10-11-2011 12:00 AM

The Effect of Biomechanical and Biochemical Factors on Endothelial Cells: Relevance to Atherosclerosis

Qiuquan Guo
The University of Western Ontario

Supervisor
Jun Yang
The University of Western Ontario

Graduate Program in Biomedical Engineering
A thesis submitted in partial fulfillment of the requirements for the degree in Doctor of Philosophy

THE EFFECT OF BIOMECHANICAL AND BIOCHEMICAL FACTORS ON ENDOTHELIAL CELLS: RELEVANCE TO ATHEROSCLEROSIS

(Spine title: Effect of biomechanical and biochemical factors on ECs)

(Thesis format: Integrated Article)

by

Qiuquan Guo

Biomedical Engineering Graduate Program

Faculty of Engineering

A thesis submitted in partial fulfillment
of the requirements for the degree of
Doctor of Philosophy

The School of Graduate and Postdoctoral Studies
The University of Western Ontario
London, Ontario, Canada

THE UNIVERSITY OF WESTERN ONTARIO
School of Graduate and Postdoctoral Studies

CERTIFICATE OF EXAMINATION

Supervisor

_____
Dr. Jun Yang

Examiners

_____
Dr. James Johnson

_____
Dr. Daniel Goldman

_____
Dr. Qingping Feng

_____
Dr. Yi Zuo

The thesis by

Qiuquan Guo

entitled:

The effect of biomechanical and biochemical factors on endothelial cells: relevance to atherosclerosis

is accepted in partial fulfillment of the
requirements for the degree of
Doctor of Philosophy

_____
Date

_____
Chair of the Thesis Examination Board

ABSTRACT

Microscale technologies create great opportunities for biologists to unveil cellular or molecular mechanisms of complex biological processes. Advanced measuring techniques, like atomic force microscope (AFM), allow detecting and controlling biological samples at high spatial and temporal resolution. Further integration with microsystems, such as microfluidic platforms, gives the ability to get detailed insight into basic biological phenomena. Highly integrated microdevices show great promise for biomedical research and potential clinical applications.

It is hypothesized that biomechanical factors play a significant role in the development of vascular diseases like atherosclerosis. To explore effects of biomechanical and biochemical stimuli on endothelial cells (ECs), AFM, which allows measurements of living cells, was utilized. Due to the heterogeneity of cells, standard characterization methods for mechanical properties of cells are still lacking. Therefore, a new quantitative method was developed for evaluation of cell elasticity correlating with cell morphology in this study. Moreover, cells are intrinsically viscoelastic materials revealed by stress relaxation measurements. A mechanically distinct bilayer model was proposed to discover the mechanical behaviour of cell components. Based on the elasticity characterization method and the stress relaxation model, the effect of cholesterol content on the mechanical response of ECs was examined, focusing on the behaviour of plasma membrane.

To mimic physiological conditions more closely for in vitro settings, a mask-free, highly integrated, low cost and time effective method was developed to rapidly fabricate a prototype of microfluidic cell culture system (MCCS). To better understand cell-cell interaction in circulatory systems like MCCS, a theoretical study of evaluating intercellular forces was also performed. Based on MCCS and microvalve technique, a novel bio-inspired and cell-based system was developed to simulate the formation of atherosclerosis plaque. Biomechanical properties of ECs, hemodynamic effects, cell rolling and adhesion events were investigated under this pathological model. The devices can be leveraged for potential applicability to biological research and clinical tests such as drug screening.

This research project has led to a better understanding of the underlying mechanisms of atherosclerosis and mechanical behaviours of ECs, as well as the development of AFM-based models that will be useful in determining cellular mechanical properties.

KEYWORDS: Atomic Force Microscopy, Atherosclerosis, Endothelial cells, Cellular elasticity, Stress Relaxation, Microfluidic cell culture, Cell Adhesion

CO-AUTHORSHIP

This doctoral thesis has been carefully prepared according to the regulations for an integrated-article format thesis stipulated by the Faculty of Graduate and Postdoctoral Studies at the University of Western Ontario, and has been co-authored as follows:

CHAPTER 2: CHARACTERIZATION OF THE ELASTICITY OF CELLS CORRELATED WITH MORPHOLOGY BY AFM

All the theoretical analyses and experiments were conducted by Q. Guo under the supervision of Dr. J. Yang. Draft of Chapter 2 was prepared by Q. Guo and reviewed by Dr. J. Yang. A paper co-authored by Q. Guo, Y. Xia, M. Sandig and J. Yang has been submitted to Journal of Biomechanics.

CHAPTER 4: THE EFFECT OF CHOLESTEROL CONTENT ON MECHANICAL PROPERTIES OF ENDOTHELIAL CELLS

All the theoretical analyses and experiments were conducted by Q. Guo under the supervision of Dr. J. Yang. Draft of Chapter 4 was prepared by Q. Guo and reviewed by Dr. J. Yang. A paper co-authored by Q. Guo and J. Yang is to be submitted.

CHAPTER 5: A RAPID PROTOTYPE OF MICROFLUIDIC CELL CULTURE SYSTEM

All the experiments were conducted by Q. Guo under the supervision of Dr. J. Yang. Draft of Chapter 5 was prepared by Q. Guo and reviewed by Dr. J. Yang. A paper co-authored by Q. Guo and J. Yang is to be submitted.

CHAPTER 6: EVALUATION OF INTERMOLECULAR FORCES IN A CIRCULATING SYSTEM

All the theoretical analyses were conducted by Q. Guo under the supervision of Dr. J. Yang. A paper co-authored by Q. Guo, M. Liu and J. Yang has been accepted on Biosystems.

CHAPTER 7: AN IN-VITRO VASCULAR MIMETIC MODEL: ENDOTHELIAL DYSFUNCTION STUDY DURING THE PROGRESSION OF ATHEROSCLEROSIS

All the experiments were conducted by Q. Guo under the supervision of Dr. J. Yang. An invention report was submitted to World Discoveries. Draft of Chapter 7 was prepared by Q. Guo and reviewed by Dr. J. Yang. A paper co-authored by Q. Guo and J. Yang is to be submitted.

ACKNOWLEDGEMENTS

I would like to acknowledge all the people who have provided me with help and encouragement during my PhD study.

I sincerely thank my thesis supervisor, Dr. Jun Yang, who showed me that perseverance and patience were the most important spirit as a researcher to hold. He introduced me to this exciting research area. I also would like to thank Dr. Yang for introducing me to work with industry partners, including LANXESS and Oxygon technologies. Dr. Yang's continuous guidance, friendly encouragement and superior expertise provided me with all the energy in my daily life. In addition, I would like to thank Dr. Chris Ellis and Dr. Leo Lau for their guidance as my advisor committee members.

My thanks also go to my colleagues and friends for their valuable help, generous suggestions and stimulating discussions. I own them tremendous gratitude. I thank the technicians in Nanofab and Machine shop of Western for their help in solving all types of technical problems.

I am deeply indebted to Dr. Ying Xia and Dr. Martin Sandig for their help with teaching me the knowledge about cell culture. Dr. Xia's expertises and valuable suggestions help me a lot with my researches.

Finally, I would like to express my sincere gratitude to family. Thanks a lot for your consistent trust in me. Thanks a lot for your patient waiting for me. It simply would not have been possible without you.

Table of Contents

List of Figures

CHAPTER 1

1 INTRODUCTION

1.1 Overview

Over past few decades, micro/nanotechnology, which grew rapidly and was widely applied in biological analysis [1-3], has allowed scientists to tackle complex research topics. There is increasing nano- and micro- scale methods introduced into routine biological labs. The increased collaborative research among physics, engineering and biology led scientists to explore new advanced techniques and models in biophysical realm. The expansion of bionanotechnology boosts understanding of various biological systems from single cell even single molecule level. From these developed experimental techniques and theoretical models, the complex living biological systems are revealed progressively.

A working hypothesis of this study is endothelial cells (ECs) playing critical roles in vascular biology. Especially, endothelium which regulates vascular tone has tremendous impact on developing vascular diseases like atherosclerosis [4]. Among various elements involved, biomechanical effect is vital factors which may play dominant role in the initiation of signalling cascades. It is expected that this research will give an insight into cellular mechanics and mechanisms of atherogenesis.

In this research, biomechanical properties of ECs were measured and well characterized using atomic force microscope (AFM). After invented by Binning in 1986 [5], AFM has been widely

used in the scope of understanding structure and mechanics of biological systems, since it is allowed to operate in living cells condition that other electron techniques, such as scanning electron microscopy (SEM) and transmission electron microscopy (TEM), are incapable of providing. With a sharp AFM probe, high resolution allows detecting surface features up to nanometre level. What is more, AFM acting as force microscope has become an essential tool in investigating cellular mechanics, cell-cell interaction forces and molecular interaction forces [6].

Microfluidics has demonstrated potential impacts on various fields from chemical synthesis and biological analysis to optic and information technology, and has dramatically expanded the capability of existing techniques [7, 8]. A bio-inspired and microfluidics-based vascular mimetic model was developed to simulate the progression status of atherosclerosis in this study. Vascular diseases like atherosclerosis are still widely lethal medical conditions. Atherosclerosis is an extremely complex inflammatory process coupled with cellular mechanical environment, both of which contribute significantly to the development and progression of the disease. The deep connection between atherosclerosis as an inflammatory disease and a biomechanical disorder primarily motivates this research. Major research topics of the thesis are briefly described as following.

In the first chapter, a literature review for atherosclerosis and biomechanical properties of cells are presented, followed by describing two main techniques employed in this research: AFM, a nano-scale tool, and microfluidic cell culture system, a microscale technique.

Chapter two and chapter three developed two characterization methods of cellular mechanics for better understanding mechanical properties of cells. In chapter two, a new quantitative method was developed to describe elasticity of single cell correlated with cell morphology. Using this

method, effects of different substrates on the mechanical property of cells were examined. In chapter three, viscoelastic behaviour of ECs was examined. A mechanically distinct bilayer structure was proposed to describe stress relaxation process of EC under constant compression.

In chapter four, based on the elasticity characterization method and the stress relaxation model, the effect of cholesterol content on cellular mechanical properties was investigated, focusing on the effect on the property of plasma membrane.

In Chapter five, a rapid prototype of microfluidic cell culture system (MCCS) was developed to generate improved physiological environment for ECs study. Chapter six gives a theoretical analysis of cell interaction forces in circulating system.

In Chapter seven, a bio-inspired vascular mimetic model was developed to mimic the formation of atherosclerotic plaque and used to investigate pathological mechanism of atherosclerosis. Biomechanical properties of ECs were explored by AFM. In addition, hemodynamic effect, rolling and adhesion events of immune cells were discussed for this model.

At last, a summary was provided and conclusions of the thesis research were drawn, followed by an overview on future study.

1.2 Atherosclerosis

1.2.1 Atherosclerosis

Atherosclerosis, with its related complications, is a leading cause of death for both men and women in developed and developing countries [9]. Research reveals that atherosclerosis is a multi-factor lesion and a chronic inflammatory disease which could also convert into acute clinical events, such as heart attack and stroke, by plaque rupture and thrombosis. A number of risk factors, including hypertension, obesity, diabetes, smoking, and especially hyperlipidemia which is elevated level of low-density lipoprotein (LDL) cholesterol, have been found to be associated with the disease [10]. However, it is much more than that. Atherosclerosis is an extremely complicated disease caused by multiple factors; the underlying pathophysiology and its associated risk factors is still unclear.

Atherosclerosis is a syndrome mainly affecting wall thickness of medium and large arterial blood vessels. Various pathology factors were investigated by researchers. For example, endothelial dysfunction has been thought to have a significant role in pathogenesis of atherosclerosis [11, 12]; Overproduction of reactive oxygen species (ROS) is also found to be related to the development of atherosclerosis [10]. At the early stage of atherogenesis, fatty materials accumulated in the wall, which thickens, hardens and even block the arteries progressively. Normally, symptoms do not occur until the blood vessels were restricted or blocked. Therefore, prevention and early diagnosis are very necessary. To help prevent complications, a healthier diet with low cholesterol is highly recommended. Screening and diagnostic tests including electro-cardiogram, stress test, CT scan or arteriography were often used to detect early development of atherosclerosis. In addition, biomarkers, such as elevated plasma concentrations

of both fibrinogen and C-reactive protein (CRP) [13], released by inflammation caused by atherosclerosis could help with the diagnosis.

The study of atherosclerosis covers a broad range of areas. The information given here is by no means complete. The current research is intended to study the mechanism of atherosclerosis progression from a basic science perspective. Due to the complexity of atherosclerosis, the review here is to give a brief introduction.

1.2.2 Hemodynamic Forces and Endothelial Dysfunction

For over a century, hemodynamic forces have been recognized as important factors regulating the structure of blood vessels [14, 15] and influencing the development of vascular pathology, e.g. atherosclerosis [16]. Shear stress, which is proportional to blood viscosity (μ), and shear rate at the wall (dv/ds), has contributed to pathogenesis of atherosclerosis in different level at various locations of blood vessels [17, 18]. Atherosclerosis shows propensity at the outer edge of blood vessel bifurcations. In these susceptible areas, blood flow is slow which results in a weaker hemodynamic shear force locally. The non-uniform shear stress will induce pro-atherogenic endothelial dysfunction and monocyte recruitment, which contributes to the development of atherosclerosis [19].

There is increasing evidence that steady laminar shear force will induce up-regulation of athero-protective (i.e. anti-inflammatory and anti-oxidant) functions in the endothelium, while unsteady or disturbed shear force can cause endothelial dysfunction then influence atherosclerotic lesion formation and progression.

Among various mechanisms of atherogenesis, endothelial dysfunction is believed to be one of the most important factors in developing atherosclerosis [12, 20]. Endothelium, due to its unique anatomical position between blood and tissue, acts as a protector by generating a repertoire of biological factors. Under various biomechanical and biochemical stimuli, endothelium produces a number of bio-active molecules performing a variety of functions. Nitric oxide (NO) generated from endothelial NO synthase (eNOS) is a major substance maintaining the balance between vasodilation and vasoconstriction [21] and regulating many aspects of cardiovascular homeostasis; other endothelium-derived vasodilators like prostacyclin works synergistically with NO to inhibit platelet aggregation [12]. Endothelium also maintains the balance between inhibition and stimulation of smooth muscle cell proliferation and migration, and thrombogenesis and fibrinolysis [22]. Damage of Endothelium will break the balance between vasoconstriction and vasodilation and initiates a number of events that promote atherosclerosis.

1.2.3 Plaque Formation

Endothelial damage or rupture will increase the permeability of endothelium. This impaired function increases the infiltration of LDL into the wall of blood vessels. Overtime, the substances such as LDL, cholesterol and fatty materials will accumulate at damaged areas. LDL will be oxidized by reactive oxygen species to form oxidized-LDL (ox-LDL). Then, ECs from the damage sites will initiate immune responses and release chemoattractants to attract monocytes from blood flow. After absorbing the oxidized-LDL, monocytes will differentiate into macrophages under the stimulation of oxidized-LDL. Macrophages continue eating and digesting the cholesterol molecules. Initially, these white blood cells intended to play a protective role. However, they are not able to process the oxidize-LDL. Finally, foam cells formed and

eventually fatty streak generated, which could be found in human aorta at the first decade of their life [4].

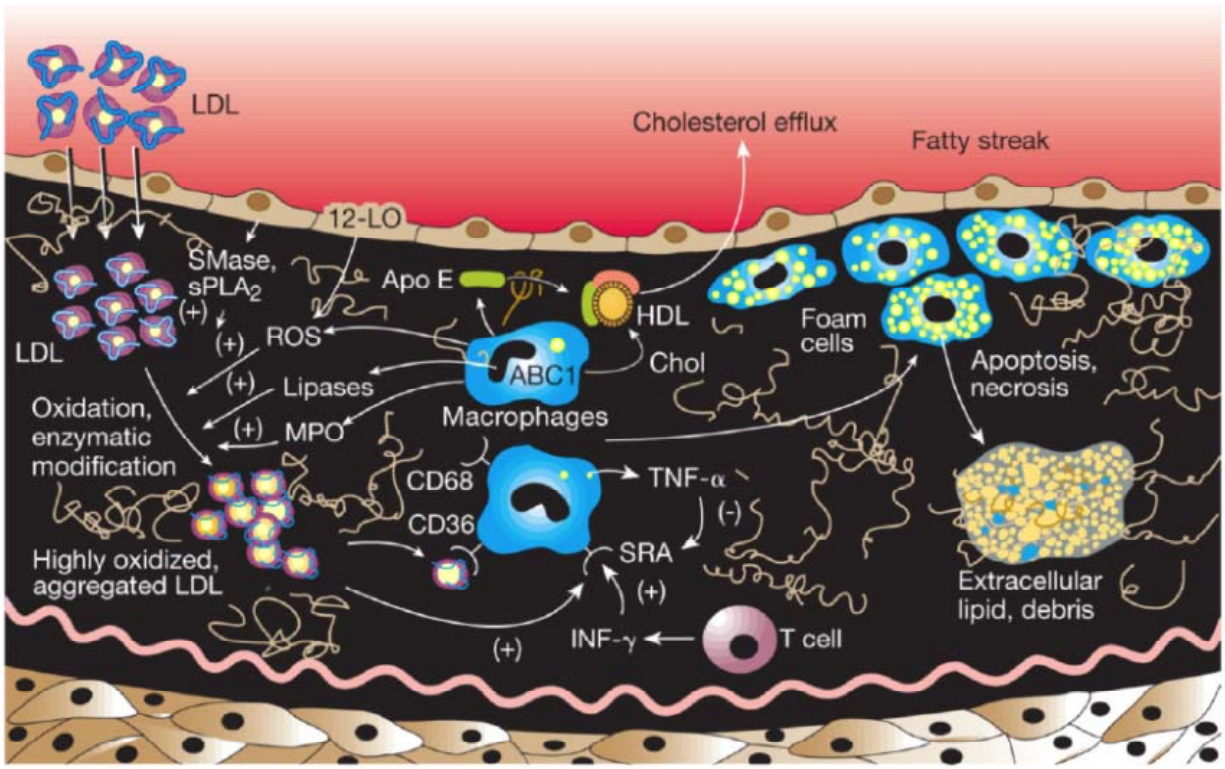

Figure 1-1. Cellular components involves with foam-cell formation. LDL was oxidized and becomes highly oxidized aggregated LDL, which is recognized by macrophage. After removal of ox-LDL, macrophage become foam cells. The death of foam cells leaves behind a growing mass of extracellular lipids and other cell debris. Reproduced from [4].

After the failure of this initial immune response, the dead cell will deposit much greater amount of oxidized cholesterol into the artery wall which triggers further cycle of immune responses. In the meantime, vascular smooth muscle cells (VSMC) begin to proliferate and migrate [9] from the media to the intima. Figure 1-1 shows different cellular components of the atherosclerotic plaque in the blood-vessel wall. As the disease continues progressing by recruiting more

inflammatory cells and lipid, more VSMCs will migrate and form a fibrous cap acting as a protective layer between the lesion and the lumen of the blood vessel. Meanwhile, the plaque will alter the geometry of the blood vessel and the local blood flow profile.

The formation of a fibrous cap is stimulated by growth factors and cytokines released from degranulated platelets, VSMCs and ECs. The composite of a plaque largely determines the risk of rupture for fibrous caps, which may cause acute ischemic event, for example a myocardial infarction or stroke.

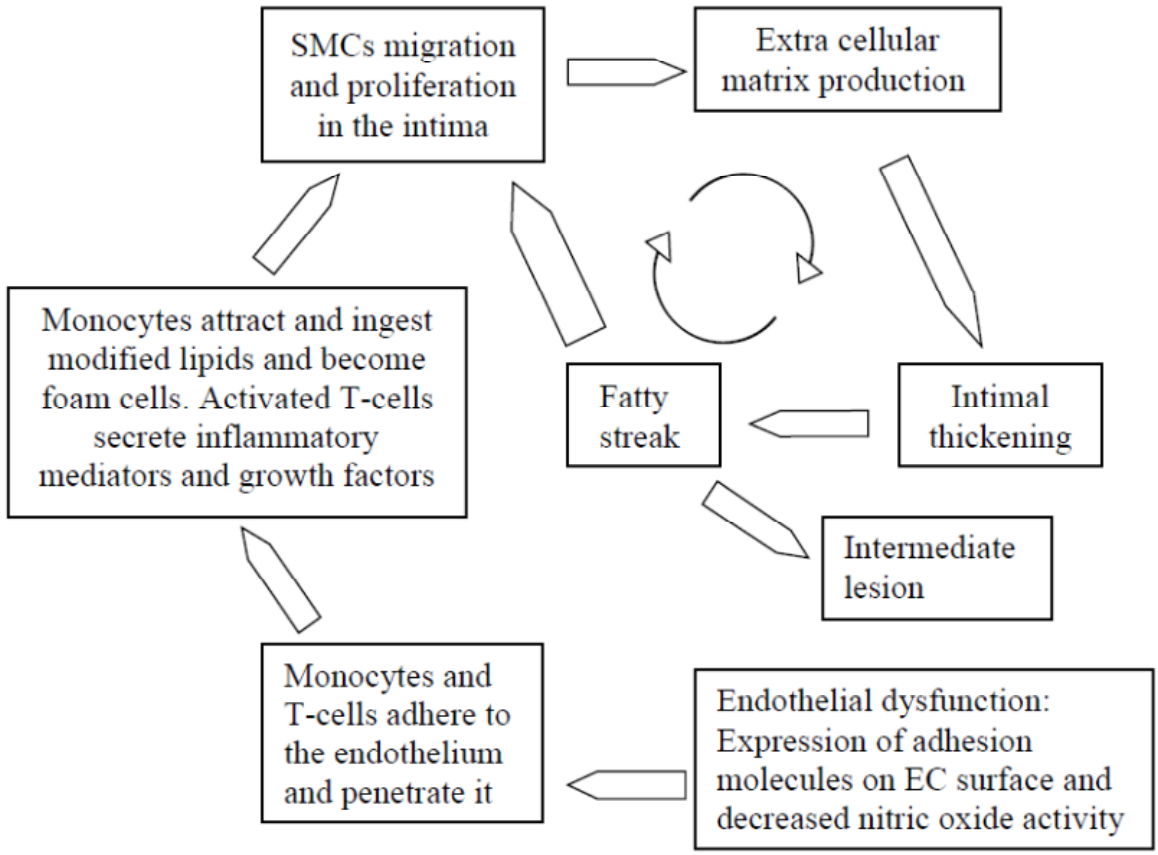

Figure 1-2. Inflammatory cells (monocytes, T-cells) and proinflammatory mediators (cytokines, interleukins) have a key role in the initial phase and progression of atheroma formation. Repeated cycles of intimal thickening lead from the first lesion of atherosclerosis, the fatty streak, to intermediate and advanced lesions. Adapted from [13].

During the formation of a plaque, numerous immune cells and signalling molecules are involved. Figure 1-2 depicts the cycle of a plaque formation process. Lipoprotein, cytokines and adhesion molecules are three main categories involved in the development of atherosclerosis.

1.2.4 Immune Responses: Promoter or Protector?

Immune responses participate in each phase of atherosclerosis after the initiation of this disease. There is no simple answer whether the immune response promotes or retards atherogenesis. As mentioned, at the early stage of plaque formation, lipid and immune cells were accumulated at the diseased site. The early plaques called as fatty streaks which are prevalent in young individuals. However, they will either progress into mature atherosclerotic plaque or disappear.

From animal model studies, there are abundant immune cells, such as T cells and macrophages, appearing in mature plaques. Many of these immune cells produce pro-inflammatory cytokines. Therefore, the plaques can continue to progress into more complex lesion. On the other hand, the disappearance of early plaque must also involve with a series of complicated immune response and intricate biological effectors.

1.3 Biomechanical Property of Cells

Mechanical properties of biological cells are determined by the structure of cells. They are highly heterogeneous in both space and time and may serve as a sensitive indicator for the health status of a cell. The biomechanical properties of tissues are often influenced by many physiologic and pathophysiologic processes. Abnormal biomechanics of tissues is often related to a wide range of diseases. The deviation from normal status will result in various dysfunction or diseases. Based on the relationship between the tissue mechanics and pathology, palpation is often used to qualify the tissue hardness for disease diagnosis. In an effort to make more quantitative examinations, other techniques have been developed to measure the elasticity of tissue in vivo [23, 24]. Recently, in vivo elastography is used for quantitative assessment of breast lesion [25].

Indeed, the property of tissue is often manifested at the cellular level. A number of studies have been conducted to find the relationship between healthy and diseased cells. As mentioned, the mechanical property of a cell is determined from the structure mainly cytoskeleton of the cell. In addition, the morphology, cell-substrate interaction and cell shape have effects on the biomechanical property of a cell. Evidence has shown that the structure of cells will be affected by different diseases to alter the mechanical properties. For example, the metastatic cancer cells were found to be much softer than the benign cells [26, 27]; the elasticities of prostate cells at different stage of the disease progress were measured which is to discriminate cancerous, non-metastatic and metastatic cells [28]; the age-related morphological and biomechanical changes of osteoarthritis were studied for early detection purpose [29]. However, there is still a long way till mechanical properties change could be applied to the clinical diagnosis.

1.3.1 Structure of a Cell

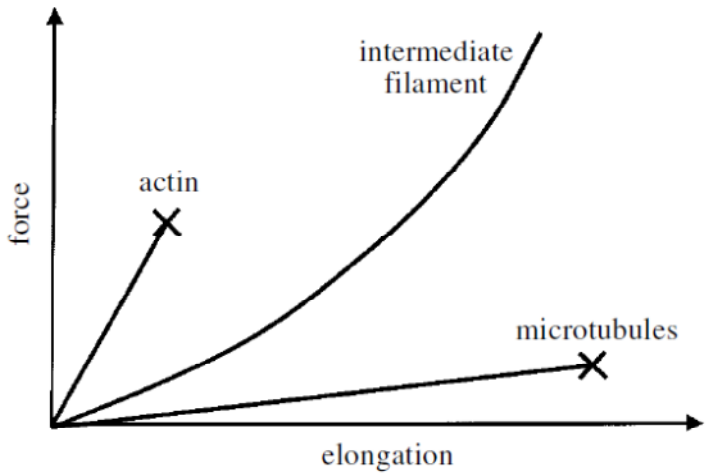

Figure 1-3. The mechanical performance of three filaments which form the cytoskeleton structure of endothelial cell. Actin and microtubules show pure elastic behaviour, while intermediate filament shows viscoelastic behaviour. Reproduced from [30].

Instead of being an inert material, cells exhibit a biological active response when a stress was applied. Thus, cells generate an internal stress on the underlying cytoskeleton structure. Even more, cells can reorganize and adjust into a new structure according to an external mechanical stimulus. Mechanical property of adherent cells is largely determined by the structure of cytoskeleton (CSK), which is a meshwork structure containing three main filaments, actin filaments (AFs), intermediate filaments (IFs) and microtubules filaments (MFs) [31]. Figure 1-3 shows the mechanical responses under different elongation for the three filaments. AFs are the smallest filaments with a diameter in the range of 5-10 nm and can be found to form bundles which are called as actin stress fibres as well. Since AFs have the highest elastic moduli among the three filaments, with a magnitude of gigapascal (GPa), the amount and distribution of AFs often determine the mechanical property of the cells. In addition, the level of crosslinking will have a dominant effect on the elastic response of a cell. The second filament is microtubule

filament, which shows pure elastic response under elongation. Microtubules are hollow tubule polymers with typical outer diameter at 24 nm and inner diameter at 12 nm. Microtubules could carry very high strain, greater than 20% [31]. Due to the largest size and special structure among three filaments, microtubules have the greatest bending stiffness. The third type of filaments is intermediate filament, with a diameter of around 10 nm. IFs have intermediate elastic performance between AF and MF. In addition, IF manifests viscoelastic property. Together with other filaments, the whole cytoskeleton is embedded in the viscous cytoplasm as well as attached to cell membrane through integrins. Thus, the overall mechanical performance of a cell falls into the class of viscoelastic materials. However, it is still not clear how the filaments, and all other associated cellular structures are arranged and coupled to respond to external biochemical and biomechanical stimuli.

1.3.2 Endothelial Mechanics

The endothelium, by virtue of its specific location in the blood vessel wall, is one of the most intensively studied tissues in cellular mechanics. Numerous studies have shown the correlation between normal functioning of endothelium and atherogenesis. Among various factors involved, mechanical force was proved to be one of the dominant influences in the progression of atherosclerosis.

As a result of their unique locations, ECs experience three primary forces: pressure, induced by the hydrostatic forces of blood; circumferential stretch or tension, generated from vasodialation and vasoconstriction; shear stress, the dragging force created by blood flow. These mechanical forces are critical regulators of endothelial function and particularly important in the whole cardiovascular system. Studies have shown that biomechanical stimuli have significant effects on

endothelial mechanical properties, functions and survival [32, 33]. Actin filaments from ECs prefer to aligning in the flow shear stress direction, which can change both the morphology and the mechanical properties of the cells [34]; different pressure will alter the function of ECs such as enhancing the release of endothelin-1 [35]. In addition, oxidized-LDL will increase the stiffness of ECs [36].

Given its anatomical position, EC is believed to be a key mediator of hemodynamic effects [37]. Of the forces mentioned above, shear force appears to be a particularly important force, since it regulates the release of vasodialation substance, cell metabolism and cell morphology [38]. There is strong relation between endothelial dysfunction and sites with low shear or turbulent flow, where demonstrate increased uptake of fatty materials [39]. Thus, laminar shear stress is essential for normal endothelial cell function and atheroprotective function [40].

1.3.3 Mechanotransduction

Mechanotransduction is describing the process of cells sensing mechanical forces from their physical surroundings, and transferring into a biochemical signals like activating signalling pathways to regulate the cell fate. The sensation of stress could occur at tissue, cellular or subcellular scales. Almost every living tissue or cell has the ability to sense mechanical stress and respond accordingly.

The mechanical forces and physical deformation of all types of cells influence cell growth, differentiation, polarity, motility, contractility, ECM synthesis, and apoptosis [41-43]. The first observed manifestation of mechanical forces on cell functions was that bone would adapt to the stress it experiences and is able to remodel if the stress changes known as Wolff's Law [44].

After that, new theories about the effects of mechanical loading on tissue differentiation were also developed [45].

Mechanotransduction not only plays a central role in normal biological functions, but also has the other side of the coin. In arterial walls, thickening and calcification are mostly contributed by the disturbed shear stress at the local region. The endothelium plays a major role in the progression of atherosclerosis, from thickening of the arterial wall intima [46], to altered endothelial permeability [47] and to activation and recruitment of monocytes [48].

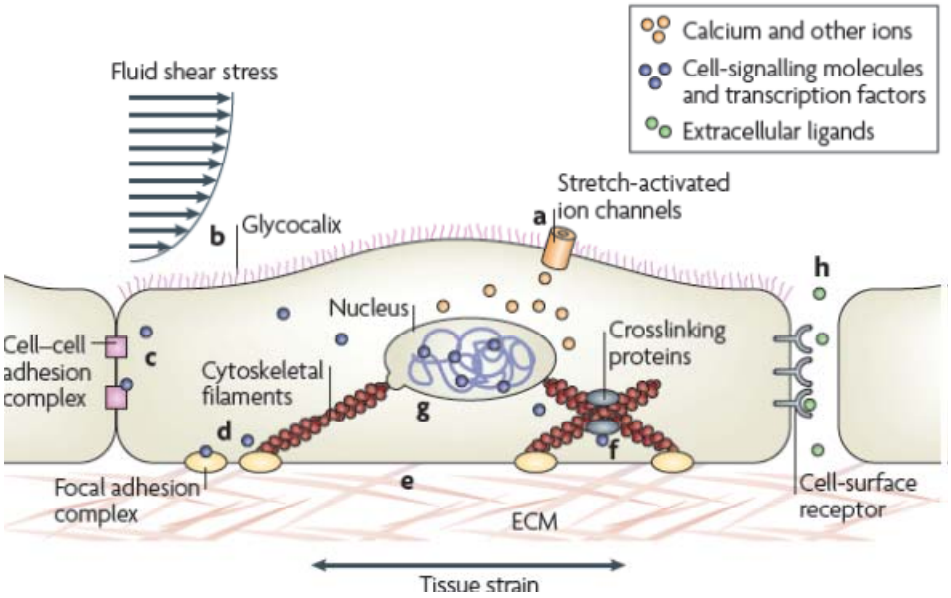

Figure 1-4. Several biological components, not mutually exclusive, have been proposed to act as cellular mechanosensors and are schematically depicted in a representative cell (see figure). Note that most of these features can be found in many cell types, although some (for example, changes in intercellular space) might only be relevant in a subset of cells. Reproduced from [49].

1.3.4 Cellular Mechanical Models

Over the last few decades, a number of studies have been conducted to study the connections among cell structure, cell responses and biological functions of cells and tissue. At the same time, scientists also developed advanced tools and techniques to manipulate single cell even single molecule to monitor the responses of biological events.

Living cells are mainly experiencing three types of mechanical stimuli, shear, tension, and compression. The forces experienced by the cells in the body vary over a wide range. Shear force exerted on vascular endothelial cell ranges between 1 and 7 Pa [50], while cartilage typically experiences stresses over 20 MPa [51]. It is useful to study the magnitude of the mechanical stimuli exerted on a biological response. Shear stress is a popular method to elicit the responses of ECs. Different geometries were developed to study the responses of ECs under shear stress. Bead forcing and scanning force microscopy (SFM) such as AFM were used to apply forces in a more localized manner, with very precise force and displacement control. The force could range from several piconewton to tens nanonewton. Other techniques such as substrate stretch and hydrostatic pressure were used to study the response of cells under defined mechanical forces and deformation. However, most of the techniques are still limited by the in vivo mimic level. In addition, the underlying physiological mechanisms are very complex. Extensive research has been conducted to indentify the molecules involved in cellular Mechanotransduction.

Mechanical properties regulate both structure and functions of biological cells. As such, a quantitative and reliable study has to be conducted to reveal the mechanics of cells. The measuring techniques can be classified into two different categories. Methods that apply forces or mechanical loads on cells and monitor the deformation are called active methods. On the other

hand, cells will also exert forces on extracellular matrix; therefore, various substrates were designed to sense the mechanical forces (mainly traction forces) generated by cells without applying external forces. These types of methods are referred to as passive methods. For active methods, a number of techniques were developed to generate compressive or tensile forces, bending forces, twisting forces, shear force, or hybrid forces by combining several different forces together.

AFM [52, 53] and MTC [54] are types of methods that can probe local sites on cells with high resolution of force and displacement. AFM is a method involving the use of a sharp tip or tips coated with spheres attached to a flexible cantilever. The applied force was monitored from the deflection of the cantilever, and the deformation of the cell was obtained from the movement of the scanner. Magnetic tweezers or magnetic twisting cytometry (MTC) use a directional magnetic field to apply either force or torque on magnetic beads which placed on the surfaces of biological tissues. The force or torque is dependent on both the properties of the applied magnetic field and the beads, while the bead movement is monitored by a CCD camera. These two techniques are primary used for local measurement; even although AFM could also be used for single cell force measurement by modifying the probe with adhering micro-size sphere [55].

Micropipette aspiration [56, 57], also known as elastimetry, is a method by applying gentle suction to a micropipette to deform the cell. The force is estimated from the applied pressure together with the deformation geometry of the cell. Micropipette aspiration is a technique measuring the overall mechanical performance of a cell. The other method used to measure the whole cell performance is optical tweezers [58, 59]. Using optical tweezers, the beads attached

on the cell surface were trapped by the high intensity laser beam to deform the cell by optical forces.

There is another pair of methods which are used to generate forces on a group of cells. The first one is shear flow method [60-62]. Different configurations were designed to provide either a constant shear over cells surface or linearly varying shear along the length or the width of cells surface. The other technique is stretching device [63, 64]. Cells are cultured on an elastic membrane modified by ECM proteins. Either constant or cyclic forces can be applied on the cells to monitor the responses. These two methods are used to investigate the flow effects or stretch effects on cell metabolism and viability; however, quantitative mechanical properties could not be determined.

Other active methods, such as micromachined force sensors [65, 66] and actuators and carbon fibre-based systems [67], are also derived from above six types of methods. Passive methods are techniques used to detect mechanical forces that single cells exert on the substrate. These methods often use soft materials as substrate [68, 69], with embedded beads [70, 71], micropatterned dots and grids [72], as well as microcantilever arrays method [73, 74] to measure the traction forces of individual cells. In addition, varieties of techniques are being developed by employing different improvements to get better force and spatial resolutions for all these methods.

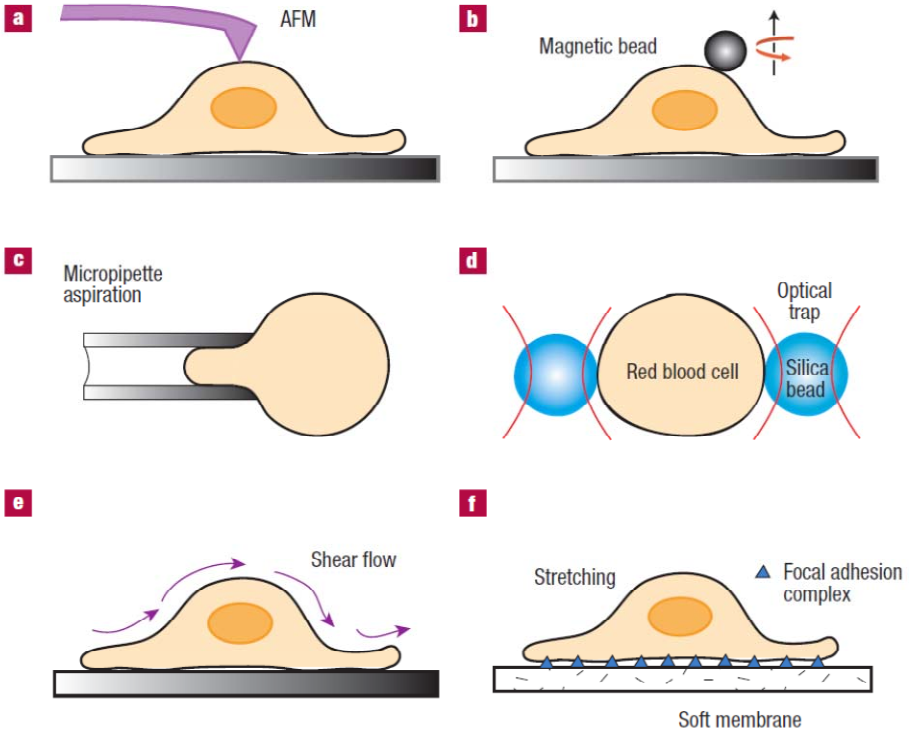

Figure 1-5. Schematic representation of the three types of experimental technique used to probe living cells. a, b, Atomic force microscopy (AFM) (a) and magnetic twisting cytometry (MTC) (b) are type A methods that can probe cell components at a force resolution of 10^{-10} and 10^{-12} N, respectively, and a displacement resolution of at least 1 nm. c, d, Micropipette aspiration (MA) (c) and optical trapping (d) are type B techniques that can deform an entire cell at a force resolution of 10^{-10} and 10^{-11} N, respectively. e, f, Shear flow (e) and substrate stretching (f) methods are capable of evaluating the mechanical response of a population of cells. Image adapted from [75].

As the development of different experimental techniques used to characterize the mechanical property of single cells, a number of mechanical models were developed by researchers to analyze the experimental data. Mechanical models of cell mechanics are derived using either the continuum approach [76] or micro/nanostructural approach [31, 77].

Despite complex and dynamic structure of cells, continuum approaches treat cells as isotropic and homogeneous composite. It is a top-down model which can't provide detailed molecular

mechanical events. The micro/nanostructural approach aims at unravelling biological complexity from physical basis. It is especially developed to investigate cytoskeletal mechanics for adherent cells, and investigates the mechanical contributions of cell membrane and spectrin network for suspension cells. The micro/nanostructural approach is a bottom-up strategy which gains more detailed molecular structural information. However, continuum approaches are relatively simple and can provide details on the distribution of stresses and strains on cells, which in turn benefits the development of more accurate micro/nanostructural approaches.

1.4 AFM and Cell Mechanics

There are a number of advanced techniques to measure cellular mechanics which were reviewed in last section. Among these techniques, AFM is one of the most versatile techniques in mechanobiology [78, 79]. AFM, invented in 1986 [5], was originally used to overcome the limitation of scanning tunnelling microscope, has shown immense impact on force-based probing of biological materials [80]. Currently, AFM has been used in a wide range of applications, such as imaging, characterization of surface property, micromanipulation, force study and molecular interaction study. AFM possesses a number of advantages, including high resolution in both spatial and force. More importantly, AFM can operate in both ambient conditions and aqueous environment, which allows to study biological materials in biophysical condition non-destructively [81].

1.4.1 Fundamental of AFM

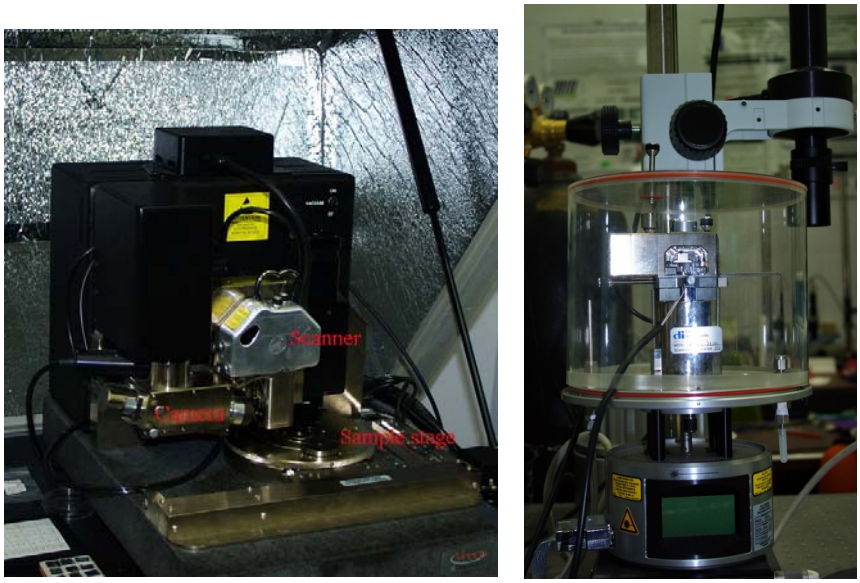

(a) (b)

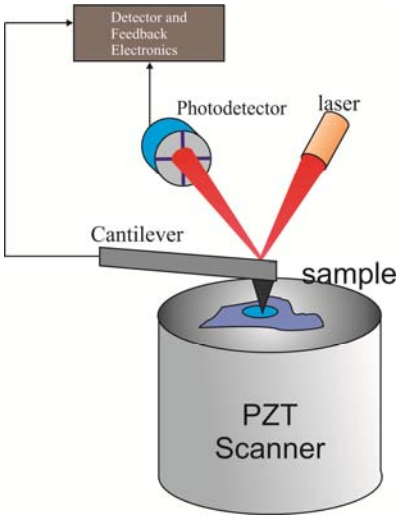

(c)

Figure 1-6. (a) Dimension AFM; (b) Multimode AFM, and (c) the schematic showing the working principles of AFM. Laser, PZT scanner, photodiode and cantilever are four main components of the system. All the operation are sent from computer to the controller throught Nanoscope software.

Figure 1-6 shows a commercial setup of AFM. There are two different types of scanning designs, tip-scanning and sample scanning. Tip-scanning is integrated in Dimension AFM (Figure 1-6a) and sample scanning is applied in Multimode AFM (Figure 1-6b). The tip-scanning design could accommodate large samples, thus, it is often employed in cellular studies, for instance cells grown on a plate or culture dish. The working principle of AFM is depicted in Figure 1-6c. The piezoelectric scanner (PZT Scanner) moves the cantilever tip from both X and Y direction (up to 100 μm for Dimension AFM) to image the sample. During scanning, the laser beam is reflected and captured by photodiode to monitor the deflection of cantilever. Meanwhile, the feedback signal is sent to the controller to move the scanner in Z direction. Topography will be obtained by rendering the data from X, Y and Z movement of the scanner.

AFM has two primary imaging modes, contact and tapping mode. How to choose the mode is mainly determined by sample property and cantilevers used. In contact mode, the tip of the cantilever is directly in contact with the sample to obtain the topography profile. Therefore, high spring constant is not recommended for contact mode since it may deteriorate the sample surface. In tapping mode, the cantilever maintains at a constant height from the sample surface while oscillating near its resonant frequency. Tapping mode is more suitable for fragile samples. The typical spring constant range of cantilevers for contact mode and tapping mode are 0.01-1 N/m and 20-100 N/m, respectively.

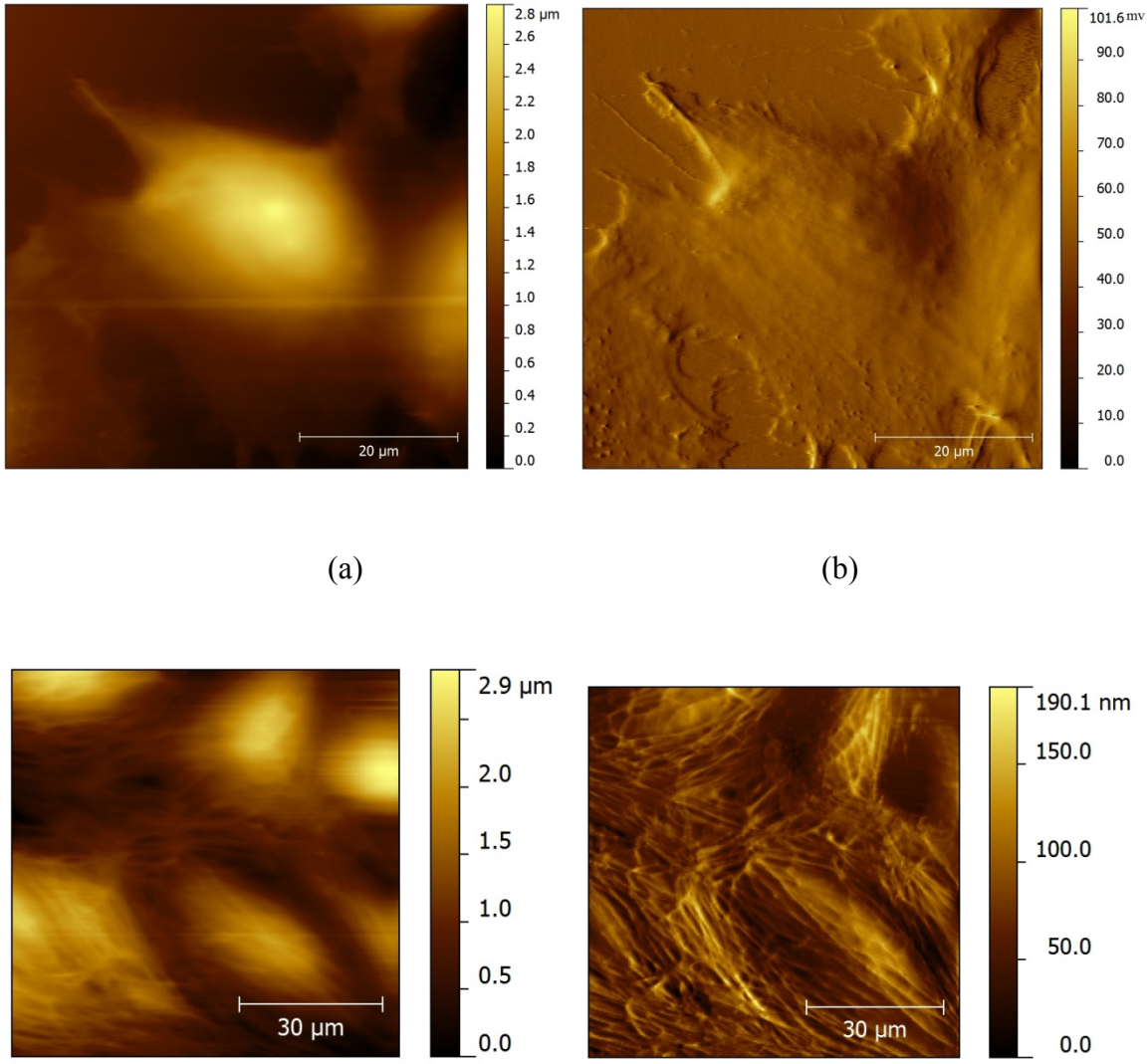

Figure 1-7. Images cells by tapping mode and contact mode. (a) Height image of a cell under tapping mode; (b) amplitude error image of a cell under tapping mode; (c) height image for confluent endothelium under contact mode and (d) deflection error image for the monolayer under contact mode.

1.4.2 AFM for Cell Mechanics

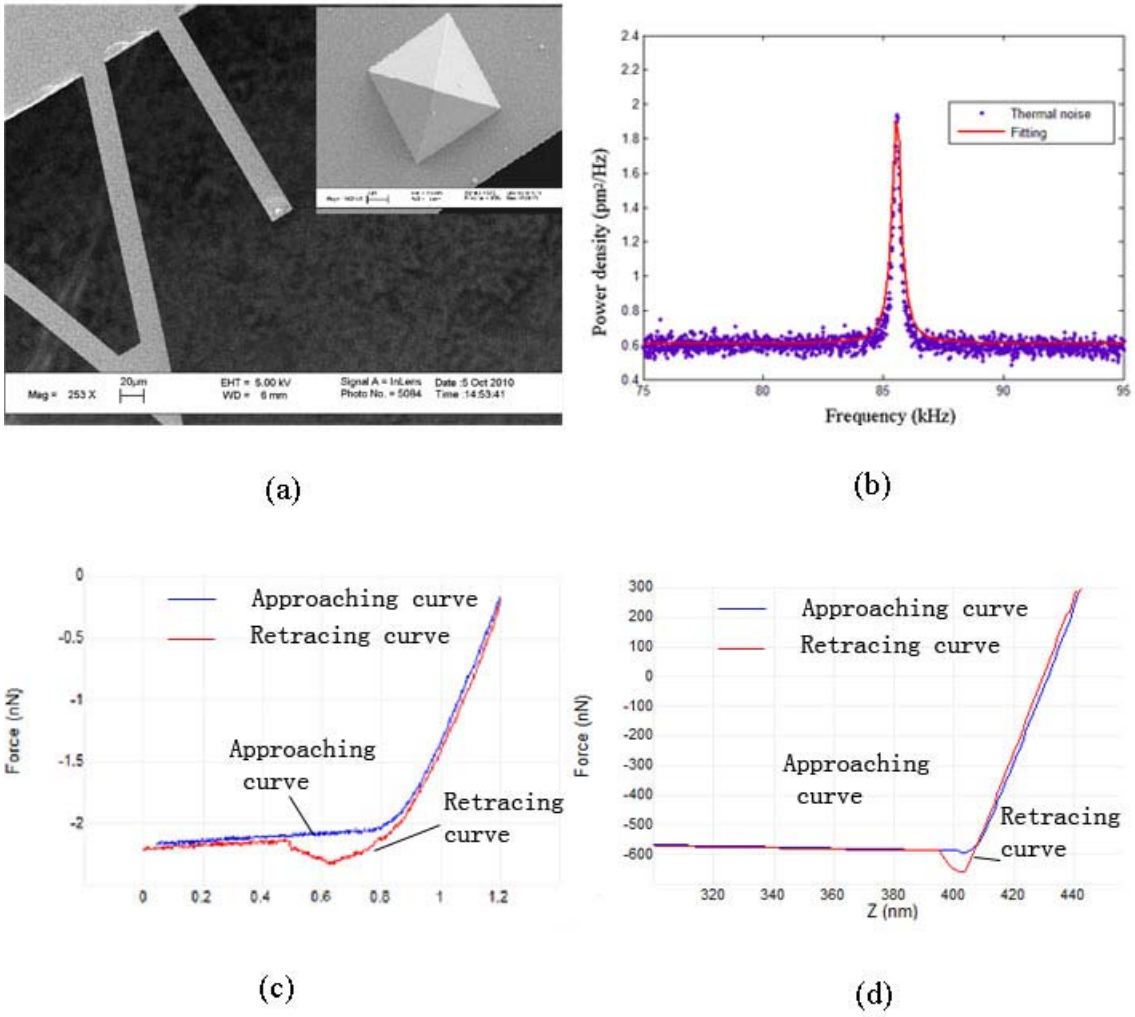

Figure 1-8. (a) SEM images of the cantilever and the probe; (b) Thermal tune data (power spectral density) extracted from time-series measurements and plotted (blue) for an AFM cantilever in air, and a Lorentzian line shape fit (red).; (c) force distance curve on soft sample (in water); (d) force distance curve on hard sample (in air).

The mechanical properties of samples are measured by force indentation in AFM. Both contact and tapping modes can perform indentation measurements while the cantilever will stop oscillating at tapping mode. To perform indentation test, the spring constant of the cantilever should be determined. Figure 1-8b shows the thermal tune method for measuring the spring

constant of a cantilever with a nominal value as 0.02 N/m. When the cantilever tip is approaching and indenting the sample, the deflection of the cantilever is monitored by the photodiode. The relation between the deflection of cantilever and the movement of the scanner is drawn in Figure 1-8c (soft samples) and d (hard samples), while the cantilever deflection is converted to force through multiplying by the spring constant of the cantilever, which results a force distance (F-D) curve.

Through force indentation measurement, F-D curves can be used to quantify stiffness, adhesion, viscoelasticity or surface charge [82, 83]. A matrix of F-D curves can be achieved by raster scanning to show the sensitivity of cytoskeleton mechanics [84] or surface receptors [85]. AFM has proven invaluable technique in the applications of probing cell microenvironment [86], molecule manipulation [87] , interaction force study [88] and single molecule recognition [89].

Other modes of operation involving oscillatory drives (tapping or force-modulation) are used to image relative viscoelastic features through simultaneous amplitude and phase detection [90, 91]. Frequency-dependent dynamic microrheology measurement by AFM are performed to obtain the viscoelastic behaviour of epithelial cells and fibroblasts [92, 93].

1.5 Microfluidic for Cell Biology

1.5.1 In Vitro and In Vivo

In vitro research is generally referred to conducting experimental biology in a well controlled and artificial environment using tissues or cells from the whole organ. Compared to in vivo studies conducting with living organisms in literally intact conditions, in vitro research possesses specific advantages. Living organisms are complex systems hindering the separation of the influence from various factors. While in vitro model allows scientists to focus on the factors of interests by isolating other components from the complex whole system. Although animal models have made essential efforts in the understanding of various diseases, in vitro technique can provide more detail information to discover the underlying mechanisms.

In an effort to develop in vitro model to more closely mimic the in vivo conditions, a number of techniques were developed by scientists. Microfluidic techniques have been proved to be an effective method in cell biology [3, 94]. With their unique phenomena, microfluidics can be leveraged to fabricate devices and components that are capable of realizing biological functions.

1.5.2 Microfluidics Cell Culture System

Varieties of factors determine phenotypes of cells in vivo and affect responses under biochemical or biomechanical stimuli. Traditional macro scale cell culture techniques, such as petri-dish and microtiter plates, become helpless in controlling the microenvironment. Micro/nano scale techniques [95] have shown great potential to replicate and increase the biological relevance of current cell-based culture models.

Microfluidics has been applied in biological studied since last two decades [96]. Compared to traditional culture methods, microscale cell cultures provide a great amount of advantages, such as manipulating micro-environment more precisely, controlling cell-cell and cell-matrix interactions, the use of small culture volumes, and the ability to integrate with microsystem technologies. Microscale techniques for cell biology have been applied in a wide range of areas, such as single-cell analysis [97] and flow cytometry-like techniques [98], patterned three-dimensional culture [99] and microscale perfusion cell culture [100, 101]. These microdevices have provided a variety of functionalities that traditional methods cannot afford. We can foresee the future that micro techniques will keep as a leading technology in answering the questions in cell biology with their unique functionalities.

Microscale technologies have shown great potential impact on cell biology and tissue engineering. However, no considerable impact has been made for routine biological assays in lab or commercial applications. Despite the advances in both microtechnology and cell biology, there are a number of challenges in integrating microtechnology with cell biology. The challenges are mostly caused by the disconnection between the engineers who design and fabricate the devices and the biologists who use them.

In this study, we will illustrate a rapid method of prototyping a vascular mimic microfluidic system from design, fabrication, assembly, sterilization and cell culture. Combined with microfluidic valve technique, a pathological model was also developed to simulate the progression of atherosclerosis.

1.6 Reference

1. Wurm, M., et al., Microtechnology meets systems biology: The small molecules of metabolome as next big targets. Journal of biotechnology, 2010. **149**(1-2): p. 33-51.

2. Folch, A. Lab-on-a-chip devices for cell biology studies: IEEE.

3. Beebe, D.J., G.A. Mensing, and G.M. Walker, Physics and applications of microfluidics in biology. Annual Review of Biomedical Engineering, 2002. **4**(1): p. 261-286.

4. Lusis, A.J., Atherosclerosis. Nature, 2000. **407**(6801): p. 233-241.

5. Binnig, G., C.F. Quate, and C. Gerber, Atomic force microscope. Physical Review Letters, 1986. **56**(9): p. 930-933.

6. Muller, D.J., et al., New frontiers in atomic force microscopy: analyzing interactions from single-molecules to cells. Current Opinion in Biotechnology, 2009. **20**(1): p. 4-13.

7. Whitesides, G.M., The origins and the future of microfluidics. Nature, 2006. **442**(7101): p. 368-373.

8. Dittrich, P.S. and A. Manz, Lab-on-a-chip: microfluidics in drug discovery. Nature Reviews Drug Discovery, 2006. **5**(3): p. 210-218.

9. Owens, G.K., M.S. Kumar, and B.R. Wamhoff, Molecular regulation of vascular smooth muscle cell differentiation in development and disease. Physiological Reviews, 2004. **84**(3): p. 767-801.

10. Victor, V.M., et al., Oxidative Stress, Endothelial Dysfunction and Atherosclerosis. Current Pharmaceutical Design, 2009. **15**(26): p. 2988-3002.

11. Hernandez-Perera, O. and S. Lamas, Endothelial dysfunction in atherosclerosis: protective role of statins. Nefrologia, 1998. **18**: p. 100-110.

12. Davignon, J. and P. Ganz, Role of endothelial dysfunction in atherosclerosis. Circulation, 2004. **109**(23): p. 27-32.

13. Kaperonis, E.A., et al., Inflammation and atherosclerosis. European Journal of Vascular and Endovascular Surgery, 2006. **31**(4): p. 386-393.

14. Kamiya, A. and T. Togawa, Adaptive regulation of wall shear stress to flow change in the canine carotid artery. American Journal of Physiology-Heart and Circulatory Physiology, 1980. **239**(1): p. H14.

15. Langille, B.L. and F. O'Donnell, Reductions in arterial diameter produced by chronic decreases in blood flow are endothelium-dependent. Science, 1986. **231**(4736): p. 405.

16. Zarins, C.K., et al., Carotid bifurcation atherosclerosis. Quantitative correlation of plaque localization with flow velocity profiles and wall shear stress. Circulation Research, 1983. **53**(4): p. 502.

17. Chatzizisis, Y.S., et al., Risk stratification of individual coronary lesions using local endothelial shear stress: a new paradigm for managing coronary artery disease. Current opinion in cardiology, 2007. **22**(6): p. 552.

18. Malek, A.M., S.L. Alper, and S. Izumo, Hemodynamic shear stress and its role in atherosclerosis. Jama-Journal of the American Medical Association, 1999. **282**(21): p. 2035-2042.

19. Cicha, I., et al., Endothelial dysfunction and monocyte recruitment in cells exposed to non-uniform shear stress. Clinical hemorheology and microcirculation, 2008. **39**(1): p. 113-119.

20. Gimbrone, M., Endothelial dysfunction, hemodynamic forces, and artherosclerosis. THROMBOSIS AND HAEMOSTASIS-STUTTGART-, 1999. **82**: p. 722-726.

21. Kawashima, S. and M. Yokoyama, Dysfunction of endothelial nitric oxide synthase and atherosclerosis. Arteriosclerosis Thrombosis and Vascular Biology, 2004. **24**(6): p. 998-1005.

22. Feletou, M. and P.M. Vanhoutte, Endothelial dysfunction: a multifaceted disorder. American Journal of Physiology-Heart and Circulatory Physiology, 2006. **291**(3): p. H985-H1002.

23. Appleyard, R.C., et al., The accuracy and reliability of a novel handheld dynamic indentation probe for analysing articular cartilage. Physics in medicine and biology, 2001. **46**: p. 541.

24. Lyyra, T., et al., In vivo characterization of indentation stiffness of articular cartilage in the normal human knee. Journal of biomedical materials research, 1999. **48**(4): p. 482-487.

25. Tanter, M., et al., Quantitative assessment of breast lesion viscoelasticity: Initial clinical results using supersonic shear imaging. Ultrasound in Medicine and Biology, 2008. **34**(9): p. 1373-1386.

26. Cross, S.E., et al., Nanomechanical analysis of cells from cancer patients. Nature Nanotechnology, 2007. **2**(12): p. 780-783.

27. Cross, S.E., et al., AFM-based analysis of human metastatic cancer cells. Nanotechnology, 2008. **19**(38): p. -.

28. Faria, E.C., et al., Measurement of elastic properties of prostate cancer cells using AFM. Analyst, 2008. **133**(11): p. 1498-1500.

29. Stolz, M., et al., Early detection of aging cartilage and osteoarthritis in mice and patient samples using atomic force microscopy. Nature Nanotechnology, 2009. **4**(3): p. 186-192.

30. Humphrey, J.D., Continuum biomechanics of soft biological tissues. Proceedings of the Royal Society a-Mathematical Physical and Engineering Sciences, 2003. **459**(2029): p. 3-46.

31. Stamenovi , D. and D.E. Ingber, Models of cytoskeletal mechanics of adherent cells. Biomechanics and Modeling in Mechanobiology, 2002. **1**(1): p. 95-108.

32. Kadohama, T., et al., Effects of different types of fluid shear stress on endothelial cell proliferation and survival. Journal of Cellular Physiology, 2007. **212**(1): p. 244-251.

33. Azuma, N., et al., Endothelial cell response to different mechanical forces. Journal of Vascular Surgery, 2000. **32**(4): p. 789-794.

34. Sato, M., et al., Mechanical stress and actin filament dynamics in cultured endothelial cell. Tissue Engineering for Therapeutic Use 4, 2000. **1198**: p. 121-130

192.

35. Hishikawa, K., et al., Pressure enhances endothelin-1 release from cultured human endothelial cells. Hypertension, 1995. **25**(3): p. 449.

36. Chouinard, J.A., et al., Oxidized-LDL induce morphological changes and increase stiffness of endothelial cells. Experimental Cell Research, 2008. **314**(16): p. 3007-3016.

37. Nerem, R., et al., Hemodynamics and vascular endothelial biology. Journal of Cardiovascular Pharmacology, 1993. **21**: p. S6.

38. Davies, P.F., Flow-mediated endothelial mechanotransduction. Physiological Reviews, 1995. **75**(3): p. 519.

39. Topper, J.N., et al., Identification of vascular endothelial genes differentially responsive to fluid mechanical stimuli: cyclooxygenase-2, manganese superoxide dismutase, and endothelial cell nitric oxide synthase are selectively up-regulated by steady laminar shear stress. Proceedings of the National Academy of Sciences of the United States of America, 1996. **93**(19): p. 10417.

40. Traub, O. and B.C. Berk, Laminar shear stress - Mechanisms by which endothelial cells transduce an atheroprotective force. Arteriosclerosis Thrombosis and Vascular Biology, 1998. **18**(5): p. 677-685.

41. Chicurel, M.E., C.S. Chen, and D.E. Ingber, Cellular control lies in the balance of forces. Current Opinion in Cell Biology, 1998. **10**(2): p. 232-239.

42. Ingber, D.E., Mechanobiology and diseases of mechanotransduction. Annals of medicine, 2003. **35**(8): p. 564-577.

43. Wang, J.H.C. and B. Thampatty, An introductory review of cell mechanobiology. Biomechanics and Modeling in Mechanobiology, 2006. **5**(1): p. 1-16.

44. Wolff, J., The law of bone remodeling. Translated by Maquet P and Furlong R. 1986, Berlin: Springer.

45. Carter, D., P. Blenman, and G. Beaupre, Correlations between mechanical stress history and tissue differentiation in initial fracture healing. Journal of Orthopaedic Research, 1988. **6**(5): p. 736-748.

46. Takahashi, M., U. Ikeda, and K. Shimada, Role of hypertension in atherosclerosis. Nippon rinsho. Japanese journal of clinical medicine, 1993. **51**(8): p. 2165.

47. Friedman, M.H. and D.L. Fry, Arterial permeability dynamics and vascular disease. Atherosclerosis, 1993. **104**(1-2): p. 189-194.

48. Nerem, R., Vascular fluid mechanics, the arterial wall, and atherosclerosis. Journal of biomechanical engineering, 1992. **114**: p. 274.

49. Jaalouk, D.E. and J. Lammerding, Mechanotransduction gone awry. Nature Reviews Molecular Cell Biology, 2009. **10**(1): p. 63-73.

50. Lehoux, S. and A. Tedgui, Cellular mechanics and gene expression in blood vessels. Journal of Biomechanics, 2003. **36**(5): p. 631-643.

51. Grodzinsky, A.J., et al., Cartilage tissue remodeling in response to mechanical forces. Annual Review of Biomedical Engineering, 2000. **2**(1): p. 691-713.

52. Radmacher, M., et al., Measuring the viscoelastic properties of human platelets with the atomic force microscope. Biophysical Journal, 1996. **70**(1): p. 556-567.

53. Hoh, J.H. and C.A. Schoenenberger, Surface-Morphology and Mechanical-Properties of Mdck Monolayers by Atomic-Force Microscopy. Journal of Cell Science, 1994. **107**: p. 1105-1114.

54. Chen, J., et al., Twisting integrin receptors increases endothelin-1 gene expression in endothelial cells. American Journal of Physiology-Cell Physiology, 2001. **280**(6): p. C1475.

55. Lulevich, V., et al., Cell mechanics using atomic force microscopy-based single-cell compression. Langmuir, 2006. **22**(19): p. 8151-8155.

56. Schmidschonbein, G.W., et al., Passive Mechanical-Properties of Human-Leukocytes. Biophysical Journal, 1981. **36**(1): p. 243-256.

57. Chu, Y.S., et al., Force measurements in E-cadherin-mediated cell doublets reveal rapid adhesion strengthened by actin cytoskeleton remodeling through Rac and Cdc42. The Journal of cell biology, 2004. **167**(6): p. 1183.

58. Henon, S., et al., A new determination of the shear modulus of the human erythrocyte membrane using optical tweezers. Biophysical Journal, 1999. **76**(2): p. 1145-1151.

59. Dao, M., C.T. Lim, and S. Suresh, Mechanics of the human red blood cell deformed by optical tweezers (vol 51, pg 2259, 2003). Journal of the Mechanics and Physics of Solids, 2005. **53**(2): p. 493-494.

60. Hochmuth, R., N. Mohandas, and P. Blackshear Jr, Measurement of the elastic modulus for red cell membrane using a fluid mechanical technique. Biophysical Journal, 1973. **13**(8): p. 747-762.

61. Ainslie, K.M., et al., Vascular smooth muscle cell glycocalyx influences shear stress-mediated contractile response. Journal of Applied Physiology, 2005. **98**(1): p. 242-249.

62. Leyton-Mange, J., et al., Design of a side-view particle imaging velocimetry flow system for cell-substrate adhesion studies. Journal of Biomechanical Engineering-Transactions of the Asme, 2006. **128**(2): p. 271-278.

63. Wang, J.H.C., P. Goldschmidt-Clermont, and F.C.P. Yin, Contractility affects stress fiber remodeling and reorientation of endothelial cells subjected to cyclic mechanical stretching. Annals of Biomedical Engineering, 2000. **28**(10): p. 1165-1171.

64. Zhuang, J.P., et al., Pulsatile stretch remodels cell-to-cell communication in cultured myocytes. Circulation Research, 2000. **87**(4): p. 316-322.

65. Yang, S. and T. Saif, Micromachined force sensors for the study of cell mechanics. Review of Scientific Instruments, 2005. **76**(4): p. -.

66. Serrell, D.B., et al., A uniaxial bioMEMS device for quantitative force-displacement measurements. Biomedical Microdevices, 2007. **9**(2): p. 267-275.

67. Yasuda, S.I., et al., A novel method to study contraction characteristics of a single cardiac myocyte using carbon fibers. American Journal of Physiology-Heart and Circulatory Physiology, 2001. **281**(3): p. H1442-H1446.

68. Harris, A.K., P. Wild, and D. Stopak, Silicone-Rubber Substrata - New Wrinkle in the Study of Cell Locomotion. Science, 1980. **208**(4440): p. 177-179.

69. Danowski, B.A., Fibroblast Contractility and Actin Organization Are Stimulated by Microtubule Inhibitors. Journal of Cell Science, 1989. **93**: p. 255-266.

70. Lee, J., et al., Traction Forces Generated by Locomoting Keratocytes. Journal of Cell Biology, 1994. **127**(6): p. 1957-1964.

71. Butler, J.P., et al., Traction fields, moments, and strain energy that cells exert on their surroundings. American Journal of Physiology-Cell Physiology, 2002. **282**(3): p. C595-C605.

72. Balaban, N.Q., et al., Force and focal adhesion assembly: a close relationship studied using elastic micropatterned substrates. Nature Cell Biology, 2001. **3**(5): p. 466-472.

73. Tan, J.L., et al., Cells lying on a bed of microneedles: An approach to isolate mechanical force. Proceedings of the National Academy of Sciences of the United States of America, 2003. **100**(4): p. 1484-1489.

74. du Roure, O., et al., Force mapping in epithelial cell migration. Proceedings of the National Academy of Sciences of the United States of America, 2005. **102**(7): p. 2390-2395.

75. Bao, G. and S. Suresh, Cell and molecular mechanics of biological materials. Nature Materials, 2003. **2**(11): p. 715-725.

76. Lim, C., E. Zhou, and S. Quek, Mechanical models for living cells--a review. Journal of Biomechanics, 2006. **39**(2): p. 195-216.

77. Boey, S.K., D.H. Boal, and D.E. Discher, Simulations of the erythrocyte cytoskeleton at large deformation. I. Microscopic models. Biophysical Journal, 1998. **75**(3): p. 1573-1583.

78. Costa, K.D., Single-cell elastography: Probing for disease with the atomic force microscope. Disease Markers, 2003. **19**(2-3): p. 139-154.

79. Kasas, S., V. Gotzos, and M.R. Celio, Observation of Living Cells Using the Atomic Force Microscope. Biophysical Journal, 1993. **64**(2): p. 539-544.

80. Jena, B.P. and J.K.H. Hörber, Atomic force microscopy in cell biology. 2002: Academic Pr.

81. Hörber, J., et al., Investigation of living cells in the nanometer regime with the scanning force microscope. Scanning Microscopy, 1992. **6**(4): p. 919.

82. Heinz, W.F. and J.H. Hoh, Spatially resolved force spectroscopy of biological surfaces using the atomic force microscope. Trends in biotechnology, 1999. **17**(4): p. 143-150.

83. Ebenstein, D.M. and L.A. Pruitt, Nanoindentation of biological materials. Nano Today, 2006. **1**(3): p. 26-33.

84. Rotsch, C. and M. Radmacher, Drug-induced changes of cytoskeletal structure and mechanics in fibroblasts: an atomic force microscopy study. Biophysical Journal, 2000. **78**(1): p. 520-535.

85. Grandbois, M., et al., Affinity imaging of red blood cells using an atomic force microscope. Journal of Histochemistry & Cytochemistry, 2000. **48**(5): p. 719.

86. Ludwig, T., et al., Probing cellular microenvironments and tissue remodeling by atomic force microscopy. Pflügers Archiv European Journal of Physiology, 2008. **456**(1): p. 29-49.

87. Kufer, S., et al., Single-molecule cut-and-paste surface assembly. Science, 2008. **319**(5863): p. 594.

88. Dammer, U., et al., Binding strength between cell adhesion proteoglycans measured by atomic force microscopy. Science, 1995. **267**(5201): p. 1173.

89. Muller, D.J., et al., Force probing surfaces of living cells to molecular resolution. Nature Chemical Biology, 2009. **5**(6): p. 383-390.

90. Putman, C., et al., Viscoelasticity of living cells allows high resolution imaging by tapping mode atomic force microscopy. Biophysical Journal, 1994. **67**(4): p. 1749-1753.

91. Haga, H., et al., Elasticity mapping of living fibroblasts by AFM and immunofluorescence observation of the cytoskeleton. Ultramicroscopy, 2000. **82**(1-4): p. 253-258.

92. Alcaraz, J., et al., Microrheology of human lung epithelial cells measured by atomic force microscopy. Biophysical Journal, 2003. **84**(3): p. 2071-2079.

93. Mahaffy, R., et al., Quantitative analysis of the viscoelastic properties of thin regions of fibroblasts using atomic force microscopy. Biophysical Journal, 2004. **86**(3): p. 1777-1793.

94. Meyvantsson, I. and D.J. Beebe, Cell Culture Models in Microfluidic Systems. Annual Review of Analytical Chemistry, 2008. **1**(1): p. 423-449.

95. Khademhosseini, A., et al., Microscale technologies for tissue engineering and biology. Proceedings of the National Academy of Sciences of the United States of America, 2006. **103**(8): p. 2480-2487.

96. Paguirigan, A.L. and D.J. Beebe, Microfluidics meet cell biology: bridging the gap by validation and application of microscale techniques for cell biological assays. BioEssays, 2008. **30**(9): p. 811-821.

97. Wheeler, A.R., et al., Microfluidic device for single-cell analysis. Analytical Chemistry, 2003. **75**(14): p. 3581-3586.

98. Culbertson, C.T., et al., Microfluidic systems and methods of transport and lysis of cells and analysis of cell lysate. 2004, Google Patents.

99. Chiu, D.T., et al., Patterned deposition of cells and proteins onto surfaces by using three-dimensional microfluidic systems. Proceedings of the National Academy of Sciences, 2000. **97**(6): p. 2408.

100. Kim, L., et al., A practical guide to microfluidic perfusion culture of adherent mammalian cells. Lab on a Chip, 2007. **7**(6): p. 681-694.

101. Hung, P.J., et al., Continuous perfusion microfluidic cell culture array for high throughput cell based assays. Biotechnology and Bioengineering, 2005. **89**(1): p. 1-8.

CHAPTER 2

2 CHARACTERIZATION OF THE ELASTICITY OF CELLS CORRELATED WITH MORPHOLOGY BY AFM

2.1 Introduction

It is well known that abnormal tissue stiffness is an indication of a wide range of diseases such as osteoporosis [1], atherosclerosis [2], etc. According to the relationship between tissue stiffness and certain diseases, palpation is clinically used to detect abnormal hardness of tissue caused by diseases like breast cancer. To achieve more quantitative examinations, elastographic techniques based on ultrasound [3] and magnetic resonance [4] imaging methods have demonstrated the ability of identifying tissue stiffness difference. Consequently, there is emerging clinical interest in finding appropriate techniques and models to diagnose diseases based on analyzing tissue mechanical properties.

Recently, studies are attempting to find a correlation of cellular elasticity with cell functions and human diseases, since changes in pathophysiological properties of tissue may be manifested at the cell level. Living cells possess specific physical and structural properties which enable them to maintain alive and functional in physiological environment. Cellular mechanics plays a major role in many cell physiological events such as cell differentiation [5], cell migration [6] and cell deformability [7]. Deviations from normal values of biomechanical properties of cells will undermine not only the physical integrity of the cells, but also their biological functions.

Understanding of cellular mechanics is critical to provide potential clinical methods that will enhance detection, diagnosis, and treatment of diseases.

Mechanical properties of cells have been studied by various single-cell techniques, such as atomic force microscopy (AFM) [8], cell poker [9], micropipette aspiration [10], scanning acoustic microscopy [11], infrared laser traps (optical tweezers) [12] and magnetic twisting cytometry [13]. At present, AFM is one of the most advanced techniques used to study biomechanical property of cells. AFM is able to quantitatively measure mechanical properties of a cell with high spatial resolution, typically at nanometre scales in biophysical environment [14, 15]. In addition, AFM has been used to image cellular microenvironments [9], surface structure, and sub-cellular structure [16]. Detection of changes in cell elasticity, measured by AFM, has been applied to distinguishing metastatic cells from benign cells, thus identifying disease states in cancer [17, 18]. What is more, AFM is applicable to detection on the pathological changes of cartilage cells in osteoarthritis [19]. AFM research conducted on endothelial cells indicated that oxidized low-density lipoproteins [20] or high plasma sodium concentration [21] increases Young's moduli of endothelial cells. All above demonstrate that AFM can be potentially developed as a diagnostic tool for detecting human disease states with fairly high efficiency and accuracy.

Although AFM is evolving rapidly in the field of biology, standard methods for achieving a comprehensive overview of mechanical properties of cells are still unavailable. In previous studies local mechanical properties of cells were often measured by AFM nanoindentation techniques [12, 22]. In order to obtain statistically meaningful data, either a number of random measurements were performed at different points on one cell, or a significant number of cells were measured. In reality, the surface of a living cell has highly heterogeneous domains containing a variety of lipid, protein, and carbohydrate components. The cytoskeleton of a cell, underlying the plasma membrane, contains many kinds of proteins forming dynamic meshworks in the cytoplasm. In addition, cell morphology is highly dependent on the substrate and the cellular microenvironment. Due to the complexity of cells, variations of cell elasticity occur not only between different cells, but also at different locations on the same cell. In order to use cell elasticity as a reliable diagnostic measure to identify cellular disease in future clinical use, the objective of our study is to develop a new evaluation method that can determine the elasticity not only of an entire cell but also of large cell sheets such as endothelia and epithelia with consideration of cell morphology.

The objective of this study is to develop a method to provide a more reliable quantification of cell mechanical property that correlates cell elasticity with morphology of the cell. In this study, through examining the local elasticity distribution of a single cell, two distinct mechanical regions which mainly affected by the underlying cytoskeleton structure were found. Based on the developed model, the effect of cell culturing substrates on the cell elasticity of HAEC was discussed.

2.2 Methods

2.2.1 Cell Culture

Human aortic endothelial cells (HAEC, Lonza) were grown in Endothelial Growth Medium-2 (supplemented with EGM-2 bulletKit, Lonza). Cells were incubated in a humidified, 5% CO_2 environment at 37 $^{\circ}$C. Culture media were changed every three days and cells were passaged after they reached 70% confluency using Trypsin-EDTA (0.05% Trypsin; 1 mM EDTA·4Na, Invitrogen). The behavior of cells remained the same during these passages, and passages 5-6 were collected in the 1 ml sterile freezing vial (90% Foetal Bovine Serum and 10% Dimethyl sulphoxide). Then cells were frozen and put into a liquid nitrogen container for later experiments.

2.2.2 Sample Preparation

Substrate preparation: Substrate A were polystyrene cell culture dishes (60 mm). Substrate B were cover glasses (20 mm in diameter) coated with Matrigel (BD Biosciences) at a 1:8 dilution of a final concentration of 1.25 mg/mL [23]. The protocol of preparation of Matrigel coated substrate is described as follows. Matrigel was prepared ahead of time and frozen as 100 µl aliquots at -20 ^{o}C. One day before AFM experiment, one aliquot (100 µl) was taken and thawed on ice for two hours (or thaw at 4 ^{o}C overnight) until matrigel liquefies. The matrigel was diluted with 700 µl cold Deionized (DI) water using prechilled pipet tips to prevent the gelation of matrigel. 4 sterilized circle cover glasses were placed in a 24-well culture plate which was placed on the ice. 200 µl of matrigel solution was placed into each coverglass-containing well and the plate was tiled until the whole coverglass is covered with liquid. 100 µl of the extra solution

from each well was pipetted and discarded. With half opening of the cover for around 30 minutes, the remaining liquid from each well was aspirated.

Cell loading: One dish of cell, which was cultured until 70% confluence, was rinsed once with HBSS and trypsinized using 4 mL of above mentioned trypsin- EDTA solution. After centrifugation at 900 RPM for 5 mins, the collected cells were dispersed into 2mL medium, and placed on two different substrates. Place the coverglasses on a parafilm (preventing suspension running away from the covergalss) and pipet 180 µl cell suspensions on each coverglass. Pipet another 300 µl cell suspension onto the 60 mm petri-dish with around 20 mm diameter area. Cell density of both substrate was around 300-600 cells/cm^2. Subsequently, cells were kept in a CO_2 incubator for 2 h for cell attachment and the medium was refreshed. Cells were cultured for 24 hours for AFM measurement till the next day.

2.2.3 AFM Experiments on Living Cells

All experiments were performed on a Dimension V AFM equipped with Nanoscope controller V and a fluid cell (Veeco, Inc.). A Silicon nitride cantilever (from Nanoscience) with a nominal spring constant of 0.03 N/m and tip radius of around 20 nm was used. The spring constant of the cantilever calibrated by the thermal tune method [24] was 0.021 N/m.

HAECs were gently rinsed with pre-warmed (37^oC) phosphate buffer saline (PBS) solution (containing Ca^{2+} and Mg^{2+}), immersed in PBS solution balance with HEPES solution to maintain right PH value (7.4), and placed under the AFM cantilever tip. Both cells and the AFM cantilever were observed with microscope of AFM. The cantilever tip can be positioned at any site of interest on cells using Nanoscope controller software (Nanoscope 7.30, Veeco).

Topography was imaged by contact mode with low deflection set point and scan rate at 0.3 Hz to minimize disturbance during the scan process. Figure 2-1lists the 2D topography image, deflection image and 3D height image of a single HAEC at contact mode AFM.

All the images were processed by Nanoscope 7.30 and Gwyddion 2.22 [25].

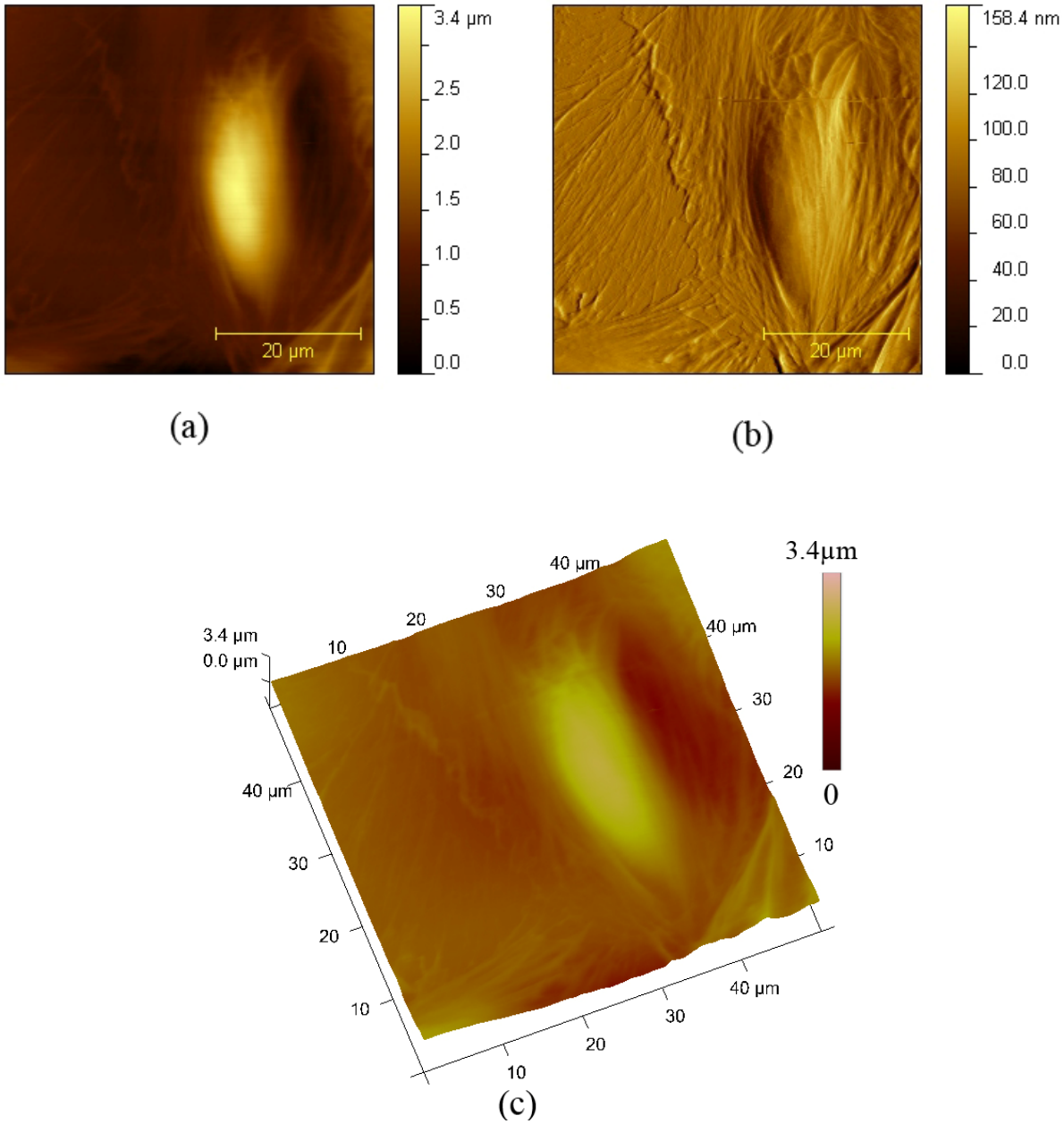

Figure 2-1. AFM contact mode image of a single HAEC . (a) 2D height image; (b) deflection image which shows the reminiscent of the structure underneath cell surface clearer than height image; (c) 3D topography image.

2.2.4 Analysis of F-D Curves and Force Volume Method

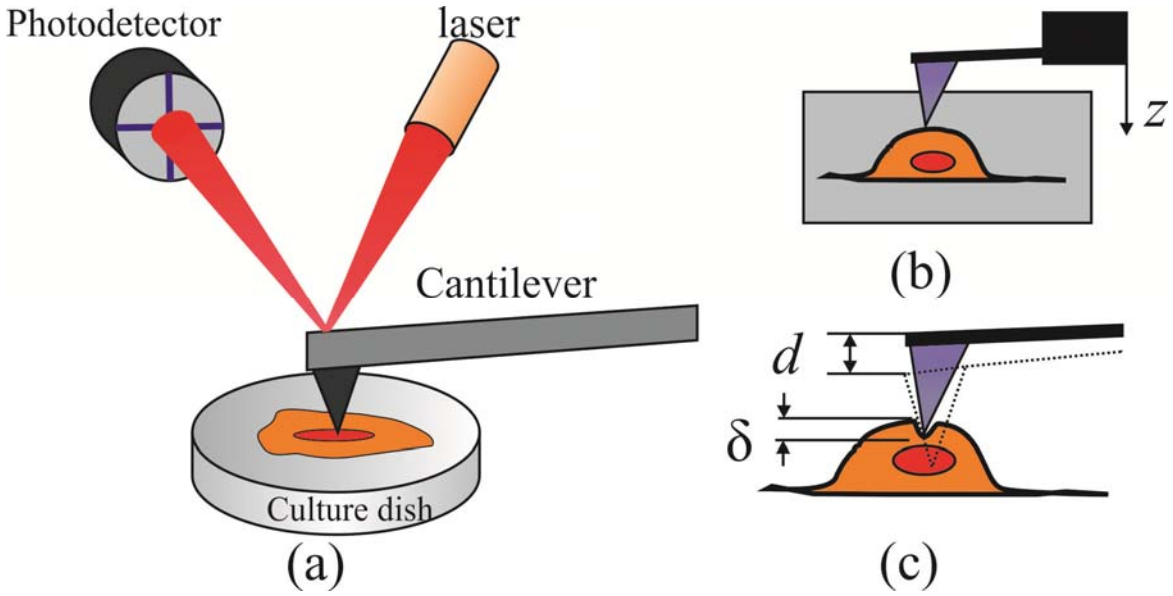

Figure 2-2. The diagram shows AFM scanning and indentation test on a cell. (a) AFM setup shows main components for AFM scanning, sample, laser, photodetector and cantilever connected with piezoelectric scanner; (b) the schema of a cantilever approaching the sample; (c) the schema of a cantilever indenting the sample. The indentation depth δ is defined as difference between the cantilever movement z and the deflection of cantilever d.

Figure 2-2 shows the schematic of AFM setup for live cell experiments and depicts the principal of an indentation test by AFM. The cantilever was moved downward by piezoelectric scanner and when the cantilever comes in contact with a sample, the cantilever starts to deflect. The split photodiode will sense changes of light intensity due to the deflection of the cantilever. The deflection was recorded as d and the movement of the scanner as z. The indentation depth is defined by the difference between the cantilever movement z and the deflection d, which is given by

$$\delta = z - d \tag{1}$$

As the scanner moving downward stepwise, the relationship between indentation depth and deflection can be obtained. The applied force on the sample can be obtained from multiplying the cantilever deflection *d* by the spring constant of the cantilever which was obtained from last section by thermal tune method. A typical force distance (F-D) curve is shown in Figure 2-3.

Several different mechanical models have been developed for analyzing F-D curves obtained by AFM. The classical Hertz model [26] is expressed as

$$F = \frac{4\sqrt{R_C}}{3}\frac{E}{1-\nu^2}\delta^{3/2} \tag{2}$$

where δ, ν, R_C, and E indicate the indentation depth, Poisson's ratio, the tip radius of the cantilever, and elastic modulus. Poisson's ratio was assumed to be 0.5 which is a typical value for soft incompressible material [27]. Classical Hertz model describing the indentation with force F into a homogeneous, soft and semi-infinite elastic material is often applied in biological samples. Compared to the size of the tip of AFM cantilevers, a cell can be seen as a very large surface. However, a fundamental assumption in the Hertz model is that the indentation depth should be less than the radius of the tip. In most cell indentation experiments, the indentation depth is up to hundreds nanometres which is much larger than the tip radius ~20 nm in our work.

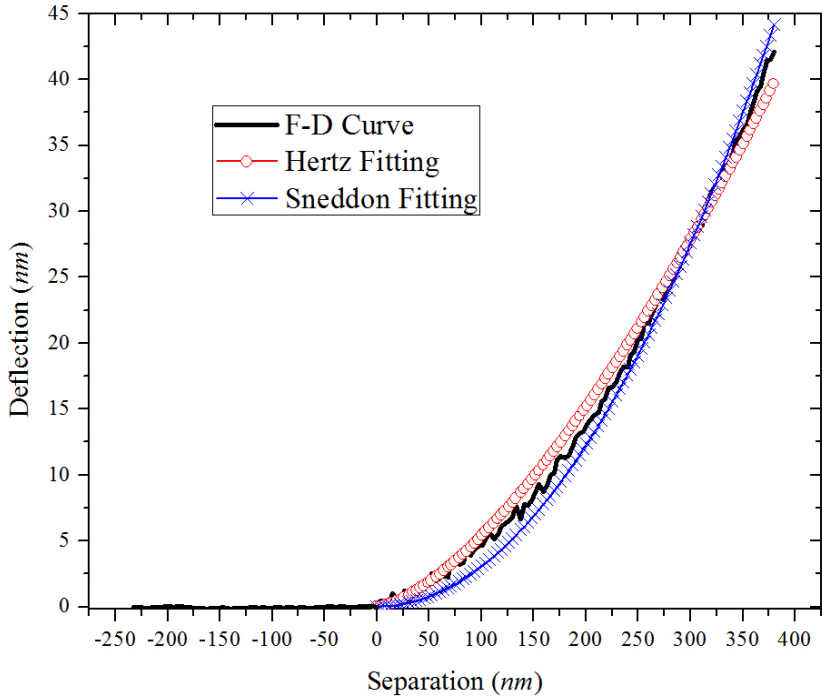

Figure 2-3. A typical cantilever deflection versus indentation depth curve (black line without symbols) taken at a random site on the cell. Young's modulus fitted by Sneddon model (blue cross symbols) is 12.35 kPa, and by Hertz model (red circle symbol) is 11.2 kPa. The spring constant of the cantilever is 0.021 N/m.

Therefore, Sneddon model [28] is used in this study for elasticity calculation. This model assumes a rigid cone indenting a soft flat surface. The load and indentation depth relation is given by

$$F = \frac{2}{\pi} \tan\alpha \frac{E}{1-\nu^2} \delta^2 \tag{3}$$

where α is half opening angle of the conical tip. In experiments, by controlling indenting rate, viscous effect of cell could be largely eliminated [29]. Figure 2-3 shows a typical F-D curve

fitted by Sneddon model and the Young's modulus is 12.35 kPa (with 95% confidence bounds), while Hertz model has underestimated the value as 11.2 kPa.

To obtain the overall elasticity map of a cell, force volume measurements were performed on HAECs. Firstly, the cells were scanned first to obtain a topography image which is to specify the area of interest. Then a single F-D curve was generated from the ramp plot to determine the relative force trigger threshold for later force volume measurement. A maximum indenting force of a cantilever was set up to 2 nN. Force plots generated at regular intervals on a sample surface were characterized as force volume imaging. If the scaned area is divided into a 32×32 array, 1024 force-distance curves will be achieved for each force volume scan. Force volume (FV) measurement was performed to simultaneously obtain a height mapping image and matrix of F-D curves, namely the matrix of elasticity, calculated by Matlab code under Sneddon model [28].

2.3 Results and Discussions

2.3.1 Morphology of HAEC

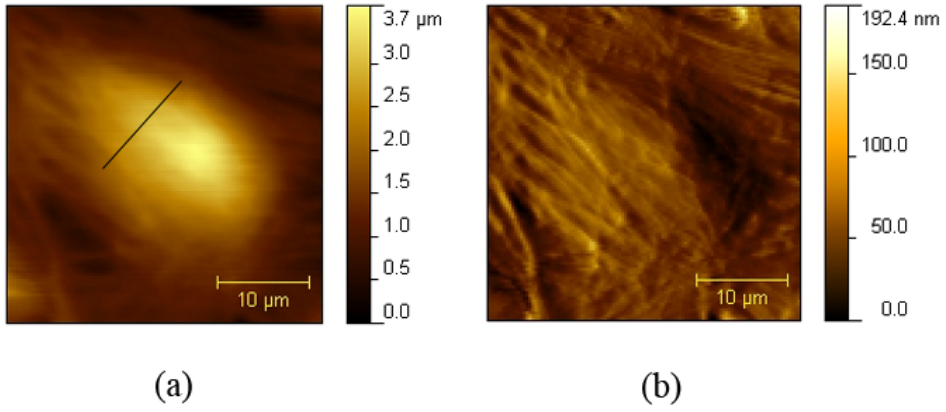

(a) (b)

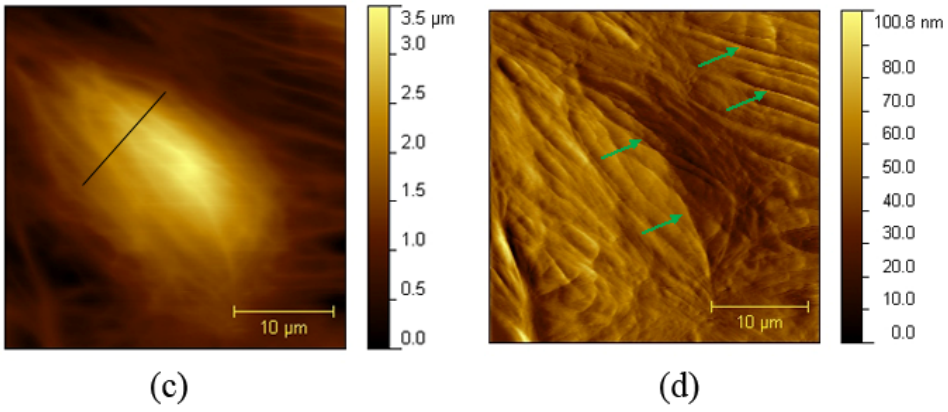

(c) (d)

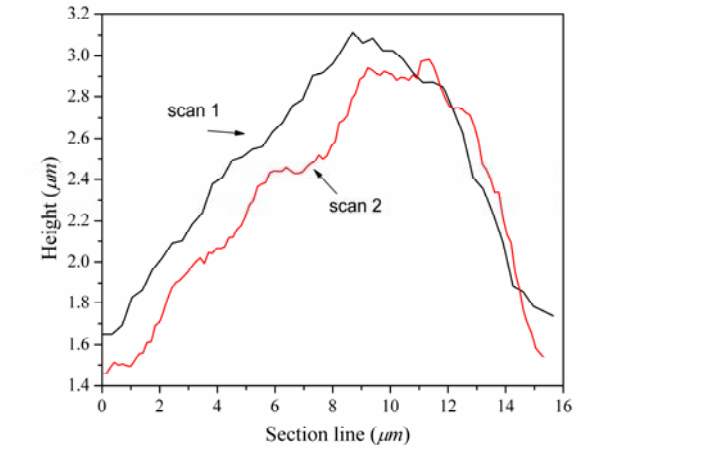

(e)

Figure 2-4. Contact mode image of a single HAEC grown on Matrigel. (a) and (c) are Height images. (b) and (d) are deflection images of cells in (a) and (c). (a) and (b) were captured within several minutes after the cells were taken out from the incubator. (c) and (d) were scanned after the cells had been equilibrating at room temperature for half an hour. The arrows in (d) indicate the reminiscent of actin cytoskeleton. (e) Cross section profiles for the two scans in (a) and (c) respectively. The two scans are indicated by arrows in this figure.

To eliminate if different environmental conditions affected AFM measurements, multiple scans were performed at different times after removal of cells from the incubator. Cells were first rinsed by pre-warmed (37^{o}C) PBS solution, a general use isotonic saline, and then quickly immersed in PBS solution for AFM imaging. Two scans were then performed. One scan was within several minutes after rinsing the cells in order to minimize the effect of the ambient environment (Figure 2-4a, b), and the other scan after the cells were equilibrating at room temperature for about half an hour (Figure 2-4c, d). The height (Figure 2-4a, c) and deflection (Figure 2-4b, d) images of a single HAEC show that the centre area of the cell has a larger height than the surrounding areas due to underlying nucleus. From the height images, we observed that the cells had shrunk and the height decreased after cells were standing in PBS for half an hour. And the height profiles of two cross sections of the cells (marked by a line in Figure 2-4a, c respectively) are shown in Figure 2-4e. Bumpy structure are visible in the second scan taken after 30 min as compared to a smoother cell surface obtained during the first scan taken shortly after removal from incubator.

In contact mode AFM, deflection image on a softer sample often reveals subsurface structures more clearly than topography Image. Therefore, deflection images of cells were also captured as shown in Figure 2-4b, d. Linear structures, reminiscent of the cytoskeleton underneath the cell membrane, became visible in the deflection images. The cytoskeleton is composed of three main kinds of filaments, actin filaments (AF), intermediate filaments (IF) and microtubules (MT). Judging from the known morphology and arrangement of cytoskeletal elements within endothelial cells [30], the filamentous structures here are likely F-actin containing stress fibres of the cytoskeleton. Cells scanned immediately after being emerged from incubator (Figure 2-4b) reveal a much smoother profile compared to those that left at room temperature for around 30 minutes (Figure 2-4d). Conjecturing that actin cytoskeleton reorganized when cells were equilibrating in PBS solution for AFM scanning, then hypothetically, the reorganization of cytoskeleton was caused by the shrinkage of the cells due to temperature and pH changes.

2.3.2 Dynamic Elasticity Change of HAEC

In order to characterize elasticity of single cell, samples were restricted in certain confluency. The images were scanned by AFM to check availability of samples preparation method (scanning images were not shown here).

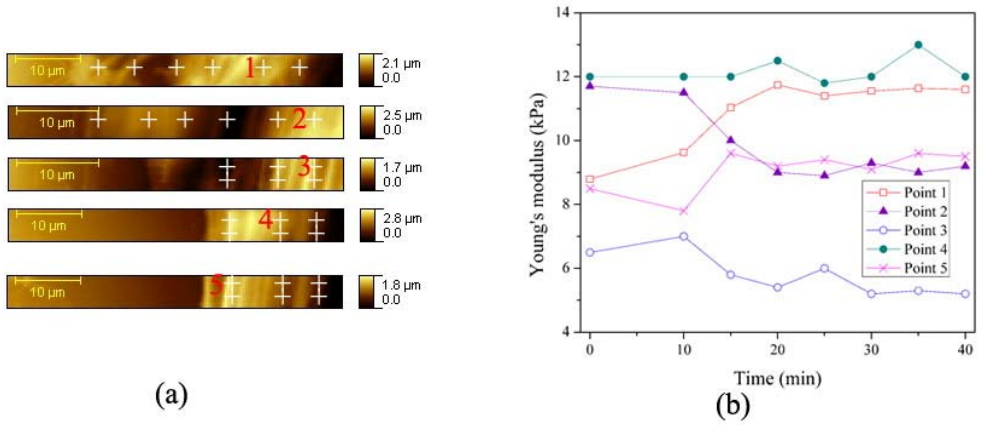

Figure 2-5. (a) Sections of several different cells, the "+" symbols are points for elasticity measurement; (b) the elasticity change with respect to time, point 1 to 5 are marked points indicated in (a).

Figure 2-5a elucidates examples of several regions of cells scanned after removal from incubator in the point and shoot module of AFM. Point and shoot module allows capturing the image first then pick up sites of interest to perform force distance curve measurements. Results showed that cells have various elasticities from different sites. Plotting the Young's moduli over time (Figure 2-5b) revealed fluctuations of elasticity during the first few minutes following removal from incubator. However, after around 20 minutes, the elasticity of HAEC became relatively stable. More cells were studied (data not shown) and we concluded that three different distinct trends can be discerned: 1) increasing and 2) decreasing of elasticity, as well as 3) relatively stable

status; therefore, following AFM experiments were performed after cells became relatively stable conditions.

2.3.3 Elasticity Characterization of a Single Cell

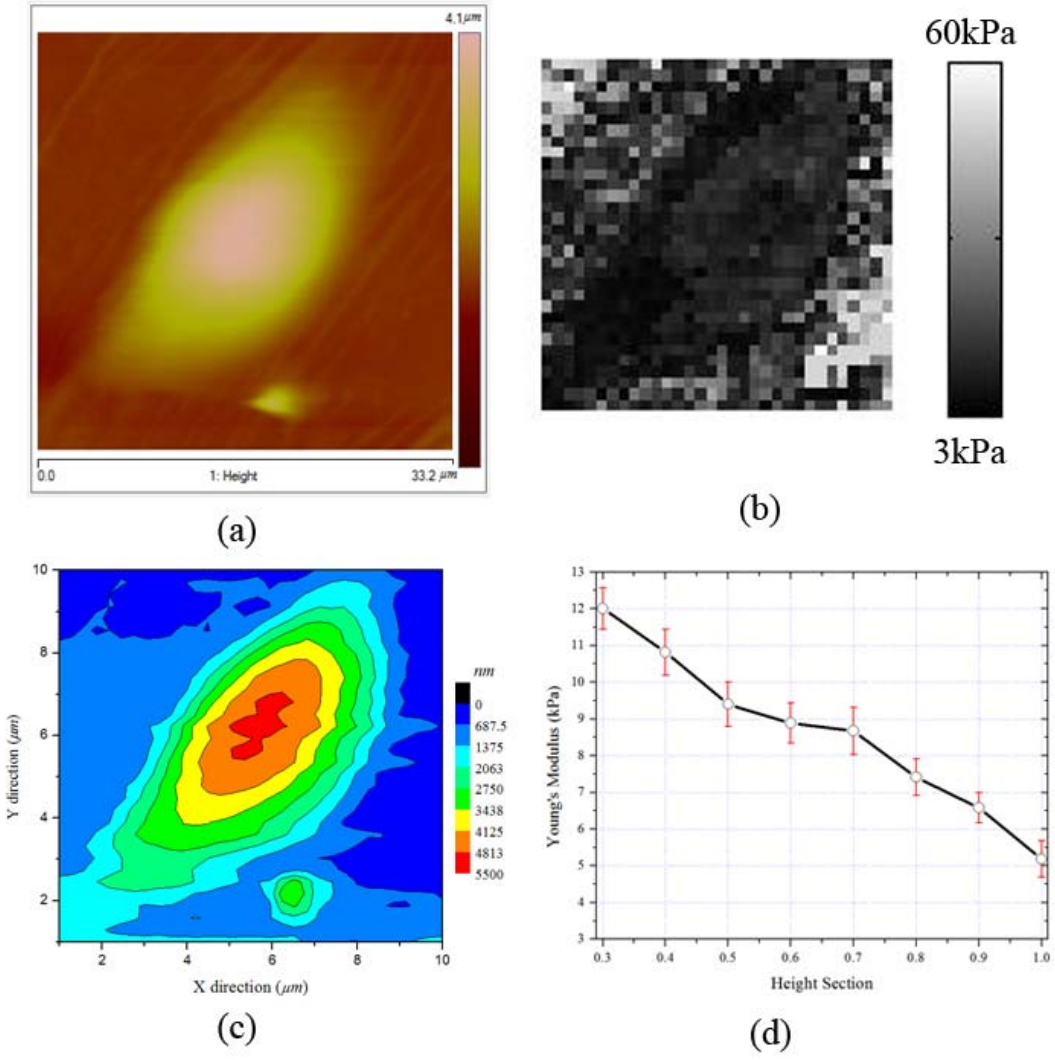

Figure 2-6. Force volume measurement of HAEC. (a) Height image; (b) elasticity map with 32 × 32 pixels; (c) the contour profile of the height image; (d) the average Young's moduli at different height intervals. 0.9 represents the height section [0.8H, 0.9H], and H is the total height of the cell.

Since HAEC in culture and in situ contains heterogeneous domains, heterogeneity and dynamic property of HAEC have increased difficulty of the elasticity measurement and characterization. Thus, to get more comprehensive information about the elasticity of a cell, force volume measurement, measuring a whole cell, is performed. Figure 2-6 shows the results of a force volume measurement of a single HAEC. When comparing Young's moduli over the entire cell in Fig. 3b, we noticed that Young's moduli vary from the nuclear area to the edge area; consequently, any data obtained from local measurement points cannot represent overall elasticity of the cell. Nevertheless, the overall average of stiffness could be used as an alternative way; the effect from substrate is inevitable at the cell edge area due to the small height. Since a cell has various heights, it is necessary to devise a method that characterizes the elasticity of a cell using the distribution of elasticity data and therefore make these results more meaningful. A criterion of defining main cell area is introduced in Figure 2-6c. After normalization, the cell height (H) is seen as 0% from the bottom of the substrate to 100% at the top. The main cell area is defined as from 30%, which can be determined by examining the height information from different cell type, to the top. On average, the elasticity of this cell on polystyrene surface is 9.45 ± 4.90 kPa (SEM).

However, the distribution of cell elasticity is highly inhomogeneous caused by heterogeneous cytoskeleton structure underneath. For further characterization, the elasticity of a cell, the cell was sliced into several different heights shown as a contour image in Figure 2-6c. The contour line comprising the same color represents a height region within the same height section. After averaging the elasticity of these height regions, an array of elasticity for different height section of the cell was obtained, shown in Figure 2-6d. It is noticeable that different height areas have a

distinguishable value compared to other cell areas. To evaluate if elasticity depends on the substrate that cells are exposed to, we cultured HAEC on basement membrane material (Matrigel) and compared measurements with those from cells grown on tissue culture plastic. Figure 2-7 is the measurement of HAECs on matrigel substrate. Under the same criteria of the definition of cell main area mentioned above, the elasticity of this cell on matrigel substrate is 8.88 ± 6.35 kPa. It is common knowledge that elasticity of cells on stiffer substrates would be slightly higher than that on compliant surface [31]; In another sense, substrate affects elasticity of cells as they grow. Our results are consistent with measurements reported by others since the Young's modulus of matrigel is much lower than that of polystyrene.

Figure 2-7b shows comparison of Young's moduli for cells on two different substrates. Although most of the area shows lower elasticity compared to cells on stiffer substrate, the elasticity of cells at the topmost of nuclear area and certain height region is very close. Measurement and comparison of small portion of a cell cannot get valid experiment results; the distribution of Young's moduli should be correlated with a great amount of surface properties of the cell which is highly heterogeneous. Instead of being separated from elasticity to claim Young's moduli in the future, the height ought to be considered as an important "weight" to define elasticity for the benefits of comparison.

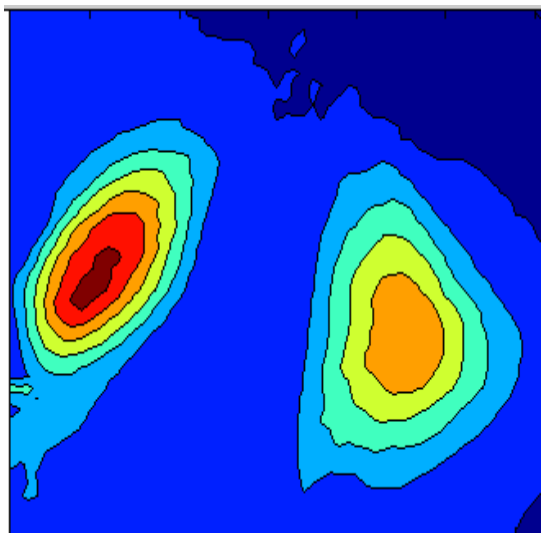

(a)

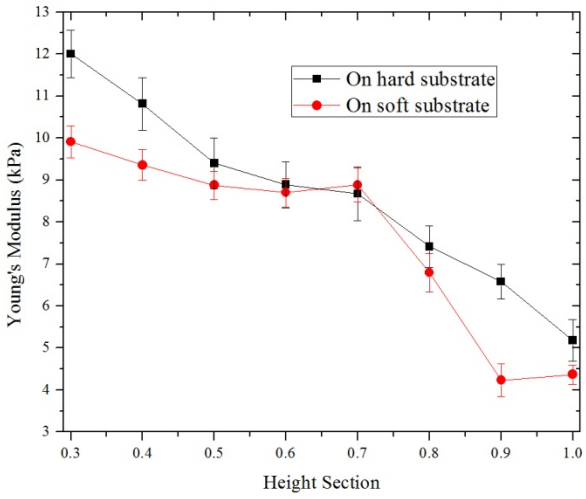

(b)

Figure 2-7. Force volume result from HAECs on matrigel substrate. (a) Cell height image; (b) the elasticity comparison of cells on two different types of substrates, the solid square symbol is for polystyrene and the solid circle symbol is for matrigel. The horizontal axis is for different height region.

2.3.4 Elasticity Distribution and Statistical analysis

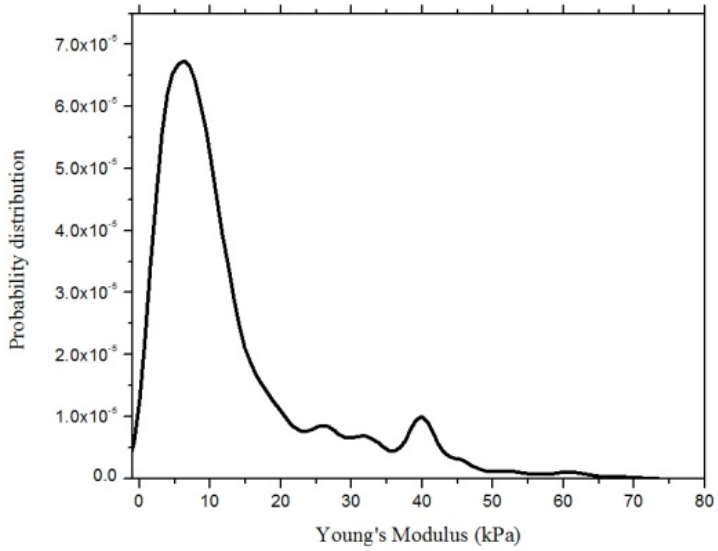

(a)

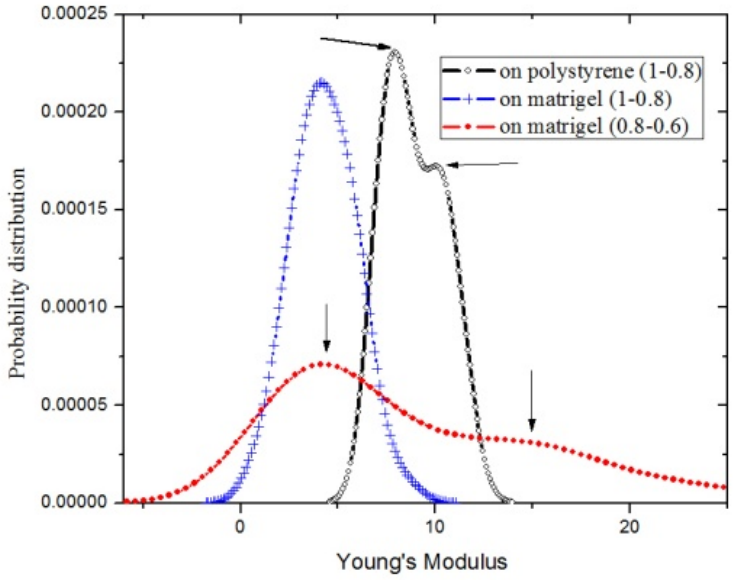

(b)

Figure 2-8. Elasticity distribution of cells from different areas. (a) The distribution of the whole scanning area. (b) The elasticity distribution for different height sections. Black hollow circle curve describes the height section from 0.8H to H on culture dish. Blue plus curve and red solid circle curve stand for the height section [0.8H, H] and [0.6H, 0.8H] of the cells on matrigel. H is the total height of the cell. The arrows indicate the peaks.

Although slicing the cell into several height sections has well improved the examination method of cell elasticity, it is still a homogenization technique ignoring the distribution of elasticity field. Figure 2-8 shows elasticity distribution from different areas of AFM mapping. Obviously the two main peaks highlighted from the multiple peaks in Figure 2-8a represent the elasticity of cell and cell edge largely affected by substrate respectively. In Figure 2-8b, double peaks are again shown in different height sections, such as the height section [0.8H, H] of the cell on culture dish and the height section [0.6H, 0.8H] of the cell on matrigel, while there is no obvious second peak shown at the height section of [0.8H, H] of the cell on matrigel.

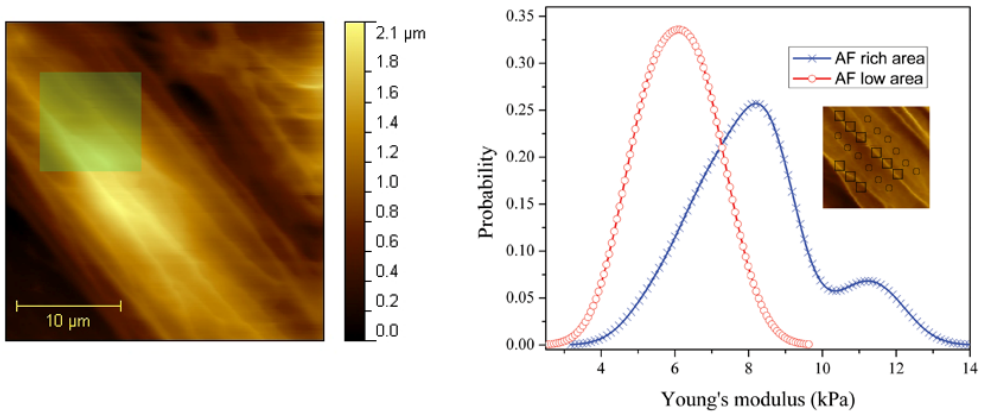

(a) (b)

Figure 2-9. (a) Height image; (b) the elasticity distribution for two different areas, one is AF affluent area, and the other is impoverish AF area. The scan area is from the square mask in (b).

In order to explain double peaks phenomenon. We slightly increased scanning force and the topography image is shown in Figure 2-9a. A small area from Figure 2-9a was chosen for force

distance curve measurement in point and shoot module. As mentioned, contact mode AFM can show more distinct features of underlying structure from deflection image. Therefore, the deflection image was captured (the enclosed image in Figure 2-9b) and used for F-D curve measurement in point and shoot module. Judging from the known morphology and arrangement of cytoskeletal elements within endothelial cells [30], the filamentous structures here are likely F-actin containing stress fibres of the cytoskeleton. Two different regions with apparent differences in AF bundle density with a small area (Figure 2-9a) were compared. One appeared to be AF rich with distinct AF bundles (square symbols in Figure 2-9b), and the other area with fewer of these bundles (circle symbols in Figure 2-9b). Since these regions were in very close proximity to each other (1-2 μm), there should not be big gap between elasticities. However, mean elasticity of AF rich area is obviously higher and the distribution extends to a higher value. The second peak here can be contributed by the elasticity of stress fibers underneath.

This explains that the double peaks of the elasticity distribution in Figure 2-8b for the cells on culture dish substrate and also in certain sections of matrigel substrate. For the cells on matrigel which is a more compliant substrate, there is no sharp second peak shown in the elasticity distribution of the topmost height section. We can predict that there are more stress fibres residing closer to the surface of the cells culturing on the hard substrate and there are more stress fibres at lower height section areas, which has caused higher elasticity because the overall stiffness of a cell is determined by cytoskeleton.

In summary, classical elasticity measurement predicts the overall mechanical properties of cells and ignored the local elasticity field distribution which is not always random in nature. However, statistic distribution often contains valuable information to complement our investigation. The

distinct double peak phenomenon of elasticity distribution reveals the discrepancy of underlying cytoskeleton structure between cells on different substrates.

2.4 Conclusion

Cell is a highly heterogeneous material and it is beneficial for evaluating the overall mechanical property instead of measuring local elasticity of cells. In this paper, AFM is used to study the morphology and the elasticity of HAEC to develop a method of characterizing the elasticity of single cell.

Force volume method with AFM was applied to study elasticity distribution on HAEC. Based on height information of a cell, a new characterization method was proposed to evaluate the elasticity. The cell height should not be separated from the discussion of cell elasticity; instead, it should be taken into consideration as a "weight" factor. This method could be leveraged for other kind of cells by normalizing height of cells. Through correlating the height with the cell elasticity, we could not only achieve a more meaningful characterization of the elasticity of cells, but also eliminate those areas which are not suitable for elasticity representation.

Through investigating the local elasticity distribution of cells, we found that cytoskeleton structure under cell surface has largely contributed to stiffness of cells. The double peak reveals more heterogeneous structure underneath while smoother distribution represents relatively homogeneous structure supporting the plasma membrane. It is concluded that elasticity of cells have a relation with the density of actin cytoskeleton: higher density area will increase the elasticity and vice versa.

To achieve comprehensive and significant cell mechanical properties for practical clinical use, there are still numerous hurdles to overcome. Nevertheless, AFM will continue severing as a powerful tool for future disease detection, diagnosis and treatment of diseases.

2.5 Reference

1. Langton, C.M., et al., Prediction of mechanical properties of the human calcaneus by broadband ultrasonic attenuation. Bone, 1996. **18**(6): p. 495-503.

2. O'Rourke, M., Mechanical principles in arterial disease. Hypertension, 1995. **26**(1): p. 2.

3. Ophir, J., et al., Elastography: ultrasonic estimation and imaging of the elastic properties of tissues. Proceedings of the Institution of Mechanical Engineers, Part H: Journal of Engineering in Medicine, 1999. **213**(3): p. 203-233.

4. Manduca, A., et al., Magnetic resonance elastography: non-invasive mapping of tissue elasticity. Medical Image Analysis, 2001. **5**(4): p. 237.

5. Fishkind, D.J. and Y.L. Wang, New Horizons for Cytokinesis. Current Opinion in Cell Biology, 1995. **7**(1): p. 23-31.

6. Lim, C., E. Zhou, and S. Quek, Mechanical models for living cells—a review. Journal of Biomechanics, 2006. **39**(2): p. 195-216.

7. Dartsch, P., et al., Morphological alterations and cytoskeletal reorganization in opossum kidney (OK) cells during osmotic swelling and volume regulation. Histochemistry and Cell Biology, 1994. **102**(1): p. 69-75.

8. Binnig, G., C.F. Quate, and C. Gerber, Atomic Force Microscope. Physical Review Letters, 1986. **56**(9): p. 930-933.

9. Zahalak, G., W. McConnaughey, and E. Elson, Determination of cellular mechanical properties by cell poking, with an application to leukocytes. Journal of biomechanical engineering, 1990. **112**: p. 283.

10. Hochmuth, R., Micropipette aspiration of living cells. Journal of Biomechanics, 2000. **33**(1): p. 15-22.

11. Bereiter-Hahn, J., et al., Mechanical basis of cell shape: investigations with the scanning acoustic microscope. Biochemistry and cell biology= Biochimie et biologie cellulaire. **73**(7-8): p. 337.

12. Svoboda, K., et al., Conformation and elasticity of the isolated red blood cell membrane skeleton. Biophysical Journal, 1992. **63**(3): p. 784-793.

13. Laurent, V., et al., Assessment of mechanical properties of adherent living cells by bead micromanipulation: comparison of magnetic twisting cytometry vs optical tweezers. Journal of biomechanical engineering, 2002. **124**: p. 408.

14. Morrow, T., et al., Programmed assembly of DNA-coated nanowire devices. Science, 2009. **323**(5912): p. 352.

15. McElfresh, M., et al., Combining constitutive materials modeling with atomic force microscopy to understand the mechanical properties of living cells. Proceedings of the National Academy of Sciences of the United States of America, 2002. **99**: p. 6493-6497.

16. Raychaudhuri, S., et al., Precise Semiconductor Nanowire Placement Through Dielectrophoresis. Nano Lett, 2009. **9**(6): p. 2260-2266.

17. Cross, S.E., et al., Nanomechanical analysis of cells from cancer patients. Nature Nanotechnology, 2007. **2**(12): p. 780-783.

18. Faria, E.C., et al., Measurement of elastic properties of prostate cancer cells using AFM. Analyst, 2008. **133**(11): p. 1498-1500.

19. Stolz, M., et al., Early detection of aging cartilage and osteoarthritis in mice and patient samples using atomic force microscopy. Nature Nanotechnology, 2009. **4**(3): p. 186-192.

20. Chouinard, J.A., et al., Oxidized-LDL induce morphological changes and increase stiffness of endothelial cells. Experimental Cell Research, 2008. **314**(16): p. 3007-3016.

21. Oberleithner, H., et al., Plasma sodium stiffens vascular endothelium and reduces nitric oxide release. Proceedings of the National Academy of Sciences of the United States of America, 2007. **104**(41): p. 16281-16286.

22. Sato, M., et al., Local mechanical properties measured by atomic force microscopy for cultured bovine endothelial cells exposed to shear stress. Journal of Biomechanics, 2000. **33**(1): p. 127-135.

23. Selvam, S., et al., Tissue-engineered tear secretory system: functional lacrimal gland acinar cells cultured on matrix protein-coated substrata. Journal of Biomedical Materials Research Part B: Applied Biomaterials, 2007. **80**(1): p. 192-200.

24. Hutter, J. and J. Bechhoefer, Calibration of atomic force microscope tips. Review of Scientific Instruments, 1993. **64**: p. 1868.

25. Klapetek, P. and D. Necas, Gwyddion. Czech Republic: Czech Metrology Institute, 2007.

26. Hertz, H., Uber die Beruhrung fester elastischer Korper. J. Reine Angew. Math, 1881. **92**: p. 156-71.

27. Matzke, R., K. Jacobson, and M. Radmacher, Direct, high-resolution measurement of furrow stiffening during division of adherent cells. Nature Cell Biology, 2001. **3**(6): p. 607-610.

28. Sneddon, I., The relation between load and penetration in the axisymmetric Boussinesq problem for a punch of arbitrary profile. International Journal of Engineering Science, 1965. **3**(1): p. 47-57.

29. A-Hassan, E., et al., Relative microelastic mapping of living cells by atomic force microscopy. Biophysical Journal, 1998. **74**(3): p. 1564-1578.

30. Hayakawa, K., N. Sato, and T. Obinata, Dynamic reorientation of cultured cells and stress fibers under mechanical stress from periodic stretching. Experimental Cell Research, 2001. **268**(1): p. 104-114.

31. Byfield, F., et al., Endothelial actin and cell stiffness is modulated by substrate stiffness in 2D and 3D. Journal of Biomechanics, 2009.

CHAPTER 3

3 A MECHANICALLY DISTINCT BILAYER MODEL FOR ENDOTHELIAL CELLS

3.1 Introduction

All living cells experience various mechanical forces, from fluid shear stress on endothelial cells to high compression forces on bone cells. The mechanical responses of cells under mechanical stimuli largely determines the subsequent biochemical signalling, which also plays significant role in the development of various diseases, including atherosclerosis [1], cancer [2] and arthritis [3]. Mechanotransduction [4, 5], converting mechanical stimuli into biochemical signals, has been found to play an important role in regulating numerous physiological processes [6]. These findings have prompted research insight mechanical properties, especially mechanical responses under biomechanical stimuli, of living cells.

Of all the different techniques, such as micropipette aspiration [7] and optical tweezers [8], available to study responses of cells under mechanical stimuli, scanning probe (SP)-based force spectroscopy like AFM [9] is suitable for obtaining mechanical behaviour for adherent cells with high spatial resolution [10]. A number of studies have demonstrated the ability of AFM in examining mechanical properties of living cells. In previous chapter, with AFM measurement, the elasticity moduli of cells were well characterized. Instead of conceiving cells as pure elastic materials, AFM has also been used to quantify viscoelastic properties of living cells through

performing stress relaxation measurement [11-13]. Typically, cells are scanned along the cell surface to reveal the heterogeneity and show the lateral distribution of mechanical property. However, cells are also non-homogeneous in normal direction of cell surfaces. During the indentation process, AFM probe will sense various cell components, from plasma membrane to underlying cytoplasm and cytoskeleton, which manifest distinct mechanical responses under stimuli. Cell membrane and cytoskeleton, with distinct architectures and mechanical properties, interact mutually and regulate the integrity along with the functions of cells. Biomechanics serves as complementary perspective to structural and cellular biology. Thus, it is necessary to find a model to indentify the contributions of different cell components on the mechanical performance of cells.

In this study, human aortic endothelial cells (HAECs) were cultured in vitro to investigate the stress relaxation behaviour. From force time curves obtained by AFM, stress relaxation responses of ECs were found to be contributed by two different stress relaxation times. Through investigating the architecture of cells, membrane skeleton and cytoskeleton, a mechanically distinct bilayer structure was proposed to explore mechanical property of ECs, focusing on discussion of the membrane behaviour for the study in next chapter.

3.2 Methods and Experiments

3.2.1 Cell culture

Human aortic endothelial cells (HAEC, Lonza), cultured in a humidified incubator at 37^{o}C with 5% CO_2, were maintained in endothelial growth media, which was supplemented with EGM2 kit (Lonza) and antibiotics (penicillin 100 U/ml and streptomycin 100 μg/ml).

3.2.2 Stress Relaxation Experiments

A commercial AFM (Dimension V, Veeco Inc.) with Nanoscope controller V and a fluid cell was used for the experiments. Triangular shape silicon nitride cantilevers (Nanoscience) with a pyramidal tip and a nominal spring constant of 0.02-0.06 N/m were used. The typical radius of curvature of tips was around 20 nm. The spring constant of cantilevers were calibrated by thermal tune method [14] before each experiment.

AFM experimental setup is the same as that in previous chapter. After ECs has formed a confluent layer (Figure 3-1). The cantilever tip was positioned at the site of interest on the sample by moving the stage using Nanoscope controller software (Nanoscope 7.30, Veeco). Low deflection set point was used to minimize forces exerted on cells and low scan rate such as 0.4 Hz was used to decrease the disturbance during scanning process.

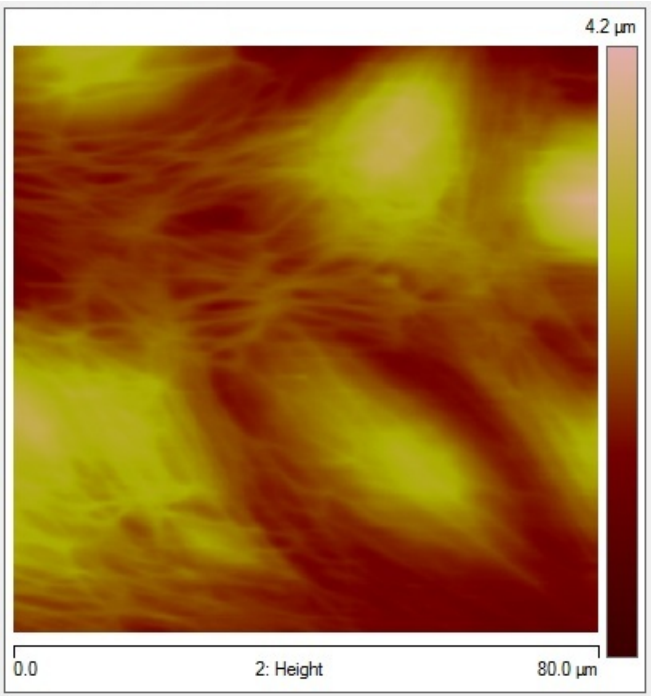

(a)

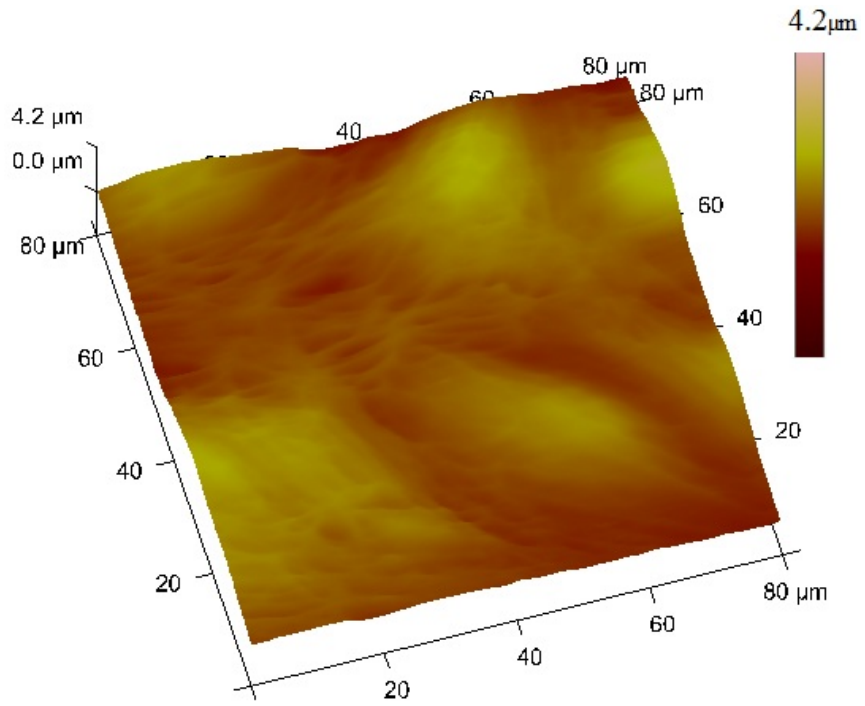

(b)

Figure 3-1. AFM images of HAEC at confluent state using contact mode. (a) 2D topography; (b) 3D height image. All images were analyzed and rendered by Nanoscope 8.10 and Gwyddion 2.24 [15].

In previous chapter, the necessary parameters such as the scan rate and loading speed were adjusted to ensure cells mainly manifest elastic properties. Although elasticity map has revealed a good perspective for mechanical properties of cells, cells are intrinsic viscoleastic materials which needs further to be understood by stress relaxation measurement. Before each stress relaxation measurement, a force distance (F-D) curve was taken to estimate the separation distance between AFM tip and cell surface. Figure 3-2 shows a typical force distance curve for indenting biological samples.

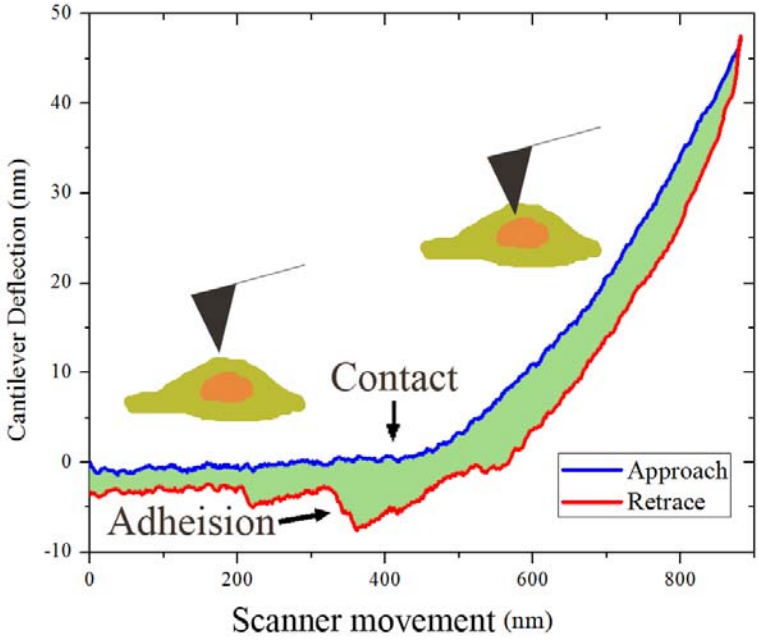

Figure 3-2. A typical indentation curve for AFM indentation on HAEC. F-D curve is obtained by multiplying cantilever deflection with spring constant of the cantilever. Blue curve is the approaching curve, while red curve is the retracing curve. Green area enclosed by approaching and retracing curves is caused by the hysteresis effect of soft materials.

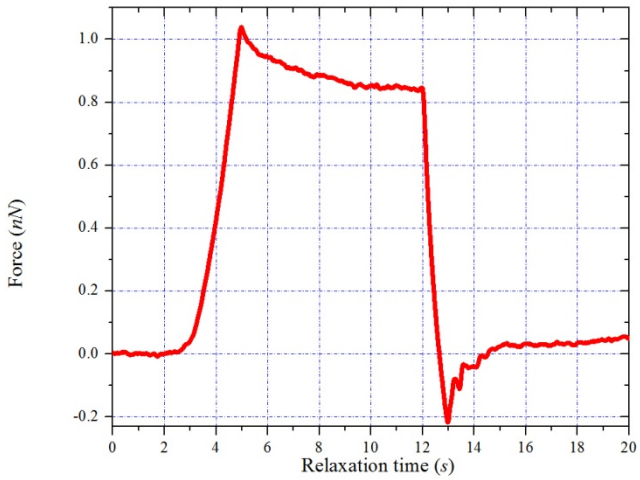

(a)

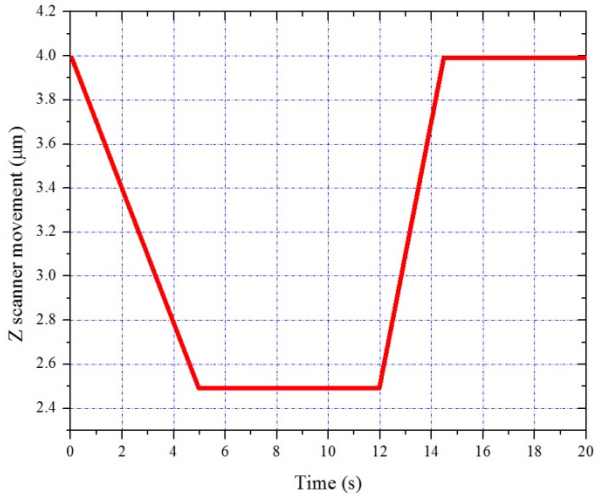

(b)

Figure 3-3. A typical force time curve obtained from PicoForce module of AFM. (a) and (b) are two channels in the strip-chart. (a) is the indentation force with respect to time, which (b) is the z movement.

PicoForce module of AFM was used to obtain the force time (FT) curves. In PicoForce mode,

Channel 1 was set to record cantilever deflection, while channel 2 was set to track the movement

of scanner. Figure 3-3 shows the test results for two channels and channel 1 was converted to force time curve by multiplying spring constant of the cantilever. A script was compiled to control the loading rate and indentation depth for force time curve measurements. Through setting x-offset, y-offset and loop count, a series FT curves can also be achieved in each engagement. A loading speed of less than 1 μm was used to ensure the membrane integrity. The maximum loading was kept under 2 nN. All data were exported as ASCII and analyzed using customized Matlab routine.

3.3 Stress Relaxation Analysis

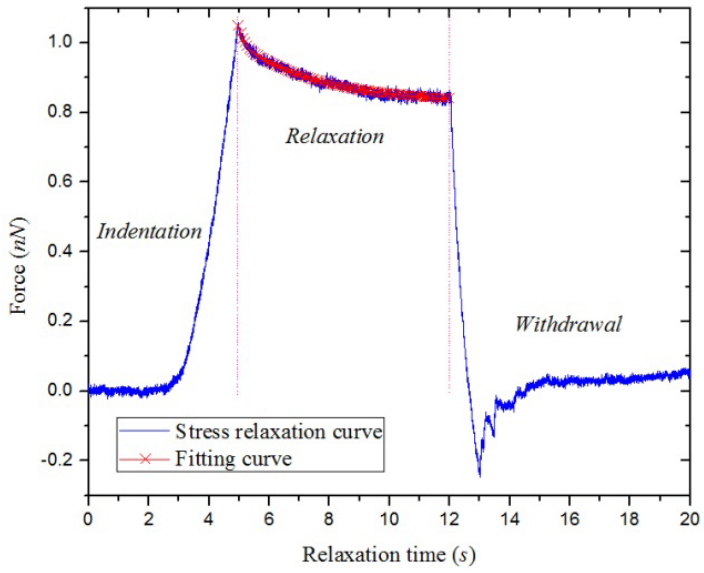

(a)

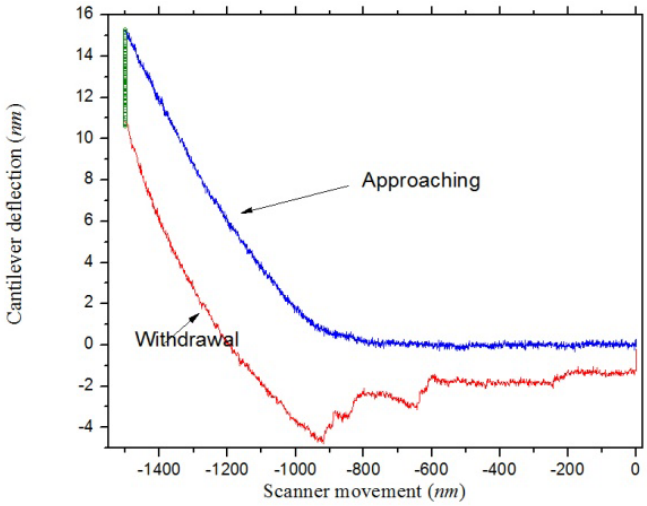

(b)

Figure 3-4. (a) Force time curve at a random site of the cell with stress relaxation part fitted by second order Maxwell model (red cross curve). Force-time curve includes indentation, relaxation and withdrawal process (separated by the red dash line). (b) The force time curve was redrawn as force distance curve to show the different between F-D curves for elasticity measurement. The offset of the two curves is caused by the energy dissipation during the measurement cycle.

Instead of applying high frequency load on cells to measure the viscoelastic response, a quasi-static loading was applied on the cell by AFM probe. Figure 3-4a shows a force time curve including three sections, indentation, stress relaxation and withdrawal. By combining with scanner movement versus time, the force time curve was able to be translated into force distance curve shown in Figure 3-4b. In stress relaxation part, the scanner movement was held constantly and the deflection of cantilever was monitored by photodiode. The change of cantilever deflection was only a few nanometres (around 4 nm shown in the green part curve in Figure 3-4b) during the stress relaxation process; thus the indentation depth change caused by the deflection of cantilever was ignored. Therefore, the indentation depth was regarded as constant during the stress relaxation process.

Generally, exponential force decay was often a method of characterizing the response of relaxation for a linear, isotropic subject like polymer [16]. Considering cells are heterogeneous materials, general Maxwell model containing N parallely arranged Maxwell elements could be give as

$$F = F_0 + \sum_{i=1}^{N} F_i \exp(\frac{-(t_i - t_0)}{\tau_i}) \tag{1}$$

$$\tau_i = \eta_i / E_i \tag{2}$$

When $N = 1$, we will get

$$F = F_0 + F_1 \exp[(-t - t_0)/\tau_1] \tag{3}$$

After fitting the stress relaxation part in Figure 3-4, we will get F_0=834.9 pN, F_1=179.8 pN and τ_1=2.18 s. F_0 and F_1 are the pure elastic load and the viscoelastic load, respectively. τ_1 is the relaxation time. From equation (2) and elasticity of EC, we will get the viscosity with the same magnitude in literature [17]. However, cells are non-homogeneous in both transverse direction and vertical direction. The linear Maxwell model still homogenizes the cell in the vertical direction. To better interpret stress relaxation response of endothelial cell under compression, the natural architecture of cells has to be considered to better characterize the mechanical behaviour.

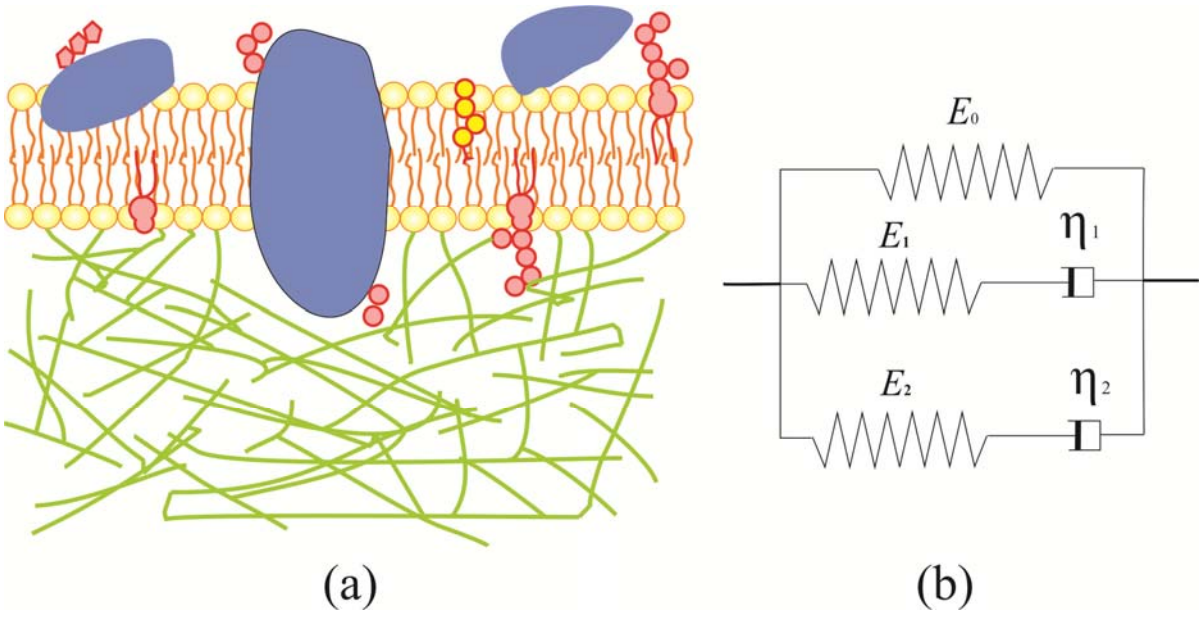

Figure 3-5. (a) Part of the cross section of a cell. The top part of a cell contains two distinctly mechanical domain, phospholipid bilayer and proteins formed as membrane skeleton and the underlying cytoskeleton structure; (b) the second order Maxwell viscoelastic model consists of a spring paralleled with two Maxwell elements.

Figure 3-5a shows a schematic of the cross section of a cell. A recent study has shown that the phospholipid bilayers of the plasma membrane are viscoelastic [18]. The very top part of a cell can be seen as the membrane skeleton connected with the underneath cytoskeleton. Instead of considering cells as a homogeneous material, the cell was seen as a spring paralleled with two

spring-dashes was shown in Figure 3-5. Unlike conventional methods, cell was treated as bilayer mechanical structure by taking account the architecture of the cell. Spring-dash 1 represents the very top part of the cell, while spring-dash 2 represents underlying cytoskeleton structure.

Figure 3-4a shows fitted curve by Maxwell model with a spring and two parallel arranged Maxwell elements. After fitting the stress relaxation part to the initial point (t_0=0), we will be able to get

$$F = F_0 + F_1 \exp(-t/\tau_1) + F_2 \exp(-t/\tau_2) \tag{4}$$

For the case in Figure 3-4a, we have F_0=828 pN, F_1=53 pN, F_2=169.6 pN, τ_1=0.175 s and τ_2 =2.68 s. F_0 is the pure elastic load. F_1 and F_2 are the viscoelastic loads on the cell membrane and underlying cytoskeleton respectively. τ_1 and τ_2 stand for the relaxation time for the two elements. Further measurement confirmed that τ_1 was the shorter response time falls in the range from 0.1 s to 1 s, while τ_2 was several seconds.

Plasma membrane is more fluid like compared to underlying cytoskeleton structure; therefore, it is hypothesized that the short relaxation response time τ_1 corresponds to the membrane part, and τ_2 indicates the response time for cytoplasm and cytoskeleton.

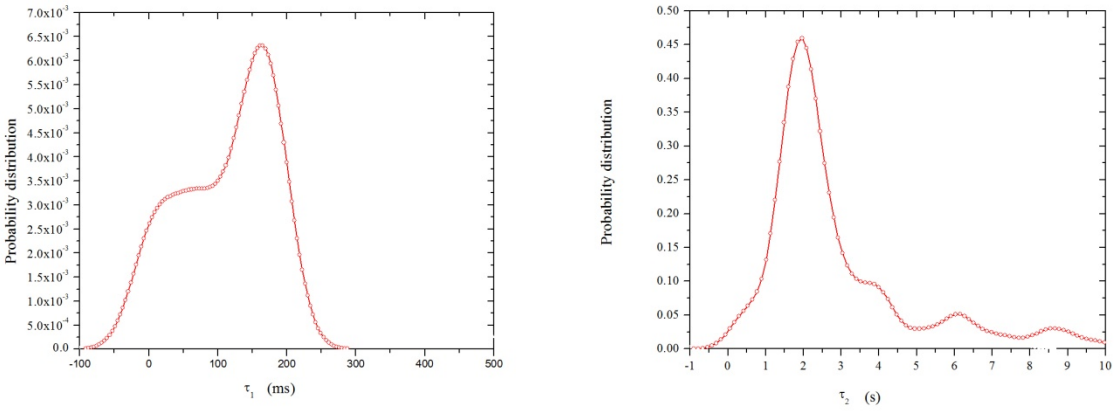

(a) (b)

Figure 3-6. Relaxation times for ECs over a certain area (100 μm^2). (a) Probability distributions of shorter relaxation time τ_1 and (b) longer relaxation time τ_2 for ECs.

Through compiling the scripts in PicoForce mode, a series FT curves were obtained over cell surface. Figure 3-6 shows the distribution of relaxation times τ_1 and τ_2 for a series of measurements for ECs. Figure 3-6a reveals that the relaxation time τ_1 falls in the range of several to 200 ms, while Figure 3-6b demonstrates that the relaxation time τ_2 is above 1 s. The difference of τ_1 and τ_2 was significant ($p < 0.0001$, student t-test).

3.4 Discussion

All living cells face not only an intricate biochemical environment, but also various biomechanical stimuli. The mechanisms of how cells converting biomechanical signal into biochemical signals to regulate cell functions are critical in homeostasis and many diseases. Cell mechanics provides new insight into underlying mechanotransduction process. With AFM, the controlled forces were applied and the responses of endothelial cells were precisely recorded.

Figure 3-5a shows the cross section of the top part of a cell, consisting of plasma membrane made of phospholipid bilayers and a number of proteins, and cytoskeleton contained within cytoplasm acting as scaffold for cells. The stress relaxation analysis has demonstrated two different relaxation times corresponding to the structure of the cell. It is hypothesized that cell consists mechanically distinct double-layer sections for plasma membrane skeleton and underlying cytoskeleton. The short relaxation time is contributed from the plasma membrane while the longer relaxation time is determined by the underlying cytoskeleton.

3.5 Conclusion

Mechanical properties are very important for cellular responses to biophysical and biochemical environment. In this study, we have measured the viscoelastic response of ECs through investigating stress relaxation behaviour under constant compression. It was hypothesized that ECs have bilayer structure in the normal direction with each layer showing distinct mechanical property. A second order Maxwell viscoelastic model was used to analyze the relaxation response. The two Maxwell elements are corresponding to the cell membrane and the underlying cytoskeleton respectively. Two relaxation times were found to correlate with the properties of plasma membrane and underlying cytoskeleton structures.

The native structure and mechanical performance are very important for the functioning of endothelial cells. ECs, lining the inner most layer of blood vessel, act as guards for the blood vessel and the body, while plasma membrane plays as a sensor to detect external signals and transmit into the cell. In the bilayer viscoelastic model, the shorter response time, corresponding to the behaviour of plasma membrane, could be used as an indicator to indentify the responses of plasma membrane under controller forces. In addition, when endothelial cells suffered from an

external mechanical stimuli or interaction with other cells such as monocytes, the shorter response time would be very critical for the membrane to sense the signal and transfer this external stimuli into the internal cells to initiate a signal cascade and take actions.

3.6 References

1. Dai, G., et al., Biomechanical forces in atherosclerosis-resistant vascular regions regulate endothelial redox balance via phosphoinositol 3-kinase/Akt-dependent activation of Nrf2. Circulation Research, 2007. **101**(7): p. 723.

2. Suresh, S., Biomechanics and biophysics of cancer cells. Acta materialia, 2007. **55**(12): p. 3989-4014.

3. Lammi, M.J., Current perspectives on cartilage and chondrocyte mechanobiology. Biorheology, 2004. **41**(3-4): p. 593-596.

4. Chen, K.D., et al., Mechanotransduction in response to shear stress. Journal of Biological Chemistry, 1999. **274**(26): p. 18393.

5. Li, S., N.F. Huang, and S. Hsu, Mechanotransduction in endothelial cell migration. Journal of Cellular Biochemistry, 2005. **96**(6): p. 1110-1126.

6. Ingber, E., Mechanobiology and diseases of mechanotransduction. Annals of medicine, 2003. **35**(8): p. 564-577.

7. Schmidschonbein, G.W., et al., Passive Mechanical-Properties of Human-Leukocytes. Biophysical Journal, 1981. **36**(1): p. 243-256.

8. Henon, S., et al., A new determination of the shear modulus of the human erythrocyte membrane using optical tweezers. Biophysical Journal, 1999. **76**(2): p. 1145-1151.

9. Weisenhorn, A.L., et al., Deformation and height anomaly of soft surfaces studied with an AFM. Nanotechnology, 1993. **4**: p. 106.

10. Huang, H., R.D. Kamm, and R.T. Lee, Cell mechanics and mechanotransduction: pathways, probes, and physiology. American Journal of Physiology-Cell Physiology, 2004. **287**(1): p. C1.

11. Moreno-Flores, S. and R. Benitez, Stress relaxation microscopy: Imaging local stress in cells. Journal of Biomechanics, 2010. **43**(2): p. 349-354.

12. Okajima, T., et al., Stress relaxation of HepG2 cells measured by atomic force microscopy. Nanotechnology, 2007. **18**: p. 084010.

13. Okajima, T., et al., Stress relaxation measurement of fibroblast cells with atomic force microscopy. Japanese Journal of Applied Physics, 2007. **46**(8B): p. 5552-5555.

14. Hutter, J. and J. Bechhoefer, Calibration of atomic force microscope tips. Review of Scientific Instruments, 1993. **64**: p. 1868.

15. Klapetek, P. and D. Necas, Gwyddion. Czech Republic: Czech Metrology Institute, 2007.

16. Riande, E., Polymer viscoelasticity: stress and strain in practice. 2000: CRC.

17. Sato, M., N. Ohshima, and R. Nerem, Viscoelastic properties of cultured porcine aortic endothelial cells exposed to shear stress. Journal of Biomechanics, 1996. **29**(4): p. 461-467.

18. Parthasarathy, R., C.W. Harland, and M.J. Bradley, Phospholipid bilayers are viscoelastic. Proceedings of the National Academy of Sciences of the United States of America, 2010. **107**(45): p. 19146-19150.

CHAPTER 4

4 THE EFFECT OF CHOLESTEROL CONTENT ON MECHANICAL PROPERTIES OF ENDOTHELIAL CELLS

4.1 Introduction

Extensive biochemical and biophysical evidence has been studied to unravel the complex picture of cell membrane structure, composition and deformability during last few decades. Various functionally and morphologically distinct microdomains, residing within or around plasma membrane, are essential for the functioning of molecules and cell membrane. Membrane proteins are not randomly floating as icebergs in a sea of the phospholipid bilayer, which was stated in Singer-Nicholson fluid model [1]. Instead, emerging evidence indicates that there are lipid microenvironments on cell surface, known as lipid rafts, which are tightly packed together with cholesterol [2]. These microdomains composed mainly of cholesterol and glycosphinolipid are critically involved with complex protein-protein interaction between ligands, receptors and kinases, to name a few. To investigate the property of plasma membrane from studying the biomechanical properties of both the cell and plasma membrane, the relation between the membrane composition and mechanical property was examined: stress relaxation responses of cells were observed through manipulating the cholesterol content in plasma membrane.

Cholesterol, as an indispensable component to keep cell membrane functional, is thought to perform as a space between hydrocarbon chains of sphingolipids and to function as dynamic glue keeping the raft assembly together. Lipid rafts containing a given set of proteins can change

composition and structure under different biochemical and biomechanical stimuli. Recent studies have shown that removing cholesterol from lipid rafts will induce changes of biomechanical properties of cells [3, 4]. Meanwhile, cholesterol is also toxic to cell if the concentration is deviated from physiological value. The natural state of plasma membrane is essential for cells to realize physiological functions. The content of cholesterol at cellular levels is kept in tight control by complex cholesterol biosynthesis and cellular uptake as well as efflux of excess cellular cholesterol, disturbance of which leads to a variety of diseases. Increasing evidences indicate that high cholesterol level or hypercholesterolaemia contribute to endothelial dysfunction [5-7] inducing cardiovascular diseases [8] like atherosclerosis. Membrane skeleton sense stimuli from external environment and transfer to internal cytoskeleton, therefore, modification of cholesterol content on the plasma membrane will alter natural biomechanical properties such as elasticity, adhesion and permeability of endothelial cells [9], which can either directly or indirectly influence cell functioning and cause dysfunction of cells to induce diseases.

In this study, two groups of human aortic endothelial cells (HAECs), cholesterol enriched cells and control cells, were studied to investigate the effect of cholesterol content on mechanical properties of ECs. Firstly, the elasticity change was observed using the method in chapter 2. From force-time curves obtained from AFM, stress relaxation responses of cells were analyzed and compared. The change of stress relaxation time has demonstrated the mechanical property of cell membrane was altered by the cholesterol content on cell membrane. It was found that cell membrane become relatively unstable compared to the reference cells without treating with high cholesterol content.

4.2 Methods and Experiments

4.2.1 Cell culture

See section 3.2.1.

4.2.2 Cholesterol Content Treatment

Cellular cholesterol content was enriched by exposing cells to methyl-β-cyclodextrin (MβCD) saturated with cholesterol. The details for preparing MβCD solution saturated with cholesterol can be found in literature [10]. In this study, dry powder of cholesterol balanced by methyl-β-cyclodextrin (Sigma Aldrich) was dissolved into endothelial growth media without serum. The solution is vortexed to bring all the powder from the wall and dissolve thoroughly. Then this 100% saturated cyclodextrin:cholesterol solution was filtered through a 0.2 μm syringe filter to remove the excess cholesterol crystal and to sterilize the solution. The final solution was incubated at 37^{o}C overnight. Immediately before using the solution, it was filter thought a 0.45 μm to remove the excess cholesterol crystals. HAECs (around 40,000 cells/cm^2) were seeded on a glass cover slip coated with gelatin. After cells attached and grew into confluent next day, the media was changed to the new cholesterol solution after washing cells twice with serum free solution (HBSS).

4.2.3 AFM Mechanical Measurements

Cellular indentation and stress relaxation measurements were performed on the two groups of cells, control and cholesterol enriched cells. The AFM setup was the same as described in previous chapters. In brief, AFM probe was first positioned over the sample and an image was

obtained to target the cell. A force distance (F-D) curve was captured to determine the force threshold for force volume measurement. Then force volume measurement was performed to get an elasticity map. For stress relaxation measurement, a quasi-static loading, with an approach speed of 500 nm/s, was applied to estimate the indentation distance through taking an F-D curve. Then the stress relaxation test was performed. All tests were done after cells grew into confluent.

4.3 Results and Discussion

4.3.1 Cholesterol Content Affects Cell Morphology

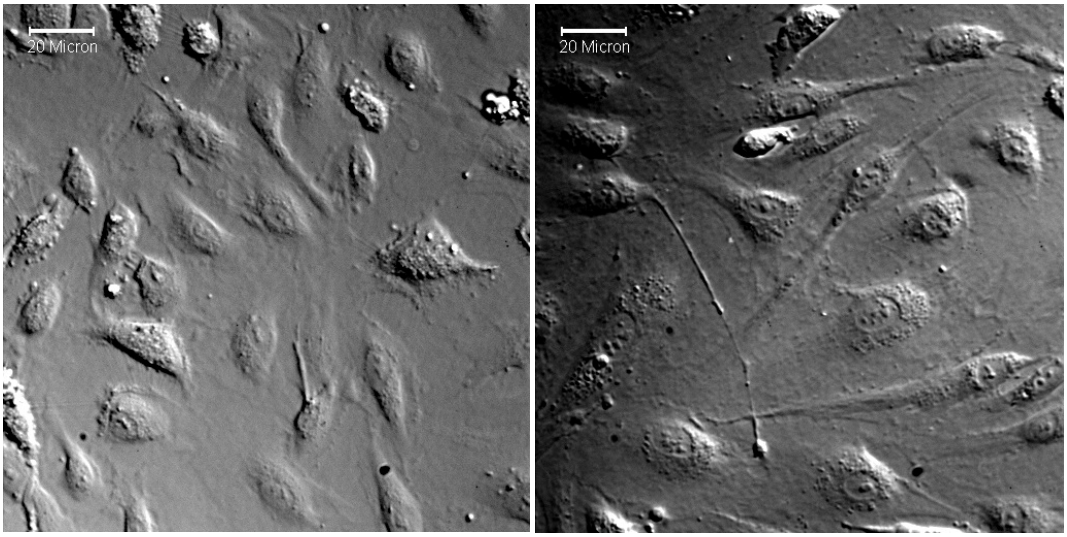

(a) (b)

Figure 4-1. DIC (Differential Interference Contrast) microscopy images of endothelial cells. (a) Control cells; (b) cells after cholesterol enrichment. Cholesterol enriched cells show blebs forming on the cell membrane.

Figure 4-1 shows images taken from DIC microscopy after cholesterol enrichment for a few hours. The membrane of cholesterol enrichment cells (Figure 4-1b) evinced more blebs than the control cells (Figure 4-1a) and larger spreading area; while the cell density doesn't show significant difference between two types of cells over a larger area. Previous works suggested the possibility that cholesterol could be enriched to certain degree in the outer monolayer [11]. In addition, cholesterol serves as glue between phospholipid bilayers. Therefore it is hypothesized that excess cholesterol may have connected the adjacent microdomains together in certain level on plasma membrane to form the blebs, which is to release the membrane lateral stress caused by the extension of cell membrane.

Predictably, excess cholesterol can increase mechanical performance of plasma membrane; therefore, the viscosity of the membrane has increased and extended the stress relaxation time as well.

4.3.2 The stiffness and intercellular interaction forces of endothelial cells

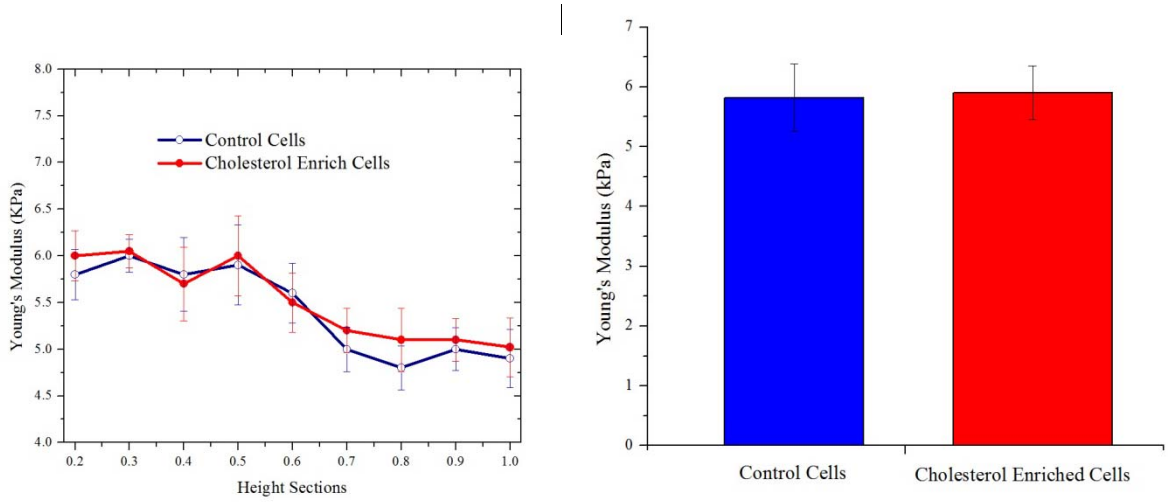

(a) (b)

Figure 4-2. Young's modulus comparison for two groups of cells. (a) The comparison of Young's modulus over the whole height sections for two groups of cells; (b) The average of Young's modulus for two groups of cells at height section of [0.3H, 0.8H]. H is the overall height of the cell. (p=0.42, student's t-test)

From the data obtained in force volume measurement, the stiffness doesn't show significant difference between cholesterol enriched cells and control cells, which were consistent from the results in literature. For force distance measurement, the indentation depth was often several hundred nanometres where the cytoskeleton has dominated the mechanical performance. In another word, the elasticity of the membrane doesn't have a significant effect on the overall elasticity of the cell.

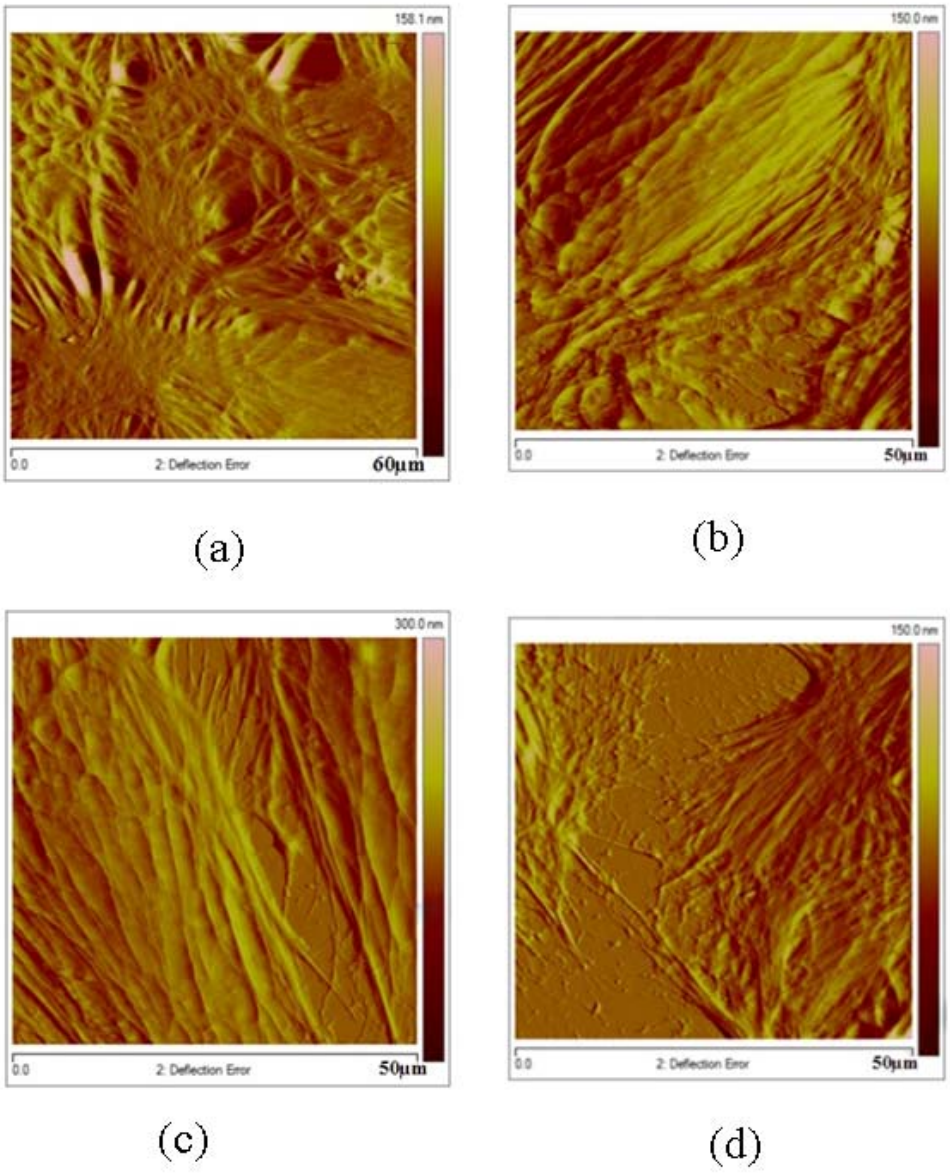

Figure 4-3. AFM deflection images (a-b) of normal cells and (c-d) cells enriched with cholesterol. Cholesterol enriched cells shows large cell separation distance compared to normal cells.

Earlier studies have shown that manipulating cellular cholesterol content will affect membrane-cytoskeleton adhesion [12]. Figure 4-3 shows the deflection images taken from AFM from both cholesterol enriched cells and control cells. From the deflection images of AFM, the underlying cytosketon structure of the stress fibres will be clearer than that from topography image. Figure

4-3a and b show that the cytoskeletons criss-cross to form a dense network in control cells, while the cholesterol enrichment cells are partially interacted with each other. Figure 4-3d shows that cells were almost separated in certain sites. Although Figure 4-3c shows that cells were connected together but the overlap level of cytoskeleton is much lower than control cells. For AFM experiments in this study, the scanning was done at room temperature and in PBS buffer solution balanced with HEPES solution to maintain the PH. Although cells were kept alive and intact during the scanning, cells still suffered from contraction due to the temperature change at the first few minutes, which is not easy to be detected from optical microscopy. Both samples were seeded with the same cell density and the time of enrichment for cholesterol was kept to shorter (around three hours) and changed back to normal medium for further growing. No obvious detachment of cells was observed. If the intercellular interaction force is weak, cells will show separation status during scanning. The limitation here is that the protocol for enrichment of cholesterol is not the same as in vivo physiologically high cholesterol condition. In addition, the enrichment happened in a relatively shorter time. Both these limitations may have enlarged the effect of the cell performance. The phenomena did show that the intercellular interaction forces were affected by cholesterol content.

Endothelium is a barrier between blood and tissue. The integrity of the barrier is the best strategy to control a right permittivity for proteins or cells. The excess of cholesterol level or hypercholesterolemia may cause abnormal functioning of endothelium which leads to a lot of diseases such as coronary artery disease or atherosclerosis.

4.3.3 Cholesterol affects the property of cell membrane

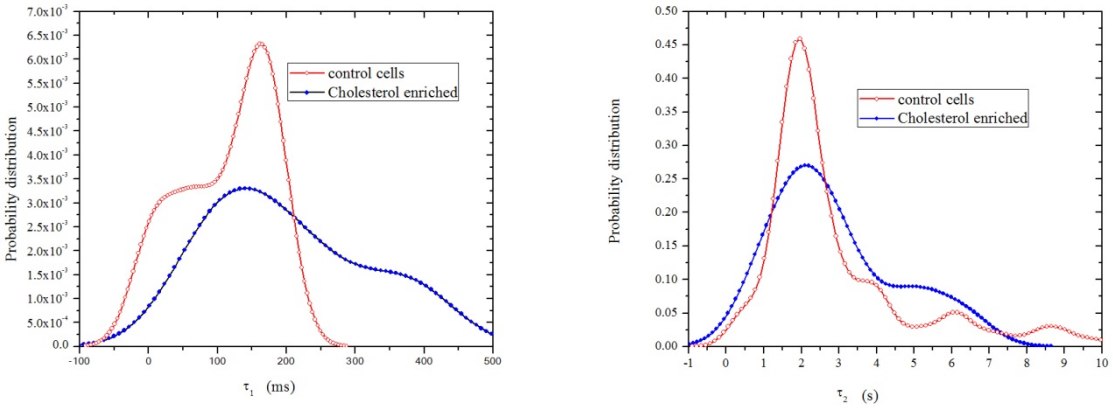

(a) (b)

Figure 4-4. Relaxation time for control cell and cholesterol enriched cells. (a) distribution of shorter relaxation time (τ_1) for control cell and cholesterol enriched cells. The shorter relaxation time for control cells is 168.7 ms, while for cholesterol enriched cells is 210.3 ms; (b) distribution of longer relaxation time (τ_2) for control cell and cholesterol enriched cells;

Figure 4-4 shows relaxation time τ_1 and τ_2 for a group of measurements for cholesterol enriched cells and control cells. Figure 4-4a reveals that the relaxation time τ_1 for cholesterol enriched cells became larger than that of control cells, while Figure 4-4b demonstrates that enriched cells and control cells do not manifest different τ_2. The difference of τ_1 was significant ($p < 0.001$, student t-test).

As mentioned, membrane cholesterol serves as glue on cell membrane, an important factor in determining the physiological properties of lipid bilayers and plasma membrane, and was believed to regulate elasticity and fluidity of plasma membrane. Thus, with excess content of cholesterol on membrane, the mechanical property of the membrane has been changed. From Figure 4-4a, cholesterol has modified the membrane into more ordered state with lower fluidity,

which increases rigidity to prolong the stress relaxation time. In addition, for the control cells shown in Figure 4-4a, the higher value may correspond to higher cholesterol site, since cholesterol is not uniformly distributed but in preferentially confined to lipid rafts which are microdomains distributed on plasma membrane. These results have further confirmed that membrane and cytoplasm can be seen as separate mechanical elements when analyzing the viscoelastic property of a cell.

In the above analysis, it was hypothesized that a cell consists mechanically distinct bilayer section, focusing on investigating mechanical response of membrane from cholesterol enriched cells. However, the membrane is not structurally separated from underlying cytoplasm and cytoskeleton. Instead of applying low forces (less than 2 nN), an increase of applying force (3-8 nN) on the cell was done to obtain the force time curves. The relaxation time is 235.5 ± 26.2 ms for the shorter relaxation time which corresponds to the property on the membrane side. This result further confirms that the two relaxation times are corresponded to the different structures of the cells.

4.3.4 Lipid raft assumption

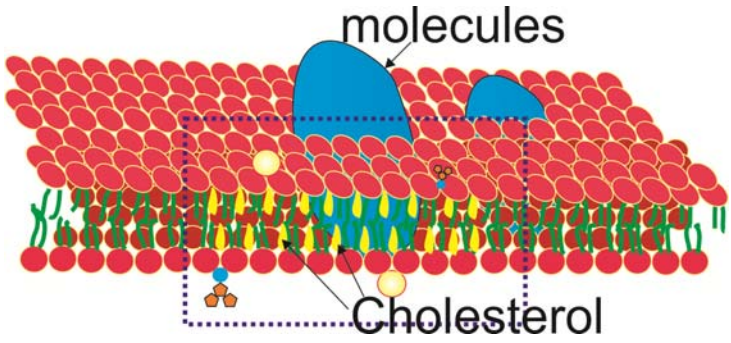

Figure 4-5. A schematic image of the cross section from part of cell membrane. The dash frame is a lipid raft with higher cholesterol content tightly packing together the lipid layer.

After the homogeneous fluid lipid bilayer model of plasma membrane has been modified, the concept of lipid raft has been widely accepted. Lipid rafts are dynamic assemblies of proteins and lipids that dispersed freely within the surrounding liquid-disordered bilayer of cellular membrane; they can also cluster to form larger ordered platforms. Figure 4-5 shows part of the plasma membrane which includes a lipid raft. As mentioned, the cholesterol functions as glue in the lipid layer organization which forms a more packed microdomain terms as lipid raft, therefore, those lipid microdomains have higher concentration of cholesterol and glycosphinolipid.

Figure 4-4a shows the distribution of the membrane relaxation time τ_1 for a larger number of measurements. From the figure we can find that there is a second peak of the relaxation time. Lipid raft is believed to be an ordered microdomain which shows lower fluidity than the surrounding environment. From the results here we could estimate that the fluidity decrease for the cholesterol enriched cells should be caused by the higher content of cholesterol forming more ordered domain on the plasmas membrane. With the excess cholesterol residing on the plasma

membrane, the fluidity of the whole membrane has decreased for the cholesterol enriched cells, although most of the cholesterol will be extracted by the cell metabolism process in the following culture.

Membrane cholesterol is an important factor in determine the physiological properties of the lipid bilayers and plasma membrane. Especially the cholesterol which is lipid raft associated has been emerging as one of the pivotal players in modulating the cellular signalling cascades.

4.4 Conclusion

Cellular homeostasis of cholesterol involves the regulation of its total cellular level and its distribution between membranes and within a given membrane. Cholesterol serves as an indispensable constituent of plasma membranes. The balance of cholesterol affects properties and functions of membrane proteins such as receptors, enzymes, or ion channels.

In this study, we have measured the mechanical properties including elasticity and viscoelasticity for two groups of cells, which are cholesterol enriched cells and control cells without special treatment. We hypothesized endothelial cell has bilayer structure in the vertical direction which shows distinct mechanical property. A second order Maxwell viscoelastic model was used to interpret the relaxation response. The results showed that the two Maxwell elements correspond to the cell membrane and the underlying cytoskeleton respectively. In addition, we used cholesterol to manipulate the structure of the cell membrane; the mechanical property change of the membrane for cholesterol enriched cell has further confirmed that the architecture of cell plays the main role for the two different relaxation response times. The morphology showed a little variance for these two types of cells and the intercellular interaction force was affected by

the different cholesterol content, however, the elasticity of two groups of cells did not show significantly difference.

In summary, cholesterol acting as biochemical stimuli on ECs has changed the mechanical performance of the plasma membrane, and altered the morphology and adhesion properties of ECs. Cholesterol was thought to be an indispensable and meanwhile toxic component for the cells. By intentionally changing the content of cholesterol in the plasma membrane, a series mechanical properties of ECs were investigated, the results shows that cholesterol has brought the membrane into chaos state which is different from their native state.

4.5 References

1. Singer, S. and G. Nicolson, The fluid mosaic model of the structure of cell membranes. Science, 1972. 175(23): p. 720-731.

2. Quinn, P.J., A lipid matrix model of membrane raft structure. Progress in Lipid Research, 2010. 49(4): p. 390-406.

3. Byfield, F., et al., OxLDL increases endothelial stiffness, force generation, and network formation. Journal of Lipid Research, 2006. 47(4): p. 715.

4. Birukov, K.G., Loose cholesterol, get stiff! Focus on "oxLDL-induced decrease in lipid order of membrane domains is inversely correlated with endothelial stiffness and network formation". American Journal of Physiology-Cell Physiology, 2010. 299(2): p. C211-C212.

5. Steinberg, H., et al., Endothelial dysfunction is associated with cholesterol levels in the high normal range in humans. Circulation, 1997. 96(10): p. 3287.

6. Shi, Q., et al., Endothelial senescence after high-cholesterol, high-fat diet challenge in baboons. American Journal of Physiology- Heart and Circulatory Physiology, 2007. 292(6): p. H2913.

7. Drolet, M.-C., et al., Early endothelial dysfunction in cholesterol-fed rabbits: a non-invasive in vivo ultrasound study. Cardiovascular Ultrasound, 2004. 2(1): p. 10.

8. Kratz, M., Dietary cholesterol, atherosclerosis and coronary heart disease. Atherosclerosis: Diet and Drugs, 2005: p. 195-213.

9. Norman, L.L., et al., Modification of Cellular Cholesterol Content Affects Traction Force, Adhesion and Cell Spreading. Cellular and Molecular Bioengineering, 2010. 3(2): p. 151-162.

10. Christian, A.E., et al., Use of cyclodextrins for manipulating cellular cholesterol content. Journal of Lipid Research, 1997. 38(11): p. 2264-2272.

11. McMullen, T., R. Lewis, and R. McElhaney, Cholesterol-phospholipid interactions, the liquid-ordered phase and lipid rafts in model and biological membranes. Current Opinion in Colloid & Interface Science, 2004. 8(6): p. 459-468.

12. Sun, M., et al., The effect of cellular cholesterol on membranecytoskeleton adhesion. Journal of Cell Science, 2007. 120(13): p. 2223-2231.

CHAPTER 5

5 A RAPID PROTOTYPE OF MICROFLUIDIC CELL CULTURE SYSTEM

5.1 Introduction

Blood vessels, which are connecting all organs in the body, maintain homeostasis of the circulatory system. Blood vessels in the body are responsible for many diseases especially cardiovascular diseases. Endothelial cells (ECs), which line at the innermost layer of blood vessel, experience shear stress, hydrostatic pressure, and cyclic strain imposed by the stretch and contraction from the surrounding smooth muscle cells [1]. Meanwhile, ECs response to these hemodynamic forces by changing morphology [2, 3], function and gene expression [4, 5]. For example, cyclic strain can up-regulate nitric oxide synthase [6]; hydrostatic pressure will induce morphology and proliferation response of ECs [7]. Overall, vascular functions are controlled by a variety of biomechanical and biochemical factors, such as hormones, cytokines and neurotransmitters, which has complicated in vivo studies.

Among all physical forces, shear force is recognized as the most important modulator in a number of physiological and pathological phenomena, such as vascular remodelling [8], angiogenesis [9] and atherosclerosis [10]. Cells sense mechanical stimuli from external environment and convert into biochemical signals to regulate cell responses. Various macro- and micro-scale perfusion cell culture systems were developed to investigate responses of endothelial cells and to clarify underlying mechanisms of shear stress mechanotransduction [11]. For

macroscale system, flow chamber is one of the most popular techniques employed as in vitro model to study responses of endothelial cells under flow condition. Recently, micro/nanoscale techniques are emerging as powerful tools in tissue engineering and biology [12]. Microfluidics, surface patterning and micro-patterning provide new capabilities for continuously unveiling cellular and molecular mechanisms underlying physiological phenomena, which are often hindered by the resolution at macroscale. Among these, microfluidic cell culture platforms have been growing rapidly in biological assays such as drug toxicity or metabolism studies [13, 14]. Micro/nanoscale techniques for cell biology range from single-cell analyses [15] to treating fields of cells in gradient generating devices [16], and from patterned three-dimensional culture [17] to miniaturized traditional cell culture assays [18]. Compared to traditional macroscale cell culture systems, such as petri-dish, microtiter plates and flow chamber, microfluidic channels provide a great amount of attractive advantages such as more precisely controlling of the microenvironment.

The plethora of microscale systems developed to date have demonstrated potential impacts of micro/nano technology in cell biology, and showcased numerous advantages at microscale that are simply not available at macroscale. However, most of microscale devices are designed and fabricated by engineers while it still lacks wide integration to biosystems as routine research tools in biological laboratories. The connection between engineers and biologists is hindered by the complexity of fabrication processes. This disconnection has induced that biologists do not have enough resources to design and validate data obtained from microdevices. Although micro/nano technologies have become more and more popular in cell biology field, new data have to be proved valid by comparing with traditional accepted results.

To pursue a more feasible and reliable fabrication method for rapid research use, a practical method was developed for making channels in poly(dimethylsiloxane) (PDMS), which could carry out a complete cycle of design, fabrication and testing of the prototype rapidly. The fabrication method will be useful for prototyping vascular mimetic microfluidic cell culture system through growing endothelial cells inside the channel. In addition, the flow channel system possesses multiple advantages including low cost, time effective and highly integrated. Compared to traditional photolithography method, this method does not require a mask and clean room environment for fabrication, which significantly facilitates fabrication processes in a routine lab.

5.2 Design and Fabrication of Microfluidic Cell Culture System

5.2.1 Materials

Building microfluidic cell culture system (MCCS) involves a series of factors, among which, selection of materials is the first important step to consider. Materials for building MCCS can be divided into two parts: microfluidic channels and substrates. Except two necessary prerequisites, biocompatibility and sterility, the materials were most restricted to be optically transparent because such devices were most used for light microscope observation. In addition, the materials of microfluidic channels have to be compatible with the following fabrication processes. Further restrictions may also be considered depending on some specific applications.

Microfluidic channels function as conduits to guide the solution to cells. In this study, PDMS (Polydimethylsiloxane, Sylgard 184 silicone elastomer kit, Dow Corning Corporation), one of the most used biomaterials in microfluidic perfusion culture system, was used to fabricate the

channel. It has many desirable qualities not only as cell culture materials but also as softlithography material. It is a non-toxic, autoclavable, transparent and gas permeable material.

The choice of substrate materials is more essential than the materials for channels. The ability of cell attachment is a primary requirement. Conventional tissue-culture polystyrene substrate and PDMS membrane were used in this study.

5.2.2 Device Fabrication

Designing a microfluidic culture system involves three main steps, fabrication of the mold, replication and assembly of the device. Among the three steps, mold fabrication is the most complex and time consuming process. Both photolithography and rapid prototype methods were described to showcase advantages of the later method.

5.2.2.1 Fabrication of Mold

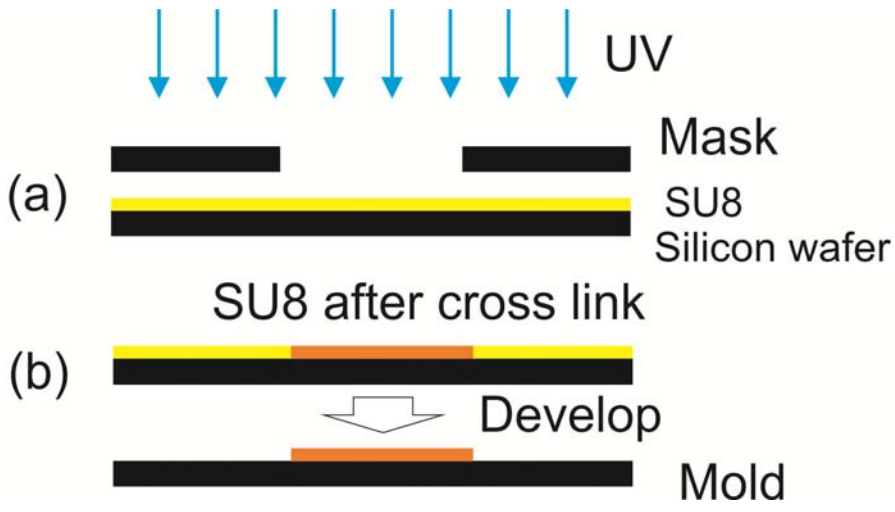

Figure 5-1. The schematic shows the mold fabrication process. (a) The silicon wafer coated with photoresist (SU8) was exposed by UV through a mask. (b) After cross-linked, the non-crosslinked photoresist was removed SU8 developed, then the mold was finished.

Figure 5-1 shows the schematic of photolithography process to fabricate the mold. Firstly, a photomask was designed with desired layout using AutoCAD software and printed on transparent sheets with high-resolution (up to 2000 DPI) image-setting system (CAD/ART Services, Bandon, Oregon). The printing system can generate a minimum feature size as small as 12.5 μm. The detailed photolithography process could be found in literature [19]. The brief processes were described here. First, the photoresist (SU8-2050) was spun across the wafer at a speed of 500 rpm for 8 sec, and then slowly increased the speed from 500 rpm to 1500 rpm for 45sec. After pre-bake process, the wafer was exposed through a mask to 10 mW/cm^2 UV light (wavelength = 365 nm) for 16 sec. Then the wafer was baked (post-bake) and then developed in SU8 developer. Finally, the wafer was baked (hard-bake) and the mold or master was achieved with designed pattern. An optional step is to coat the master with a layer of HMDS to facilitate later peeling-off of PDMS.

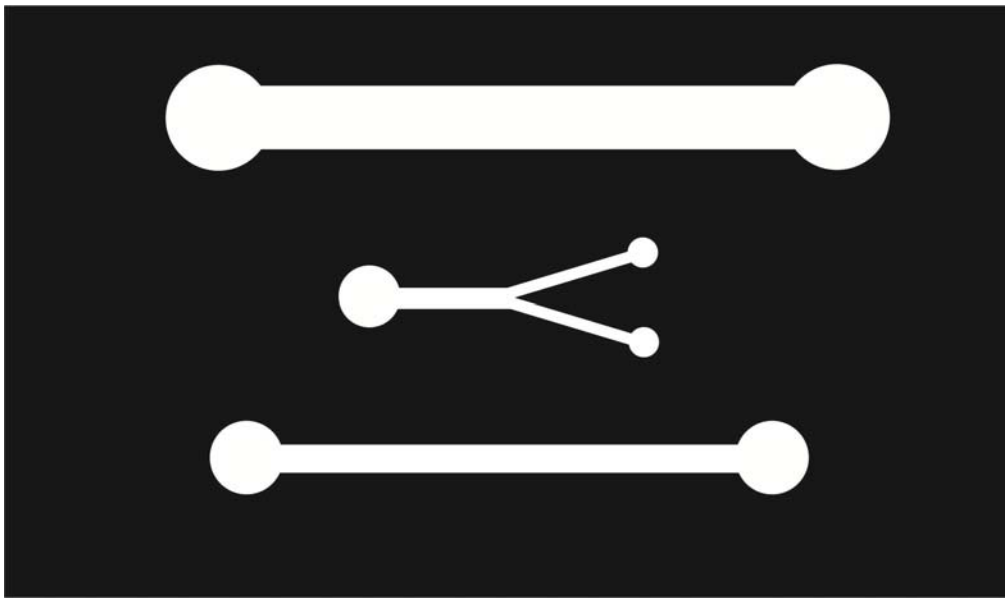

Figure 5-2. The designed photomask for a device. The while part is the pattern for the final channel. Photomask will be printed with high-resolution (up to 2000 DPI) image-setting system (CAD/ART Services, Bandon, Oregon)

The objective of this study is to simplify the standard fabrication processes for more practical use in a routine biological lab. Without compromising high resolution in devices fabricated by photolithography, it can be proved that simplified processes can also achieve adequate resolution for most of applications. Instead of printing out photomask as shown in Figure 5-2, the same desired pattern was drawn in the equipment software and a vinyl sheet was cut by the cutting plotter (Craft ROBO Pro, Graphtec). Within minutes, the pattern could be printed out. The adhesive coated backside of the pattern was stick to a petri-dish or silicon wafer to achieve the final mold.

5.2.2.2 Replication of the Mold

Softlithography represents a non-photolithographic based mostly on replica molding for carrying out micro-fabrication. PDMS is cured by crosslinking reaction to give an optically transparent polymer with the ability of reproducing surface feature. It is commonly used as a stamp resin in the procedure of soft lithography, one of the most common materials to make microfluidic chips.

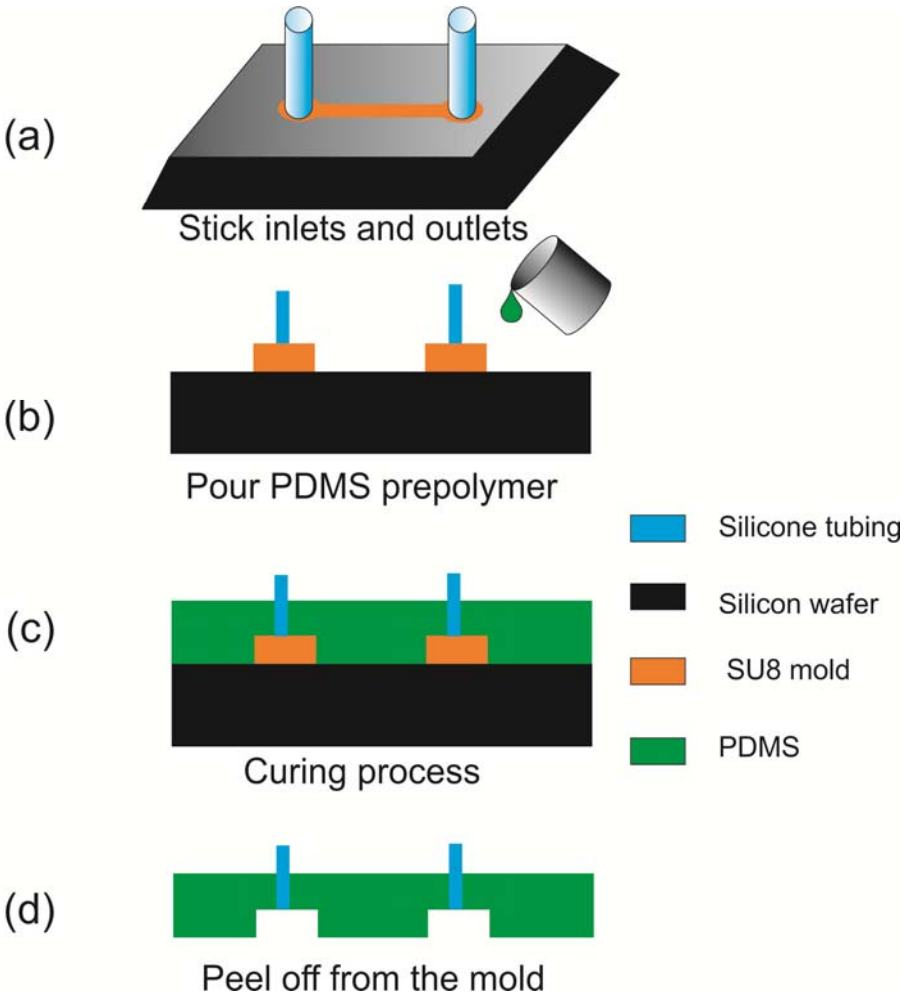

Figure 5-3. Schematic process of the soft-lithography process. (a) Inlets and outlets part of the mold were stick with silicone tubing; (b) PDMS solution was pouring on the mold; (c) the mold and PDMS solution was cured; (d) after cured, PDMS layer was peeled off from the mold.

The replication processes are illustrated in Figure 5-3. After sticking the silicone tubings to the inlets and outlets, PDMS kit by mixing the base and the curing agent in 10:1 was slowly poured on the mold, paying attention not to disturb the silicone tubings. The mold was placed in the vacuum chamber for degassing and then cured. After that, the chip was peeled off and the adhesive at the inlets and outlets was removed to get the channel side of the device shown in Figure 5-3d.

The experiment protocol is listed below:

1. Cut several silicone tubings with 1 cm length and stick to inlets and outlets of the mold. Place the mold into a petri-dish (Fisher brand, 100×15mm) and make sure no tubings are too high for the cover.

2. Weigh out 50 g PDMS base and 5 g curing agent. Use a clean spoon to mix the base and curing agent by both swirling and folding the mixture for about 5-10 minutes to ensure that the curing agent is evenly distributed in the base.

3. Degass the mixture by placing the beaker in a vacuum desiccator and evacuating the chamber. Bubbles will appear, rise to the surface of the mixture, and pop. Vent the chamber and evacuate it again. Repeat this 2-3 times for 30 min. Degassing is complete when there are no longer bubbles visible in the mixture.

4. Pour ~30 g of mixed, degassed PDMS onto each mold placed in the petri-dish. Thickness of PDMS replica made in experiment is ~0.4 cm, taken the experimental errors into account. Using a pair of 200 μL pipet tips, push on the edges of the master mold to force out any air bubble that may be trapped underneath, and make sure it does not float up from the bottom. Let them stay for another 20 min for further degassing. Make sure that PDMS pattern is thicker than 4 mm, or it will be deformed easily and not convenient to manipulate later.

5. Pour ~1.4 g of PDMS solution in another petri-dish to form a PDMS membrane. The thickness is around 100 μm.

6. Once all bubbles have been removed, place the petri-dish with mold on a hotplate at 70ºC for 1.5 hours to cure the PDMS uniformly. The hotplate surface needs to be level. If heated time is not sufficient, the replica will not polymerize thoroughly, and will be sticky. It will be rigid and brittle if over-heated. At the last 5 minutes of heating, place the other petri-dish on another hotplate at 80ºC.

7. Peel the cured PDMS casting (channel side) off the mold when it is still warm, remove the adhesive at inlets and outlets, and then place it on a clean petri-dish. Cut out the desired structure;

8. If the glass substrate is needed, clean the glass slide with Nanostrip at 120ºC and then with DI water beforehand;

9-1. For PDMS substrate, place the channel side PDMS on the other petri-dish with membrane. After heating them for another 1 hour at 80ºC, cast the device along the edge of channel side, and peel off the whole device while it is warm.

9-2. For glass substrate, bring the PDMS casting and the clean glass slide into contact, allowing intimate contact to occur spontaneously without external assistance. Put bonded device on hot plate at 80°C for at least 2 hours. Then allow the bond to anneal for at least 15-20 min at room temperature before using the devices. For stronger bond, it is recommended that the devices anneal overnight (8-10 hrs), or heat the device at 150°C for 1h.

To achieve better bonding performance, the PDMS device and the substrate can be treated by oxygen plasma oxidation. The oxidation of PDMS is believed to result in a surface that comprises SiOH groups. The contact angle of water on oxidized PDMS is less than 15° [3]. The

recipe for O_2 plasma cleaning with STS Reactive Ion Etch in Nanofab is: Chamber Pressure: 50mTorr; O_2 flow rate: 40±5% sccm; Power: 30 W; Reacting time: 30 min.

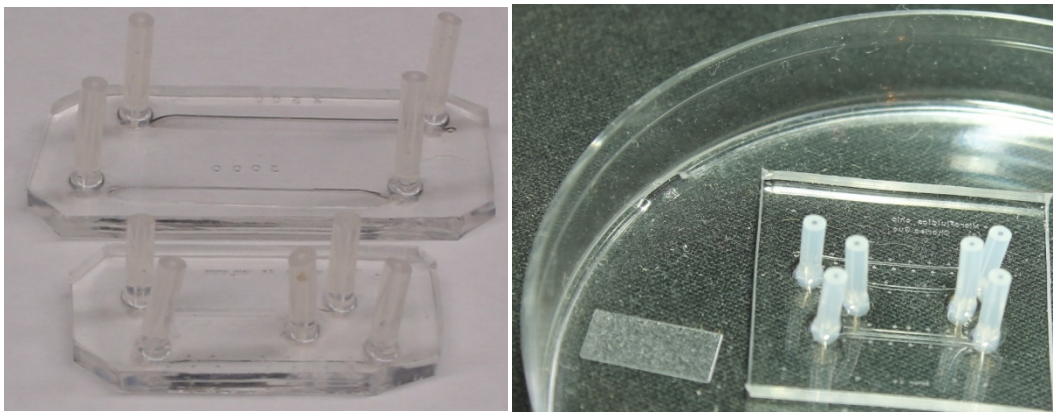

(a) (b)

Figure 5-4. The finished devices with different sizes and on different substrates. (a) Chips with PDMS membrane as substrate; (b) chips with cell culture dish (polystyrene) as substrate.

Figure 5-4 shows the fabricated devices on different substrates, glass substrate and PDMS membrane.

5.2.2.3 Device Assembly

In the assembly process, the chip-to-world interface connecting the chip to peripheral equipments is one of the most critical steps. Instead of punching the PDMS with blunt syringe needle, which needs skilled operation as well, the chip-to-world interface was done by embedding short silicone tubings at inlets and outlets in advance during the replication processes shown in Figure 5-3a. Traditionally, the inlets and outlets were punched after the PDMS was cured and peeled off, and then the metallic tubings with diameter larger than the holes were inserted to function as inlets and outlets for further connection. Obviously, the thermal expansion coefficient between metallic and PDMS are different, the device will suffer from potential

leakage issue after the autoclave process. In addition, the intricate processes will possiblely introduce contamination into the devices. Since the silicone is similar in composition with PDMS, the inlets and outlets were permanently bonded with PDMS, which eliminates any potential leakage and simplifies further operations.

The creation of robust sealed flow channels between the channels and the substrates is crucial requirement for microfluidic culture system. However, there is trade-off here because we need to peel off the device to perform further study of the culturing cell. In this study, the polystyrene culture dish substrate and PDMS substrate were used to create a reversible bonding between PDMS and the substrate.

All the peripheral connections were assembled by silicone tubing and Teflon tubing.

5.2.2.4 Sterilization Techniques

In cell culture, sterile environment is essential for conducting successful experiments. Thus, an effective sterilization technique is very critical to maintain a sterile environment for long period of culture time. Various techniques were employed for sterilizing perfusion culture systems, including autoclaving, flushing the devices with 70% ethanol and exposing the devices to UV light or oxygen plasma, among which, autoclaving is the most simplest and effective method, which was popularly used by biologists.

However, autoclaving is not always compatible with microfluidic device and peripheral components. With this consideration, all the materials chosen for the device and peripheral connections, such as the tubes, were allowed to be autoclaved. To ensure the sterilization efficiency, most of the components were flushed with 70% ethanol and then autoclaved at 121^{o}C

for 30 minutes. All the components were placed into sterilization pouches (Fisher Scientific, Canada) to avoid contamination during transportation from equipment room to the biosafety cabinet.

5.2.3 Perfusion Culture System

The vascular mimic microfluidic system is operated in dynamic conditions differing from conventional cell culture. Cell seeding needs to ensure a reasonable density for cells to interaction with other cells and extracellular matrix (ECM). The immobilization strategies need to be considered due to the non-standard culture surfaces used. In addition, the efficient supply of nutrient and oxygen are also important factors to ensure cells grow successfully. All the following processes will ensure that the cells are cultured in healthy conditions, such as the media temperature and PH. A few technical issues were also addressed.

5.2.3.1 Cell Loading/Seeding

It is a dynamic procedure for loading cells in perfusion culture system, where cell suspension is infused into the microfluidic channels. The cell density is very important to ensure enough coverage of cells on the substrate for the interaction of cells to each other. It is different from the static culture where the required cell number could be easily determined from area. The infused cell density is mainly affected by the height of the channel used. A channel with 100 μm height normally needs the cell density to be 2×10^6 cells/ml, while 400 μm height channels require the cell density as 5×10^5 cells/ml or less. Another influence factor is the loading rate. The seeding flow rate must be relatively slow to avoid compromising cell viability. However, too low flow rate may also cause cells to settle down in the connections before entering into the effective areas,

which will cause non-uniformity of the cell density. Thus, it is better to form a standard procedure to improve the seeding performance.

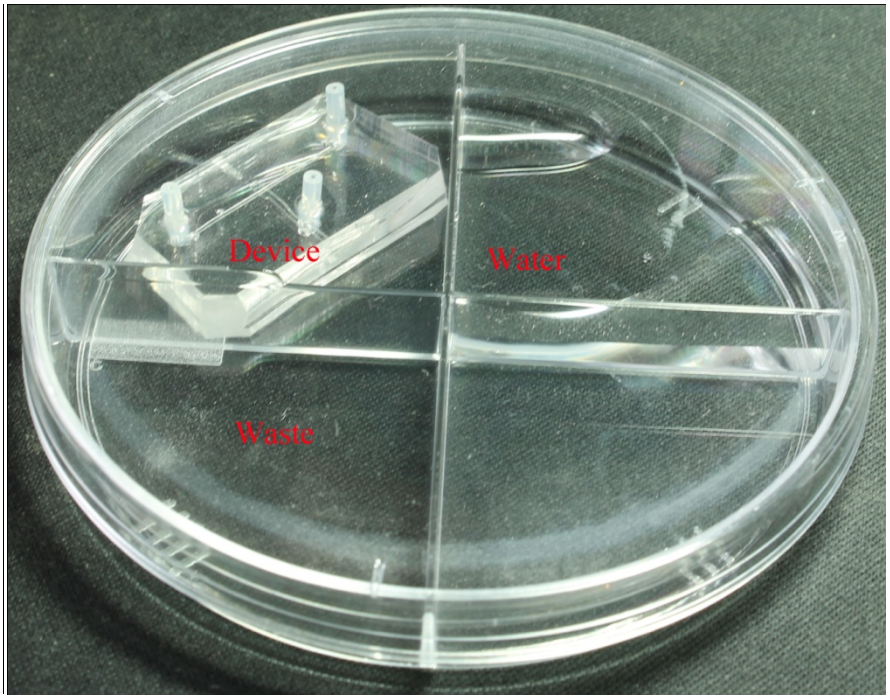

Figure 5-5. The schematic shows the local culture environment which is realized by a four-section petri-dish. The main device was place in one of the section, while another section was partially filled with clean water and the other two sections were leaving for storing waste.

Firm cell attachment is critical in the perfusion culture. After being autoclaved with peripheral connections, the device was filled with 0.01% poly-D-lysine (PDL) solution and kept overnight in a humidified incubator. In the following day, PDL was replaced with gelatin solution (0.1%) which serves as ECM for cell attachment. In above and all the following culture processes, it is very important to avoid air bubbles generating in the channel. Therefore, the device is placed in a petri-dish with four sections as shown in Figure 5-5. One of the sections was filled with 3 ml autoclaved water to provide a locally humidified environment for the device, which is to avoid evaporating of solution in the device and forming bubbles. In addition, placing the device overnight in the humidified incubator is to make sure PDMS absorb water to saturation. Other

than preventing self-generated air bubbles, it is also important not to introduce air bubbles into the device. Thus, drop merging technique was used during each of the injection steps.

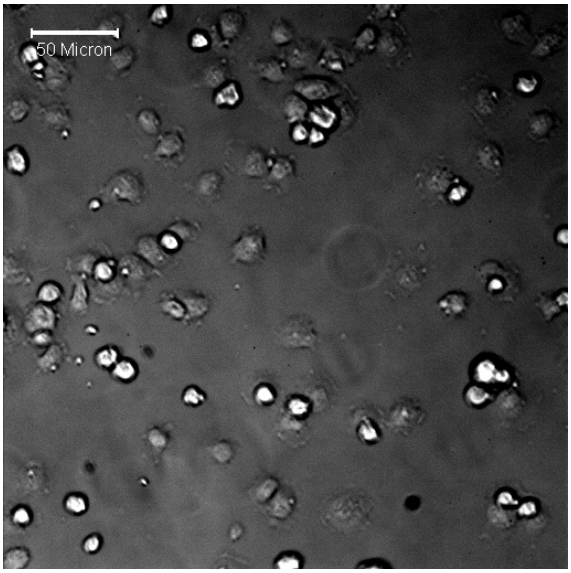

Figure 5-6. Distribution of cells in the channel after cells were loading into the channel. In a few minutes, some cells were already partially attached on the substrate.

After coating with gelatine solution for 4-8 hours, a dish of 70% confluent cell was rinsed with 5 ml HBSS twice and trypsinized with 4 ml trypsin solution for 4 minutes. Before centrifugation, 10 ml of the cell suspension was collected for cell number counting using hemocytometer. Remaining solution was centrifuged at 900 RPM for 4 minutes and the cell pellet was collected. From the counted number by hemocytometer, certain amount of balance medium was added in the cell pellet to achieve the cell density required. To avoid the unnecessary influence from the connections and to decrease the loading distance, the device was not assembled with peripheral connections during the cell loading process. The cell suspension was collected with a 1 ml syringe and infused into the channel carefully with drop merging technique. Optical microscope

was used to examine the cell density. Cells are often allowed to attach to the substrate for around 2 hours, which may vary depending on the different cell types.

5.2.3.2 Perfusion of the Culture System

There are two different modes of perfusion, non-circulating [20-22] and re-circulating [23, 24] culture. In non-circulating culture system, the culture media is perfused directly into the waste reservoir, thus, cells are fed with fresh media all the time. While in re-circulating system, the culture media is re-circulated back into the media reservoir with big amount of volume; the waste and the secreted factors are diluted and the oxygen level is re-equilibrated. Different techniques and equipment are used for the perfusion culture system. The non-circulating culture is often driven by syringe pumps or gravity, while re-circulating culture is often driven by peristaltic pumps including external and on-chip [24] types.

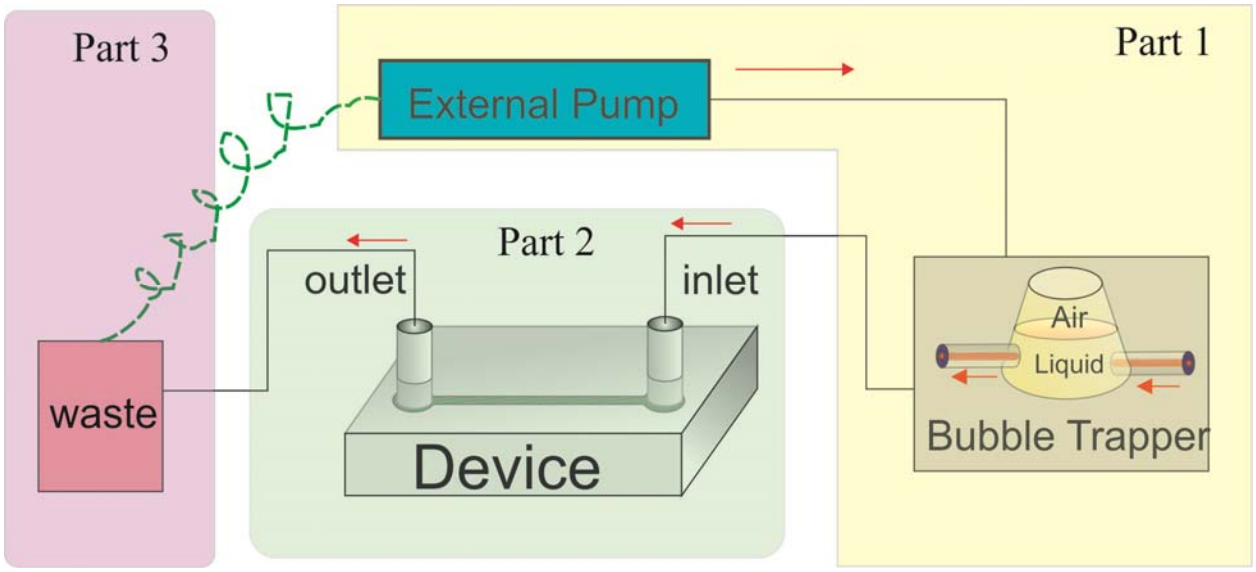

Figure 5-7. The schematic of the perfusion culture system, including three parts: external pump with connections as part1, the device with chip-to-world interfaces as part2 and the waste, which is either re-circulated into the pump or disposed depending on the type of the pump used, with connections as part 3.

Once cells were attached to the substrate firmly, the perfusion of the medium was started. 10 ml warmed media (37^{o}C) was pre-equilibrated in the incubator for at least one hour. The whole system was separated into three parts: part 1 is the pump connected with a bubble trapper; part 2 is the main part which is the device for culturing cells, and part 3 the waste reservoir which is either re-circulated into the pump or disposed depending on the type of the pump used. Part 1 with peristaltic pump or the syringe filled with pre-equilibrated media was connected with the chip-to-world inlet of the device by drop merging technique to avoid inducing bubbles. Then the outlet of the device was connected with part 3. For syringe pumps, the pump was kept outside the incubator while other parts were placed into the incubator. For small size peristaltic pump as we used, all the parts could be put inside the incubator. Till now, the microfluidic perfusion system was finished.

5.2.3.3 Immunoassay

The sample was rinsed with around 1 ml of PBS by connecting the syringe to the inlet and fixed by 3.7% formaldehyde solution in PBS for 10 minutes at room temperature, followed by washing cells with another 1 ml PBS. Cells were permeabilized with 0.1 % Triton X-100 in PBS for 3 minutes, washed by PBS and blocked with 1% bovine serum albumin (BSA) for 20 minutes. Then cells were stained with Hoechst 33342 at a final concentration at 5 μg/mL in PBS for 10 minutes and washed with PBS. The sample was filled with fluoroshield and examined by fluorescent microscope (IX81, Olympus).

5.3 Experiments and Results

5.3.1 Cells Morphology

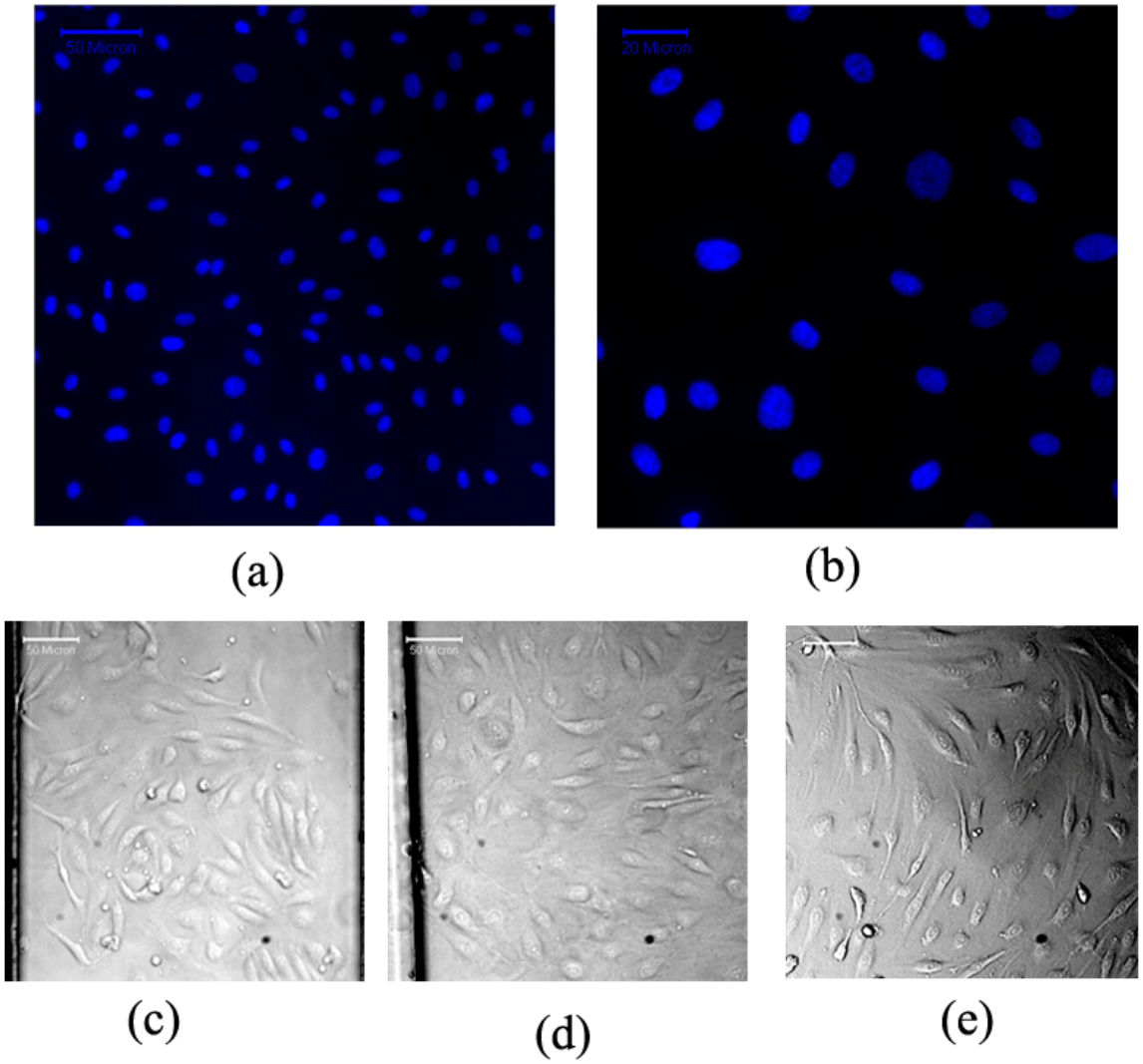

Figure 5-8. (a) and (b) are staining of nuclei for different density of endothelial cells inside culture channels; (c) and (d) show endothelial cells in the small channel (300 μm width) and bigger channel (1000 μm width) at shear force of 1 dyne/cm^2, respectively; (e) is cells growing at shear force of 20 dyne/cm^2.

Figure 5-8 shows cells in channels growing into confluent after around 48 hours. Cell density at confluent can range from 1200 cells/mm^2 to 2500 cells/mm^2, which largely depends on the

loading density of cells. Figure 5-8a has a cell density around 1300 cells/mm^2 while Figure 5-8b shows a cell density around 1500 cells/mm^2.

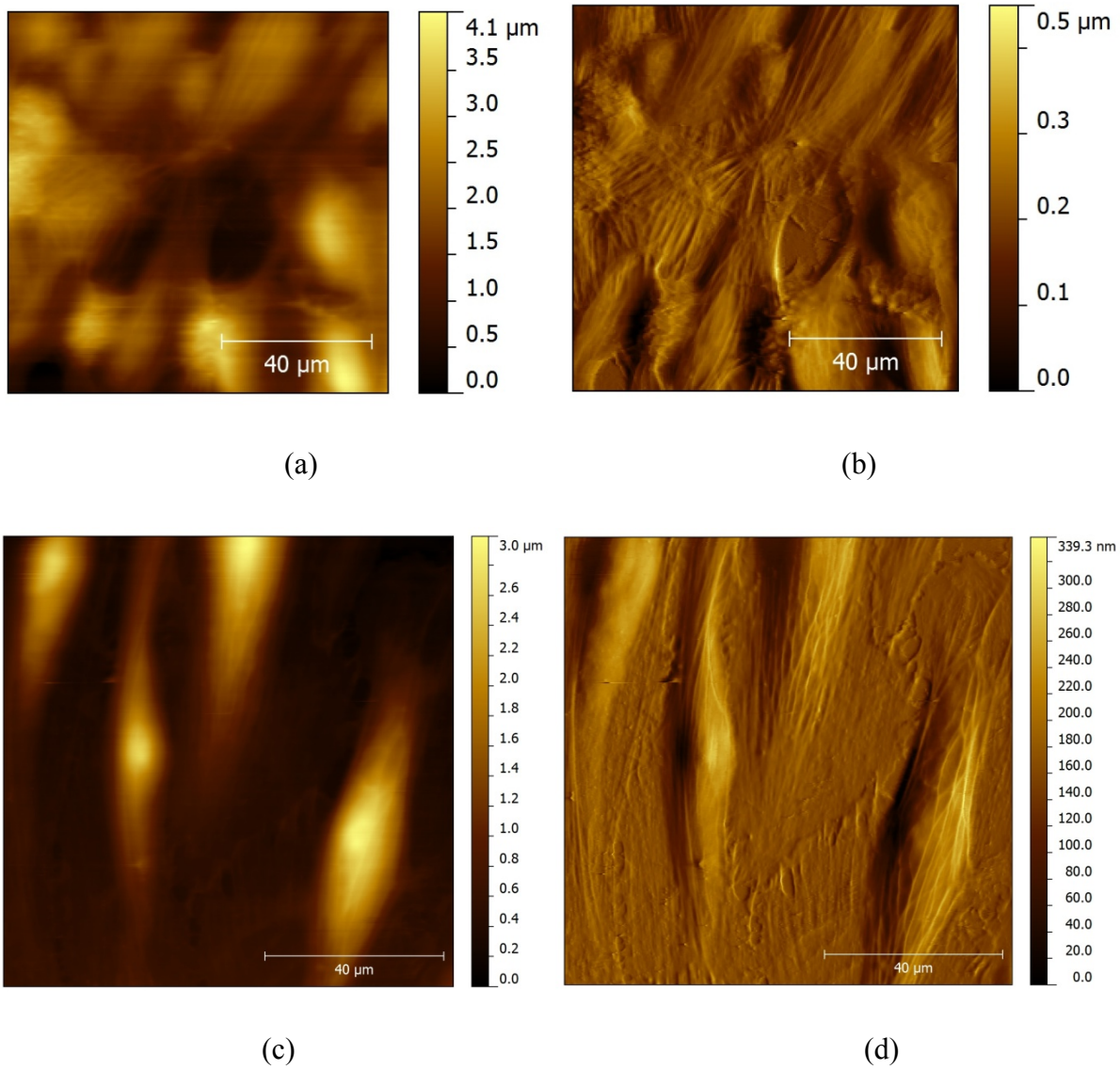

Figure 5-9. Morphology and deflection images of endothelial cells scanned by AFM. (a) and (b) are cells at shear force of 1 dyne/cm^2, while (c) and (d) are at 20 dyne/cm^2.

After around 24-48 hours perfusion, the device was dissembled for AFM experiments. Figure 5-9 shows the height image and deflection images for cells growing at the second day of perfusion. From deflection images, underlying stress fibres indicate the flow direction.

5.4 Discussion and Conclusion

Microfluidic cell culture systems are becoming more attractive because they extend the capabilities of macroscale perfusion. However, due to the complexity of microfabrication techniques, for instance photolithography which needs to be done in clean room, biologists cannot yet benefit from microscale techniques. Microfluidic technique has been widely employed in a wide range of applications, and various techniques were developed to replace the complex microfabrication process.

In this study, we have demonstrated an easy way to realized microfluidic cell culture for vascular mimicking application. A rapid prototype to mimic the vascular vessel in vitro was constructed. Several highlighted technical procedures guarantee the success in building up the prototyping. Firstly, using cutting plotter significantly decreases the preparation time of mold and increase the feasibility of fabrication in almost any lab. Secondly, the world-to-chip connection is one of the keys to success in connecting microfluidic device to peripheral equipments. Thanks to highly flexible property of silicone, it allows the following connections to be sealed perfectly. Through introducing silicone tubings as the connection between the chip and peripheral equipments, we were able to fabricate a highly integrated device for the cell culture application, which not only guarantee all the connections seamlessly. Thirdly, the procedures applied to avoid bubbles ensure cells grow healthy in the channel. Last but not least, gas permeability of PDMS allows the static culture possible when the membrane is not covered. Each of these is crucial for successful implementation of a leak-free, bubble free and highly integrated device for cell culture application.

Recent advances in microfluidics have brought forth new tools for studying flow-induced effects or other biophysical stimuli on mammalian cells especially on endothelial cells. The plethora of microscale systems developed to date demonstrate flexibilities of microfluidic designs, and showcase advantages of the microscale that are simply not available at the macroscale. With the development of more microscale techniques, a standard and practical microscale fabrication method will be available in a routine lab. Microfluidic cell culture will potential solve a number of biological and medical difficulties.

5.5 References

1. Bundey, R.A., Endothelial cell mechanosensitivity. Focus on" Cyclic strain and motion control produce opposite oxidative responses in two human endothelial cell types". American Journal of Physiology-Cell Physiology, 2007. 293(1): p. C33.

2. Langille, B.L. and S. Adamson, Relationship between blood flow direction and endothelial cell orientation at arterial branch sites in rabbits and mice. Circulation Research, 1981. 48(4): p. 481.

3. Nerem, R.M., M.J. Levesque, and J. Cornhill, Vascular endothelial morphology as an indicator of the pattern of blood flow. Journal of biomechanical engineering, 1981. 103: p. 172.

4. Rubanyi, G.M., J.C. Romero, and P.M. Vanhoutte, Flow-induced release of endothelium-derived relaxing factor. American Journal of Physiology-Heart and Circulatory Physiology, 1986. 250(6): p. H1145.

5. Boo, Y.C. and H. Jo, Flow-dependent regulation of endothelial nitric oxide synthase: role of protein kinases. American Journal of Physiology-Cell Physiology, 2003. 285(3): p. C499.

6. Awolesi, M.A., W.C. Sessa, and B.E. Sumpio, Cyclic strain upregulates nitric oxide synthase in cultured bovine aortic endothelial cells. Journal of Clinical Investigation, 1995. 96(3): p. 1449.

7. Acevedo, A.D., et al., Morphological and proliferative responses of endothelial cells to hydrostatic pressure: role of fibroblast growth factor. Journal of Cellular Physiology, 1993. 157(3): p. 603-614.

8. Kamiya, A. and T. Togawa, Adaptive regulation of wall shear stress to flow change in the canine carotid artery. American Journal of Physiology-Heart and Circulatory Physiology, 1980. 239(1): p. H14.

9. Hudlicka, O. and M. Brown, Physical forces and angiogenesis. 1993, Futura Publishing. Mount Kisco, NY. p. 197-241.

10. Malek, A.M., S.L. Alper, and S. Izumo, Hemodynamic shear stress and its role in atherosclerosis. Jama-Journal of the American Medical Association, 1999. 282(21): p. 2035-2042.

11. Young, E.W.K. and C.A. Simmons, Macro-and microscale fluid flow systems for endothelial cell biology. Lab on a Chip, 2009. 10(2): p. 143-160.

12. Khademhosseini, A., et al., Microscale technologies for tissue engineering and biology. Proceedings of the National Academy of Sciences of the United States of America, 2006. 103(8): p. 2480-2487.

13. Odijk, M., et al., A microfluidic chip for electrochemical conversions in drug metabolism studies. Lab on a Chip, 2009. 9(12): p. 1687-1693.

14. Toh, Y.C., et al., A microfluidic 3D hepatocyte chip for drug toxicity testing. Lab on a Chip, 2009. 9(14): p. 2026-2035.

15. Wheeler, A.R., et al., Microfluidic device for single-cell analysis. Analytical Chemistry, 2003. 75(14): p. 3581-3586.

16. Keenan, T.M. and A. Folch, Biomolecular gradients in cell culture systems. Lab on a Chip, 2008. 8(1): p. 34-57.

17. Meyvantsson, I., et al., Automated cell culture in high density tubeless microfluidic device arrays. Lab on a Chip, 2008. 8(5): p. 717-724.

18. Fisher, R. and R. Peattie, Controlling tissue microenvironments: biomimetics, transport phenomena, and reacting systems. Tissue Engineering II, 2007: p. 1-73.

19. Gad-el-Hak, M., The MEMS handbook. 2006: CRC.

20. Chung, B.G., et al., Human neural stem cell growth and differentiation in a gradient-generating microfluidic device. Lab on a Chip, 2005. 5(4): p. 401-406.

21. Bettinger, C.J., et al., Three Dimensional Microfluidic Tissue Engineering Scaffolds Using a Flexible Biodegradable Polymer. Advanced Materials, 2006. 18(2): p. 165-169.

22. Kim, L., et al., Microfluidic arrays for logarithmically perfused embryonic stem cell culture. Lab on a Chip, 2006. 6(3): p. 394-406.

23. Leclerc, E., Y. Sakai, and T. Fujii, Cell culture in 3-dimensional microfluidic structure of PDMS (polydimethylsiloxane). Biomedical Microdevices, 2003. 5(2): p. 109-114.

24. Gu, W., et al., Computerized microfluidic cell culture using elastomeric channels and Braille displays. Proceedings of the National Academy of Sciences of the United States of America, 2004. 101(45): p. 15861.

CHAPTER 6

6 EVALUATION OF INTERMOLECULAR FORCES IN A CIRCULATING SYSTEM

6.1 Introduction

The association and dissociation of interactions between molecules of cells and surrounding environment play a critical role in biological events such as cell signalling, cell proliferation and cell migration. Cells like platelets and leucocytes often need help of erythrocytes to realize their functions [1]. In addition, cell adhesion mediates pathogenesis of many inflammatory diseases. For example, in a circulating system, accumulation and aggregation of cells can promote certain critical pathological issues, like atherosclerosis and thrombosis. The characterization of molecular interaction is fundamental quest in biology. Quantitative study of molecular interaction force is very important for unveiling the underlying mechanisms and future predictive biology.

Identities of most cell adhesion molecules have been elucidated, for instance, E-selectins, ICAM-1 and VCAM-1 on endothelial cells; L-selectins, β1-, β2- and β6- integrins, PECAM-1 on leukocytes; Rap1 on sickle red blood cell, etc. Additionally, cell-cell interaction and cell-substrate interaction are regulated by many molecules due to the complexity of cell surfaces. To bypass complex multiple molecular interaction, researchers developed various experimental and theoretical methods to study the intermolecular forces at single molecule level. Several popular experimental techniques include atomic force microscopy (AFM) [2], biomembrane force probes

(BFP) [3], surface force apparatuses [4], optical tweezers [5], micropipettes [6], microplates and flow chamber [7, 8]. Direct force measurement by AFM and BFP can achieve ultrahigh resolution for single molecular interaction force analysis by coating probes with specific molecules of interest. Flow chamber experiment is a method which not only can provide high accuracy, but also more closely mimic the in vivo biophysical environment. Furthermore, flow chambers are ideally used to study a number of molecular interactions in parallel to obtain more statistically meaningful data. During last decade, the sensitivity of flow chambers has been largely improved, which can analyze interactions with a resolution of lower than a piconewton.

Flow chambers have long been used to study receptor-ligand interactions, such as determination of bond lifetime and unbinding force calculation. A recent paper did a comprehensive review for studying molecular interactions with a laminar flow chamber [9]. As a result of the irregular shape and uncertain bond length for cells, which would cause the unqualified calculation of forces, molecule-coated spheres rather than cells are usually used in flow chamber experiments to eliminate the unexpected phenomena. The key information achieved in flow chamber experiments is monitoring the molecular bond formation and rupture in a defined hydrodynamic environment. There is a simple formula suggested by Bell [10]used to describe a given receptor-ligand behaviour:

$$k_{\text{off}}(F) = k_{\text{off}}(0)\exp(\frac{F}{F^0}) \tag{1}$$

where $k_{\text{off}}(F)$ is the dissociation rate as a function of applied force F . F^0 was approximated as $k_{\text{B}}T/\delta$, where k_{B} is Boltzmann's constant, T is the absolute temperature, and δ is the bond distance. In flow chamber experiment, the hydrodynamic force of breakup exerted on a

circulating cell doublet has been calculated [11], and generally used to predict the force strength of intermolecular bond [12]. Currently, several theoretical methods mostly used to evaluate interparticle interactions in colloidal suspensions [13-16] have been adapted and applied in biological systems to study the cell-cell interaction forces [11, 17].

However, in reality, intercellular forces are a complex mixture of various interactions such as electrostatic forces, van der Waals (VDW) forces and steric forces etc. The contribution of these forces depends on both the separation distance and local environment. When cells are brought to a distance less than several nanometres, those molecules mediated forces and short distance forces like ionic bond may become critical, which further complicates the interaction forces. Only considering the hydrodynamic forces may underestimate or overestimate the interaction forces of molecular bonds in flow chamber experiments. To more quantitatively interpret flow chamber experiment results like the bonding life time study, these additional non-neglectable intercellular forces, for example, the DLVO (Derjaguin-Landau-Verwey-Overbeek) force, need to be taken into consideration. DLVO forces, which combine the effects of the London-van der Waals attraction and the electrostatic repulsion due to the electric double layer (EDL) interaction, has been successfully used in biological application [18-20]. In this study, circulating cell doublets and the cell-substrate interaction model with several ten nanometres separating distance are investigated. Excluding hydrodynamic forces, the DLVO forces are taken into account of the interaction force calculation.

In order to quantify the molecular interaction forces of cell-cell and cell-substrate in a circulating system, such as flow chamber and microfluidic culture system, Low-Reynolds number hydrodynamic theory and Goldman's theory are employed to calculate the hydrodynamic force

generated from the flow field effect for a cell doublet and the cell-substrate interaction respectively, followed by the DLVO theory analysis. The results demonstrate that DLVO forces have the scale as large as 14.6% of the exerted hydrodynamic force for cell doublets model, and for intermolecular force analysis of cell-substrate interaction, it can go up to 30%. Both cell doublet and cell-substrate models are subject to nonlinear effect of intermolecular forces as the distance changes. This analysis is beneficial to predict the biophysical properties of receptor-ligand bonds more quantitatively.

6.2 Models and Methods

6.2.1 Statement of the Assumptions and Models

Intercellular interactions are essential for cells to realize their functions. To study the intercellular interaction forces in a circulating system, three main factors need to be considered: the strength of the force, the separating distance and the environment it acts in. The acting distance of forces varies from several angstroms to hundreds of nanometres [21]. Every surface force has its own cutoff distance depending on the environment and also the specific problem being solved. Cells and biomolecules exposed to a circulation system experience hydrodynamic forces that affect their function. In literature work, the hydrodynamic interaction on cells or hard spheres in flow chamber system has been studied. Mostly, the hydrodynamic force has a much higher magnitude which dominates the overall interaction forces. However, the electrostatic force is largely screened at biological solution which has high salt concentration. Thus, the acting distance of electrostatic forces is largely decreased, leading to unbalanced DLVO forces. Therefore, DLVO forces cannot be neglected. In this study, the intermolecular forces of a

circulating cell doublet and cell-substrate interaction model are predicted by the hydrodynamic and DLVO forces.

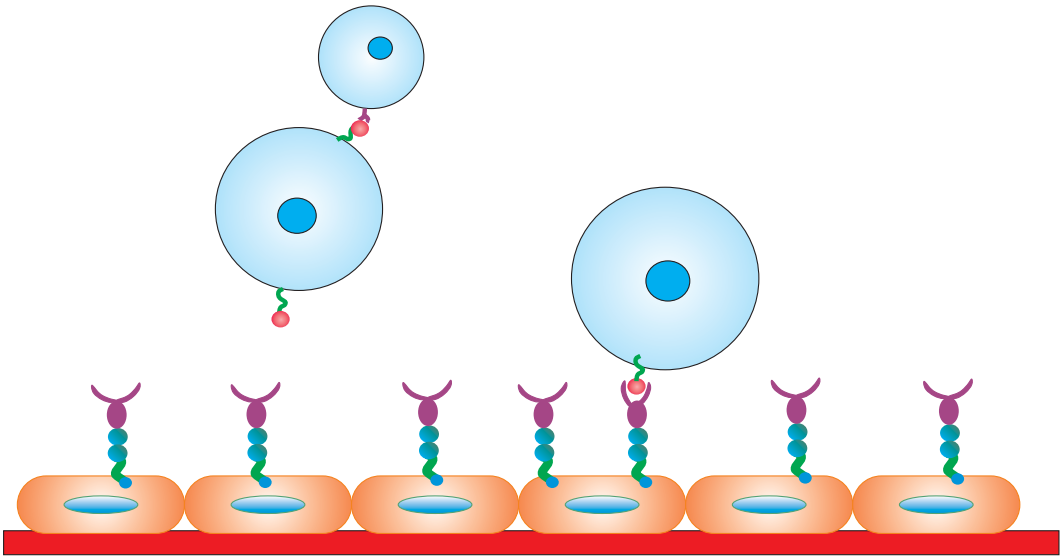

Figure 6-1. Schematic of cells in a circulating system. Two models are illustrated, one is the cell doublet linked by a receptor-ligand bond, and the other is the cell-substrate interaction model.

To elucidate the complex biophysical environment that affecting or governing cells interaction processes, in vitro flow chamber assays like parallel plate flow chamber (PPFC) have been developed to study the intermolecular interaction. In order to eliminate the affect of multiple molecular interactions, microspheres coated with specific molecules are placed into the flow chamber as shown in Figure 6-1. Herein, two models are illustrated, one is the cell doublet which represents a pair of microspheres linked by a rigid tether and the other is the cell substrate interaction model. The detailed models will be analyzed in section 6.2.2.

Normally, biological cells have the size ranging from a few micrometers to several ten micrometers and are exposed in the microenvironment. Hence, activities of microorganisms and living cells in fluid are usually characterized by low Reynolds number flow**.**

6.2.2 Hydrodynamic Force Analysis

In colloidal particles system, well-defined solutions have been developed for hydrodynamic force analysis, which aided in explaining the intercellular force in biological area. Analytical computation of hydrodynamic forces applied on aggregates composed of two equal-sized particles under simple shear force was solved [22], which has been applied in investigation of neutrophil, platelet, and red blood cell homotypic aggregation [23-25]. In reality, there are cell doublets composed of both equal-sized and unequal-sized cells. Hence, a common method in applied in the previous study for arbitrary size cells [12] was recruited in biological systems.

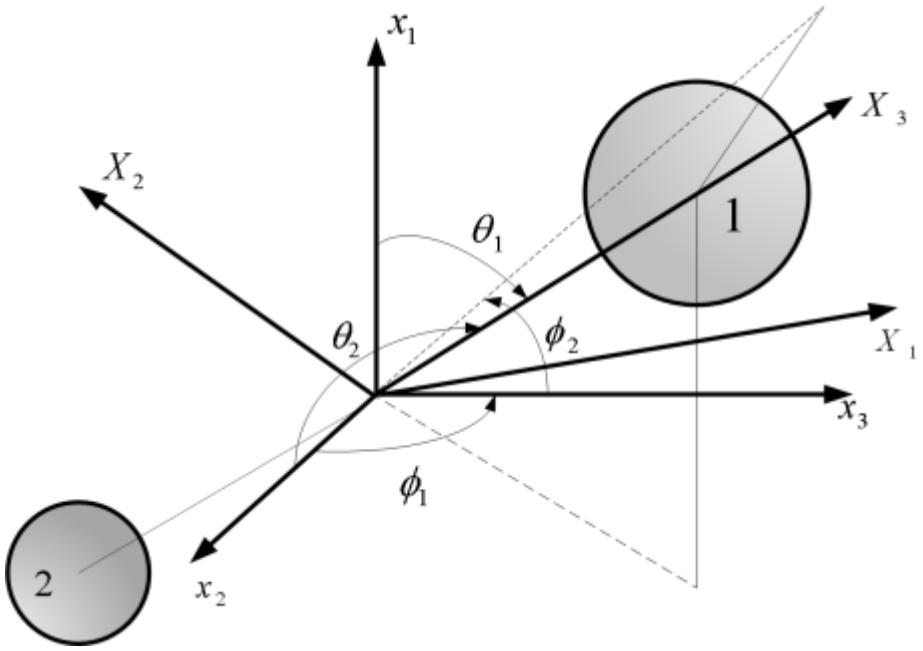

Figure 6-2. Schematic of the cell doublet. Biological cells (particles) are modeled as a pair of unequal spheres of radii a_1 and a_2, which are separated by a rigid tether of length d. Space-fixed coordinate system is designated x_i. x_3 coincides with the direction of fluid flow, x_2 is the direction of the velocity gradient, and x_1 is the vorticity axis. The origin O lies at the midpoint of the line joining the centers of the two spheres. X_i describes the particle-fixed coordinates. X_3 lies along the line joining the centers of the two spheres. It is directed toward the larger sphere. X_2 is coplanar with the x_1-x_3 plane, and X_i is perpendicular to X_2 and X_3. (θ_1, Φ_1) and (θ_2, Φ_2) are polar and azimuthal angles with respect to the axes x_1 and x_2, respectively. (Figure adapted from [12])

When the distance between two particles falls into less than 100 nm, it could be regarded as a cell doublet. Both individual spheres do not undergo free rotation about the tether in the cell doublet. Figure 6-2 shows the schematic of a cell doublet. In a cell doublet, there are two spheres, whose radii are a_1 and a_2, exposed to a linear shear flow. In this study, a simple shear of magnitude G ($u_3 = Gx_2$, $u_1 = u_2 = 0$) is chosen. There are three key geometric parameters of this doublet: the radii a_1 and a_2 for the unequal-sized spheres, a tether of length d, which is the separating distance of two spheres surfaces, represents the receptor-ligand bond length. Usually, these three parameters are replaced by the radius of the larger sphere a_1 and other two dimensionless parameters: the radius ratio $\lambda = a_2/a_1$, and the dimensionless separation distance $\delta = d/a_1$. Excluding geometry parameters, the orientation of the axis connecting two centers of spheres with respect to the flow direction is another contribution factor. Other flow parameters influencing the magnitude of applied force and force loading rates are the shear rate, G, and the fluid viscosity μ. All these parameters contribute to the hydrodynamic behaviour of the cell doublet.

When a cell doublet is subject to a low Reynolds-number flow, the force and torque acting on particles could be written in matrix expression as [26]

$$\mathbf{F}=-\mu(\mathbf{RU}+\mathbf{\Phi\varepsilon}) \tag{2}$$

where **F** is the 1x12 force-torque vector, **R** is the 12x12 grand resistance matrix, **U** is the 1x12 relative velocity-spin vector, **Φ** is the 12x12 shear resistance matrix, and **ε** is a 1x12 shear vector.

On the right side of Equation (2), **R** and **Φ** are flow-independent resistance matrices that are functions of a_1, λ and δ [27, 28], **ε** is obtained in a straightforward fashion from the rate-of-strain tensor, **U** is determined using knowledge of doublet motion in linear shear field [14].

After defining all the items on the right side, the forces and torques for the cell doublet can be solved; then intercellular bonding forces are to be predicted by the hydrodynamic force. Since only normal force can be sensed by molecular bonds, the normal force F_N extracted from the third item of the vector **F** becomes critical. For a cell doublet containing two arbitrary sized particles, the tensile force is:

$$F_N = \alpha_N(a_1, \lambda, \delta) G \eta a_1^2 \sin\theta_1 \sin 2\phi_1 \tag{3}$$

where $\alpha_N(a_1, \lambda, \delta)$ is the force coefficient which is a function of a_1, λ and δ. For two unequal rigid spheres in low-Reynolds-number flow, $\alpha_N(a_1, \lambda, \delta)$ has the form as

$$\alpha_N(a_1, \lambda, \delta) = \frac{1}{4X_{11}^A + X_{11}^A(\lambda^{-1}) + (1+\lambda)X_{12}^A}\pi$$
$$\left[\begin{array}{l} -3(1+\lambda)^2(1+\delta+\lambda)X_{12}^{A\,2} + 2X_{11}^A\left[6X_{11}^A(\lambda^{-1})(1+\delta+\lambda) + (-4X_{11}^G(\lambda^{-1}) + (1+\lambda)^2 X_{12}^G\right] + 2X_{11}^A(\lambda^{-1}) \\ \left[-4X_{11}^G + (1+\lambda)^2 X_{12}^G(\lambda^{-1})\right] + (1+\lambda)X_{12}^A\left[-4X_{11}^G - 4X_{11}^G(\lambda^{-1}) + (1+\lambda)^2(X_{12}^G + X_{12}^G(\lambda^{-1})\right] \end{array}\right]$$

where X_{ij}^X and $X_{ij}^X(\lambda^{-1})$ are resistance and mobility functions mentioned in **R** and **Φ** above [27, 28]. For two equal size particles, $\alpha_N(a_1, \lambda, \delta)$has a more straightforward form, equation (3) will become as

$$F_N = a_1 / 2G\eta \sin^2\theta_1 \sin 2\phi_1 \left[3rX_{11}^A - 3rX_{12}^A - 4a_1(X_{11}^G - X_{12}^G)\right] \tag{4}$$

where $r=a_1+a_2+d$.

For cell-substrate interaction, according to Goldman's theory [15, 29] a substrate-bound cell exposed to a laminar flow experience a drag force F and torque Γ given by

$$F = 32.05\mu a^2 G \tag{5}$$

$$\Gamma = 11.86\mu a^3 G \tag{6}$$

where a is the sphere radius.

6.2.3 DLVO Forces Analysis

DLVO theory has been used as a qualitative model [30], also in a quantitative way in biological application. DLVO theory proposes that an energy barrier resulting from the repulsive force prevents two cells (particles) approaching one another and adhering together. When there is sufficient energy to overcome that barrier, the attractive force will pull them into contact where they adhere strongly and irreversibly together. This is one of the critical conditions called cell aggregation and deposition in biological area. DLVO theory suggests that stability of particles in solution is dependent upon its total potential energy function V_T. This theory recognizes that V_T is the balance of several competing contributions:

$$V_T=V_A+V_R+V_S \tag{7}$$

where V_S is the potential energy contributed by the solvent, usually, it only makes a marginal contribution to the total potential energy over the last few nanometres of separation. Much more important is the balance between V_A and V_R, which are the attractive and repulsive contributions.

They are potentially much larger and operating over further distance. The attractive contributions attribute to London-van der Waal interaction. For unequal spheres, V_A can be written as [30]

$$V_A = -\frac{A_H}{6}\left[\frac{2a_1a_2}{d^2+2a_1d+2a_2d}+\frac{2a_1a_2}{d^2+2a_1d+2a_2d+4a_1a_2}+\ln\left(\frac{d^2+2a_1d+2a_2d}{d^2+2a_1d+2a_2d+4a_1a_2}\right)\right] \quad (8)$$

The attractive force generated from the attractive potential energy is

$$F_A = \frac{32A_Ha_1^3a_2^3r}{3d^2(2a_1+d)^2(2a_2+d)^2(2a_1+2a_2+d)^2} \quad (9)$$

where A_H is the Hamaker constant and d is the particle separation, a_1 and a_2 are the radii of two spheres respectively. If $a_2 = \infty$, then the particle could be seen as a flat plate, which becomes the cell-substrate interaction case.

Several theories have been developed in literature to investigate the repulsive potential V_R, and here the linear superposition approximation (LSA) is used for the estimation [30].

$$V_R = 4\pi\varepsilon\varepsilon_0\left(\frac{k_BT}{ze}\right)^2\Psi_1\Psi_2\frac{a_1a_2}{r}e^{-kd} \quad (10)$$

The repulsive force generated from the potential will be

$$F_R = 4\pi\varepsilon\varepsilon_0\left(\frac{k_BT}{ze}\right)^2\Psi_1\Psi_2\kappa^2a_1a_2\frac{1+\kappa r}{(\kappa r)^2}e^{-kd} \quad (11)$$

where k_B is the Boltzmann constant, T is the Kelvin temperature. ε and ε_0 are the dielectric constant of the fluid and the permittivity of vacuum respectively, Ψ_1 and Ψ_2 are the electrostatic potential for two spheres surface, κ^{-1} is the Debye length, which is a function of the ionic

concentration. The same as VWR force analysis, the cell-substrate interaction could be seen as $a_2 = \infty$.

6.3 Results and Discussions

6.3.1 Hydrodynamic Force of a Cell Doublet

Both experimental and theoretical works have confirmed that the strength of many biologically relevant receptor-ligand bonds ranges between 10 pN and 40 pN [10, 31]. Typical receptor has a length of 30 nm [21]. Cells are assumed to have a 15 nm glycocalyx, which means the lower limit of a receptor length is 15 nm. In this study, all the parameters being used are consistently within these scales.

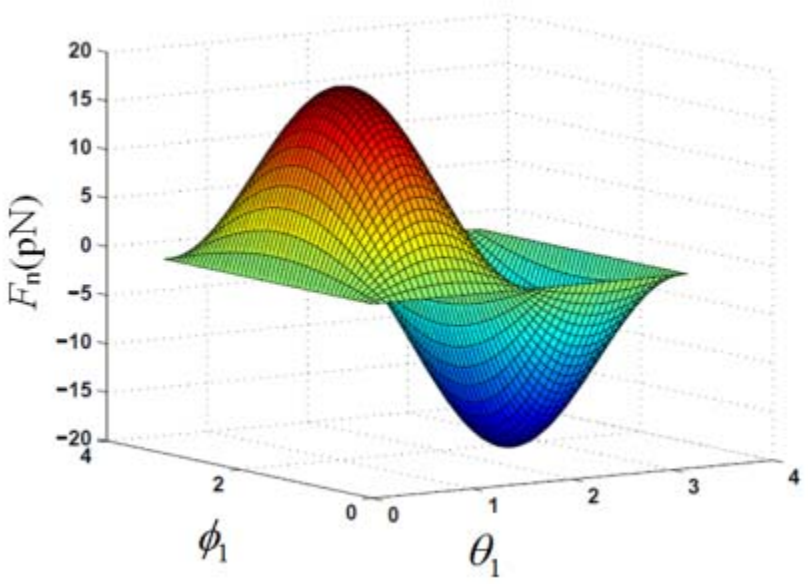

Figure 6-3. Normal force (F_N) with respect to polar and azimuthal angles of doublet axis to the vorticity axis, which are $0<\theta_1<\pi$ and $0<\Phi_1<\pi$, here $\eta = 0.01$ Poise (1cP), $G = 1000$ s^{-1}.

For equal size spheres cell doublet, the hydrodynamic force of two platelets with $a_1 = 1$ μm, $a_2 = 1$ μm and $d = 20$ nm in a laminar flow chamber is calculated. Values for platelets are from [32].

Polar and azimuthal angles of doublet axis to the vorticity axis are $0<\theta_1<\pi$ and $0<\Phi_1<\pi$. The hydrodynamic force applied on different locations on the cells will be varied. Figure 6-3 depicts the variation in normal force (F_N) with respect to the orientation of axis applied on this cell doublet subjected to a linear shear flow, which has η = 0.01 Poise (1cP), G=1000 s^{-1} which is arterial shear rate varies from 50-1500 s^{-1}. Since molecular bonds can only sense the tensile force, we integrate the positive F_N from equation (3) to get the averaged tensile force:

$$\frac{\int_0^{\pi/2}\sin(2\phi)d\phi+\int_{\pi}^{3\pi/2}\sin(2\phi)d\phi}{\pi}=\frac{2}{\pi} \tag{12}$$

$$\frac{\int_0^{\pi}\sin(\theta)^2 d\theta}{\pi}=\frac{1}{2} \tag{13}$$

Then substitute equation (12) and (13) into equation (3), we have

$$F_N=\alpha_N(a_1,\lambda,\delta)G\eta\times\frac{2}{\pi}\times\frac{1}{2} \tag{14}$$

As mentioned in previous section, force coefficient $\alpha_N(a_1,\lambda,\delta)$ is the function of motility and resistance functions, which are the sum of series functions. Thus, analytical solution could not be obtained because of the recurrence calculations involved in those series functions. The first 150 terms of the series are used to calculate the numerical results for all the motility and resistance functions. 0.01% (pN) accuracy is obtained in the numerical calculation in this study.

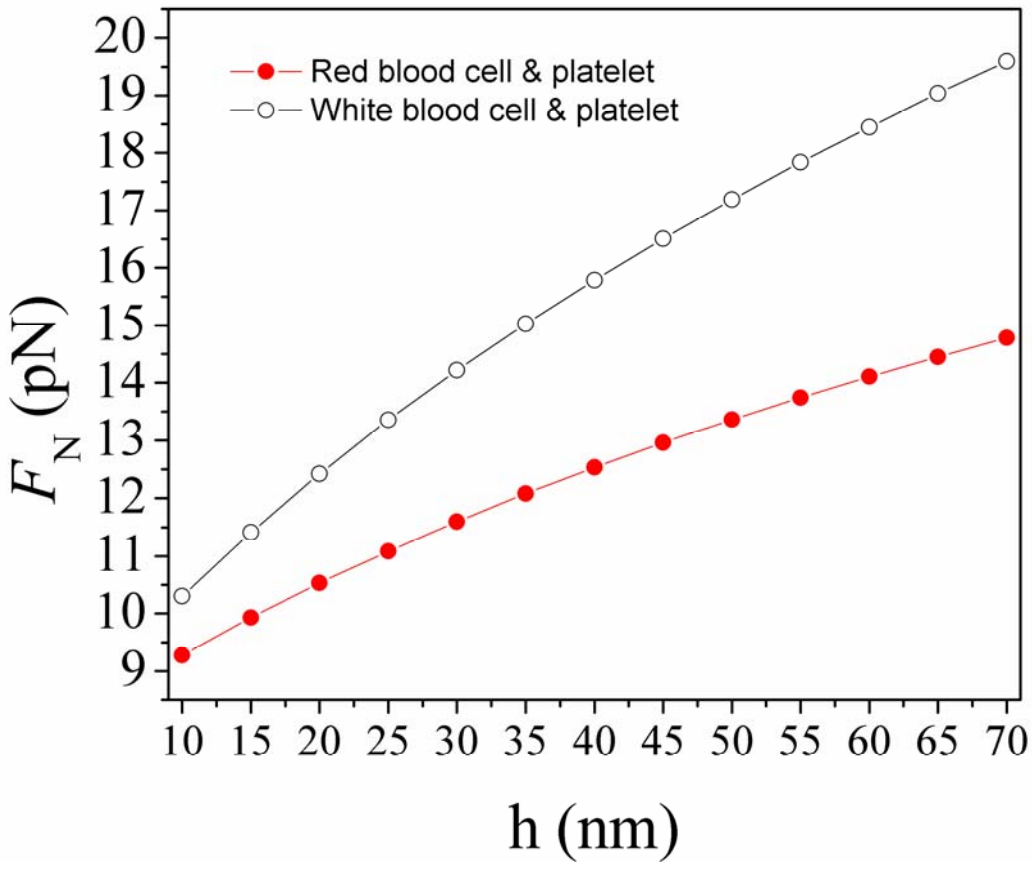

Figure 6-4. Average tensile hydrodynamic force with respect to the separation distance of cell doublets. The hydrodynamic force will keep increasing until the bond ruptures. Solid and hollow circles represent red blood cell and white blood cell interaction with platelet respectively. Here a_1 = 3 μm for red blood cell and a_1 = 4 μm for white blood cell a_2 = 1 μm, η=0.01 Poise (1cP), G=1000 s^{-1}.

In the following analysis, different sizes of microspheres doublet and blood cells doublet were selected for calculation. The results are shown in Figure 6-4. In blood flow system, red blood cell (RBC) or white blood cell and platelet could be simplified as a cell doublet. Normally, the diameter of RBC (swollen) is around 6-8 μm [31], and platelet around 2-3 μm. White blood cells, such as lymphocyte and monocyte with diameters ranging from 7 μm to 21 μm, have an intrinsic sphere shape, which are suitable for cell doublet analysis. Figure 6-4 shows the average tensile

hydrodynamic forces applied on the doublets have continuous increase with respect to the separation distance until the bond breaks. Two pairs of cell doublets (an analogy of real blood cells) with a_1 = 3 μm (red blood cells), a_2 = 1 μm and a_1 = 4 μm (white blood cells), a_2 = 1 μm were put into a flow field as η=0.01 Poise (1cP), G=1000 s^{-1}.

6.3.2 DLVO forces of a Cell Doublet

DLVO forces are a ubiquitous force in both colloidal system and biological area. In flow chamber systems, microspheres experience changing DLVO forces all the time due to the dynamic condition. There are two factors which mainly determined the attraction and repulsive forces magnitude. One is the separation distance of particles which will be at fluctuating distance, and the other one is the local ionic concentration which may vary time to time as well. Both the attractive and repulsive forces may dominate due to the changing of condition.

In biological system, the ion concentration (above 0.1M of NaCl) is higher than that of normal colloidal system. Therefore, the electrical double layer will be largely screened, which means the electrostatic force will be less significant compared to VDW force. Hence, VDW force will dominate DLVO forces in the biological environment. There are several other interaction forces such as polar interactions from extended DLVO theory which may affect intermolecular interactions. As studied, short range forces accounted in extended DLVO theory will have significant effect when two particles are brought into very short distance. Especially in colloidal system or molecular interaction, the separation distance of two particles could reach down to a few nanometres. As mentioned by B.W. Ninham [33], when dealing with electrostatic force in biological system, specific ion effect needs to be considered when the separation distance of two molecules or cells becomes very small (less than 5-10 nm). However, in this paper, the receptor-

ligand interaction and the separation distance of cells is above 15 nm and what we are dealing with is above 20 nm, which is consistent with literature study [31].

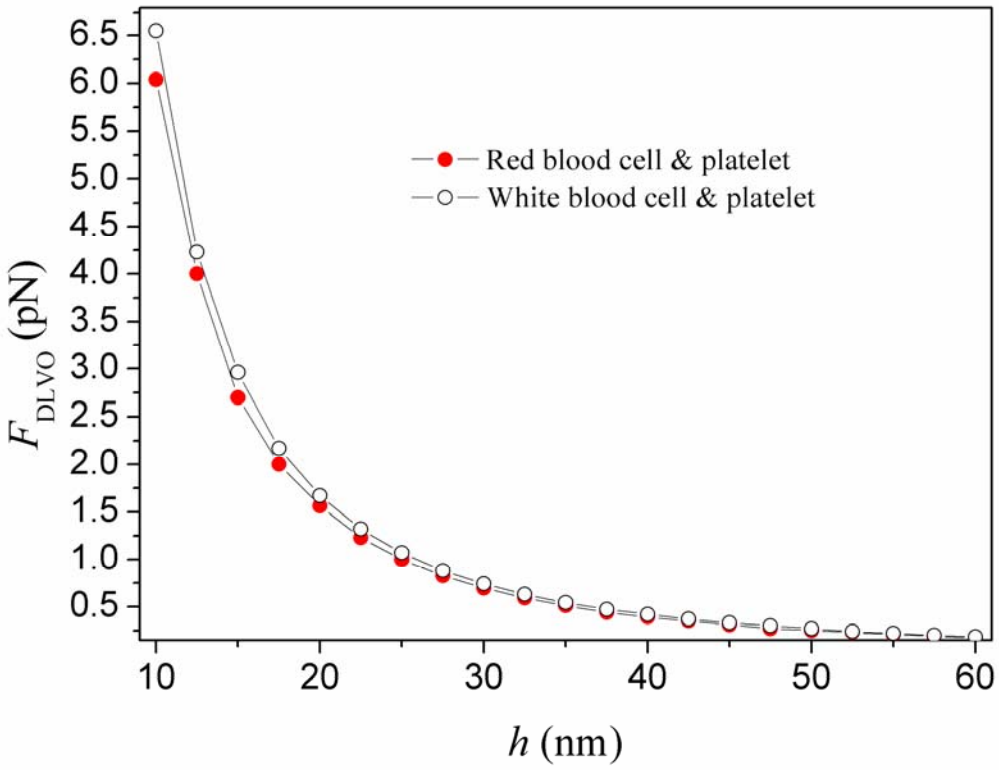

Figure 6-5. DLVO forces with respect to the separating distance (F_{DLVO} is attractive force). The curve with solid circles represents red blood cell and platelet interaction force (a_1 = 3 μm, a_2 = 1 μm). The curve with hollow circles represents white blood cell and platelet interaction force (a_1 = 4 μm, a_2 = 1 μm).

For DLVO forces, several parameters need to be given. A critical one is the Hamaker constant. A reasonable value of the Hamaker constant of interaction between two lipid media embedded in water is 5×10^{-21} J [34], and higher values were used for red blood cells (9×10^{-21} J) and platelets (10^{-19} J) [35]. Considering various beads may be used in flow chamber study, the Hamaker constant may vary. Plasma dielectric constant is 78.54; the elemental charge is 1.602×10^{-19} C;

the surface potential of two particles is assumed to be around 100 mV. The surface potential constant of platelet and red blood cells are -60.0 mV and -34.0 mV respectively [35, 36]. Figure 6-5 shows the DLVO forces as function of the separation distance for two pairs of blood cells with radii a_1 = 3 μm, a_2 = 1 μm and a_1 = 4 μm, a_2 = 1 μm. Swollen sphered red blood cells were often used to diminish the asperities for more accuracy experimental research [31].

6.3.3 Intermolecular Forces of a Cell Doublet in a Circulating System

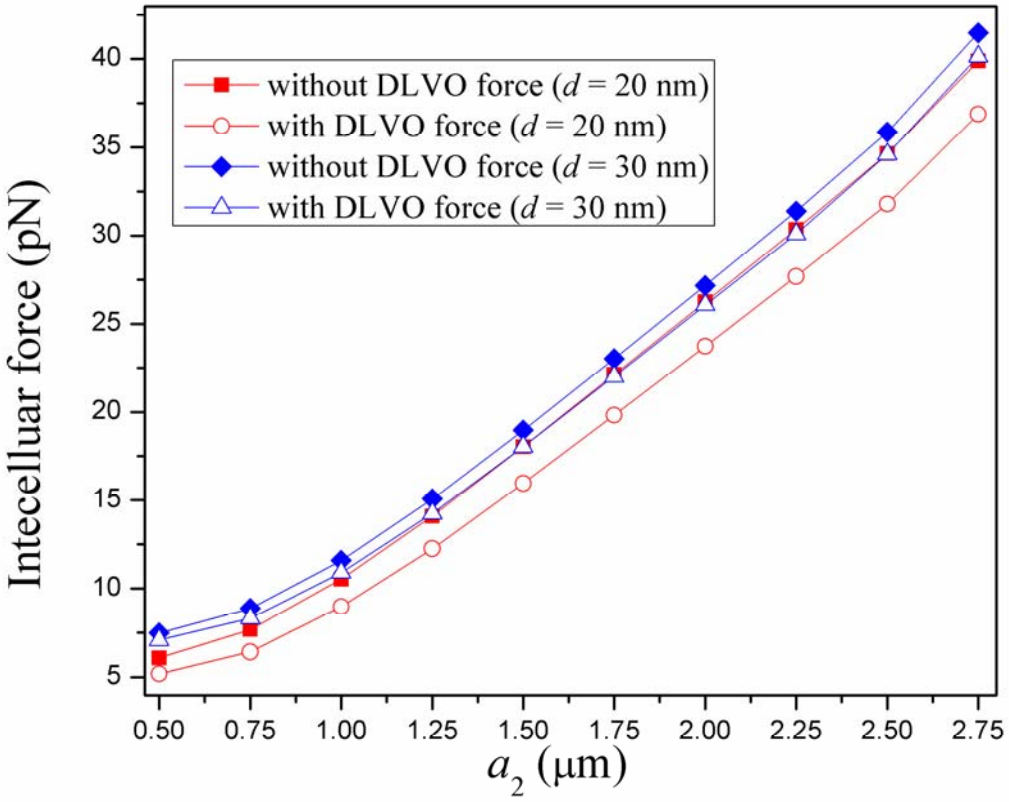

Figure 6-6. Intercellular force analysis results. Microspheres with a_1=3 μm and different radius of a_2 are studied. The separation distance are d = 20 nm (square symbol curves) and 30 nm (circle symbol curves) respectively.

Figure 6-6 shows the intercellular forces of a cell doublet with a_1= 3 μm and various a_2. The effect of DLVO forces may become as high as 14.6% when the radius of a_2 is smaller (0.5 μm) for d = 20 nm. The smaller radius is considered, the more distinct effect will become. For the cell doublet of RBC and platelet, the effect of DLVO forces is 14.5%.

Figure 6-4 shows that the hydrodynamic force increases as the increasing of the separation distance and Figure 6-5 shows that DLVO forces decrease as the separation distance grows. Hence, the intercellular forces will rise up as the separation distance increases. If the molecules still keep bonded and the bond life time increases as the separation distance increases, the bond is called catch bond. As the separation distance changes, DLVO forces will have a nonlinear effect on the intercellular forces. When d = 30 nm, the effect of DLVO forces becomes 6% or less and will become negligible after the separation distance comes above 50 nm.

6.3.4 Intermolecular Forces of Cell-Substrate Interaction in a Circulating System

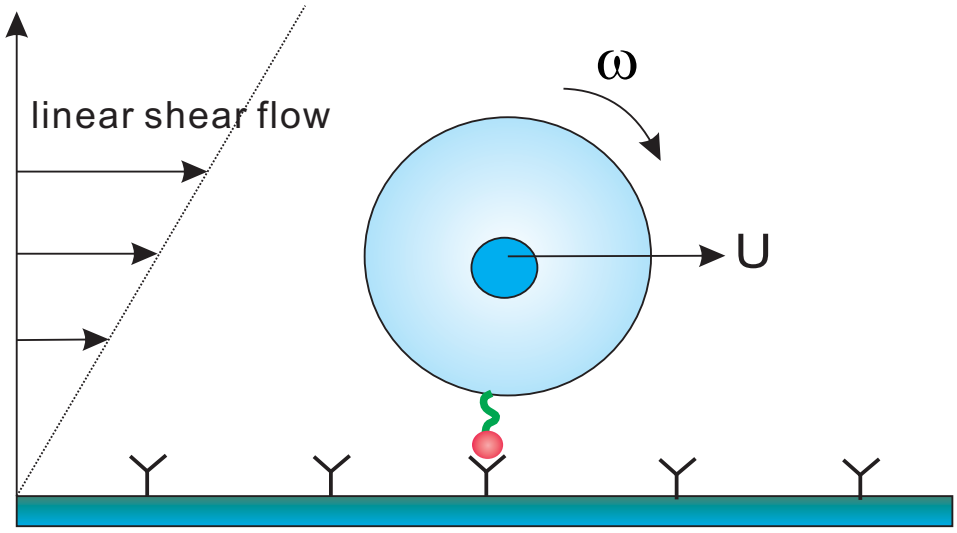

Figure 6-7. Receptor-coated particles or cells are driven along a ligand coated surface by a linear shear flow. U is translational velocity and ω is angular velocity.

As shown in Figure 6-7, cells are viewed as spheres coated with molecular protrusions. The tangential force can be calculated by equ. (5) and the vertical force is calculated by $F_V = \Gamma / a$. Since molecule can only sense the vertical force, F_V is used to calculate the intermolecular forces in the following analysis. DLVO forces are calculated by equ. (9) and (11) with $a_2 = \infty$. The intermolecular force results of two cases with the receptor-ligand interaction force of 20 pN and 30 pN which falls into the range of typical receptor ligand interaction forces [10, 31], are shown in Figure 6-8. In order to study the bonding kinetics, we have to mimic the same scale of forces on the receptor-ligand interaction. The linear shear rate for these two cases can be calculated from equ. (6), which are G = 187 s^{-1} and G = 281 s^{-1} respectively. These shear rates still fall in the range of arterial shear rate. For the intermolecular force of 20 pN case, the effect of DLVO forces could go up to 30%.

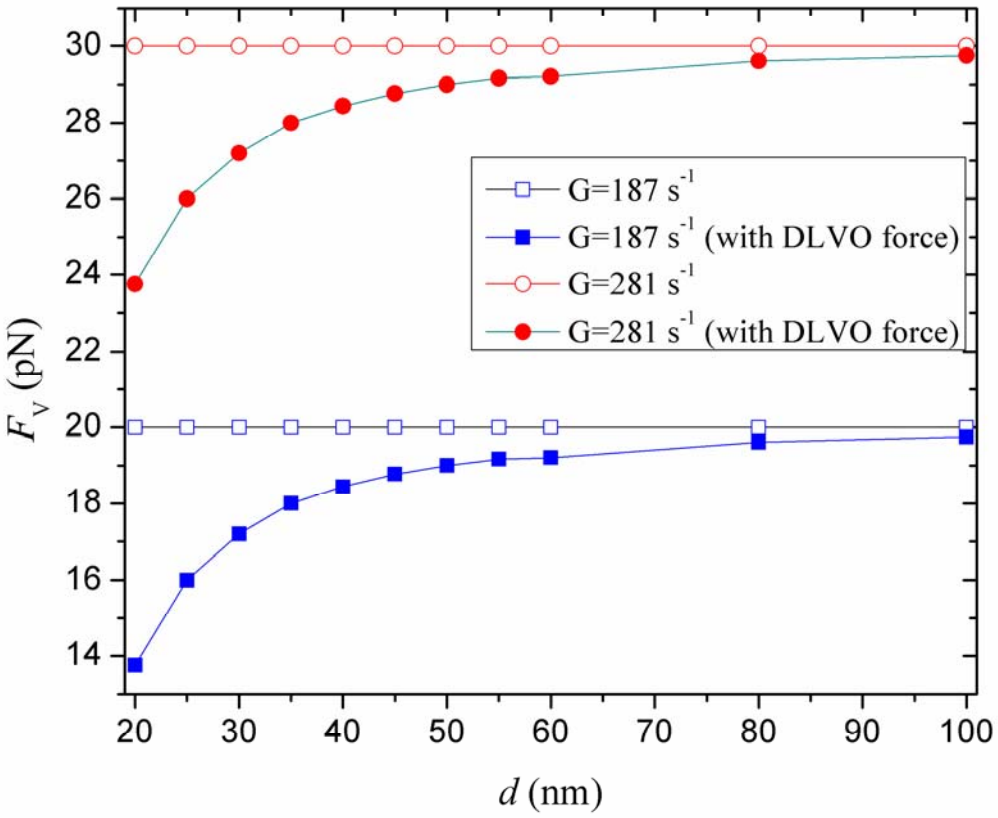

Figure 6-8. Intermolecular forces with respect to the separation distance. Square symbol line is for G = 187 s^{-1} and Circle line is for G = 281 s^{-1}.

In circulating systems, the separation distance of a substrate-bound cell would display a moderate variation, leading to a nonlinear effect on the intermolecular forces. For a specific receptor-ligand interaction study, if the force history is important, the nonlinear effect has to be considered.

In both cell-cell and cell-substrate interactions studied above, the interaction of single receptor-ligand bond was studied. If there are multiple receptor-ligand bonds and breaking up at the same time, the estimated intermolecular forces will be much larger than single bond force. DLVO will

have less effect and become negligible. However, breaking up multiple bonds at the same time is rare, and the last bond rupture was often captured and studied.

6.4 Summary and Conclusion

This paper presented a method to quantitatively determine the intermolecular forces for a cell doublet and cell-substrate interaction model. In flow chamber experiments, the hydrodynamic force is usually taken as the operating force to quantify the intercellular forces of molecular bonds. Due to the high ionic concentration in biological system, the EDL effect is largely screened. As a result, the unbalanced DLVO forces have a non-neglected effect on intermolecular force analysis. Results show that DLVO forces would cause up to more than 14% discrepancy for a cell doublet analysis if only the hydrodynamic force is considered. For cell-substrate interaction, the intermolecular force calculation shows higher discrepancy for a single molecular bond study. Both cell-cell and cell-substrate model indicated that DLVO forces have nonlinear effect on the intermolecular forces as the separating distance changes. If the force history has to be considered in the analysis, DLVO forces could not be excluded in the analysis.

A recent research study has shown that the interaction between live cells and micro-particles would be affected by their metabolic states [37]. Although dead cells or microspheres were investigated mostly, several pieces of experimental evidence support that experiment data need to invoke a fitting parameter for compensation, which may contribute more uncertainty to the data. For above analysis, if the receptor-ligand length is long enough, the effect of DLVO forces will be smaller. It is important to know the length of the receptor-ligand bond being studied, like E-selectin or P-selectin has a longer length compared to cadherin which would decrease the influence of the nonlinear effect. To minimize this kind of influence for short interaction distance,

a possible way is to introduce spheres with protrusions then coated with molecules, which could increase the separating distance of cell-cell and cell-substrate interaction. Meanwhile, the model of hydrodynamic force analysis may need further modification.

To summary, in biological region where the ion concentration is high, it is important to take into account DLVO forces to study intermolecular forces more accurately. Since DLVO forces are ubiquitous forces in biological area, this effect may need to be considered in other cell-cell interaction measurement apparatus as well. This proposed correction would be beneficial for later data analysis of intercellular and molecular bond forces study.

6.5 Reference

1. Sun, C.H., C. Migliorini, and L.L. Munn, Red blood cells initiate leukocyte rolling in postcapillary expansions: A lattice Boltzmann analysis. Biophysical Journal, 2003. 85(1): p. 208-222.

2. Moy, V.T., E.L. Florin, and H.E. Gaub, Intermolecular Forces and Energies between Ligands and Receptors. Science, 1994. 266(5183): p. 257-259.

3. Merkel, R., et al., Energy landscapes of receptor-ligand bonds explored with dynamic force spectroscopy. Nature, 1999. 397(6714): p. 50-53.

4. Morrow, T., et al., Programmed assembly of DNA-coated nanowire devices. Science, 2009. 323(5912): p. 352.

5. Litvinov, R.I., et al., Binding strength and activation state of single fibrinogen-integrin pairs on living cells. Proceedings of the National Academy of Sciences of the United States of America, 2002. 99(11): p. 7426-7431.

6. Chu, Y., et al., Force measurements in E-cadherin-mediated cell doublets reveal rapid adhesion strengthened by actin cytoskeleton remodeling through Rac and Cdc42 JP Thiery and S. Dufour were co-principal investigators. Journal of Cell Biology, 2004. 167(6): p. 1183-1194.

7. Perret, E., et al., Fast dissociation kinetics between individual E-cadherin fragments revealed by flow chamber analysis. Embo Journal, 2002. 21(11): p. 2537-2546.

8. Thoumine, O. and J.J. Meister, Dynamics of adhesive rupture between fibroblasts and fibronectin: microplate manipulations and deterministic model. European Biophysics Journal with Biophysics Letters, 2000. 29(6): p. 409-419.

9. Bongrand, P., A.M. Benoliel, and A. Pierres, Studying molecular interactions at the single bond level with a laminar flow chamber. Cellular and Molecular Bioengineering, 2008. 1: p. 247-262.

10. Tha, S.P. and H.L. Goldsmith, Interaction Forces between Red-Cells Agglutinated by Antibody .3. Micromanipulation. Biophysical Journal, 1988. 53(5): p. 677-687.

11. Tha, S. and H. Goldsmith, Interaction forces between red cells agglutinated by antibody. I. Theoretical. Biophysical Journal, 1986. 50(6): p. 1109-1116.

12. Shankaran, H. and S. Neelamegham, Hydrodynamic forces applied on intercellular bonds, soluble molecules, and cell-surface receptors. Biophysical Journal, 2004. 86(1): p. 576-588.

13. Jeffrey, D. and Y. Onishi, The forces and couples acting on two nearly touching spheres in low-Reynolds-number flow. Zeitschrift für Angewandte Mathematik und Physik (ZAMP), 1984. 35(5): p. 634-641.

14. Nir, A. and A. Acrivos, On the creeping motion of two arbitrary-sized touching spheres in a linear shear field. Journal of Fluid Mechanics, 1973. 59(02): p. 209-223.

15. Goldman, A.J., R.G. Cox, and H. Brenner, Slow Viscous Motion of a Sphere Parallel to a Plane Wall .2. Couette Flow. Chemical Engineering Science, 1967. 22(4): p. 653-&.

16. Lyklema, J., Fundamentals of interface and colloid science. 2005: Academic Pr.

17. Smith, M.J., E.L. Berg, and M.B. Lawrence, A direct comparison of selectin-mediated transient, adhesive events using high temporal resolution. Biophysical Journal, 1999. 77(6): p. 3371-3383.

18. Hermansson, M., The DLVO theory in microbial adhesion. Colloids and Surfaces B-Biointerfaces, 1999. 14(1-4): p. 105-119.

19. Hayashi, H., et al., Soft particle analysis of bacterial cells and its interpretation of cell adhesion behaviors in terms of DLVO theory. Colloids and Surfaces B-Biointerfaces, 2001. 22(2): p. 149-157.

20. Rijnaarts, H.H.M., et al., DLVO and steric contributions to bacterial deposition in media of different ionic strengths. Colloids and Surfaces B: Biointerfaces, 1999. 14(1-4): p. 179-195.

21. Becker, J.W., et al., Topology of Cell-Adhesion Molecules. Proceedings of the National Academy of Sciences of the United States of America, 1989. 86(3): p. 1088-1092.

22. Arp, P.A. and S.G. Mason, Kinetics of Flowing Dispersions .8. Doublets of Rigid Spheres (Theoretical). Journal of Colloid and Interface Science, 1977. 61(1): p. 21-43.

23. Goldsmith, H.L., et al., Time and force dependence of the rupture of glycoprotein IIb-IIIa-fibrinogen bonds between latex spheres. Biophysical Journal, 2000. 78(3): p. 1195-1206.

24. Shankaran, H. and S. Neelamegham, Nonlinear flow affects hydrodynamic forces and neutrophil adhesion rates in cone-plate viscometers. Biophysical Journal, 2001. 80(6): p. 2631-2648.

25. Tees, D.F.J., O. Coenen, and H.L. Goldsmith, Interaction Forces between Red-Cells Agglutinated by Antibody .4. Time and Force Dependence of Break-Up. Biophysical Journal, 1993. 65(3): p. 1318-1334.

26. Brenner, H. and M.E. Oneill, Stokes Resistance of Multiparticle Systems in a Linear Shear Field. Chemical Engineering Science, 1972. 27(7): p. 1421-&.

27. Jeffrey, D.J., The Calculation of the Low Reynolds-Number Resistance Functions for 2 Unequal Spheres. Physics of Fluids a-Fluid Dynamics, 1992. 4(1): p. 16-29.

28. Jeffrey, D.J. and Y. Onishi, Calculation of the Resistance and Mobility Functions for 2 Unequal Rigid Spheres in Low-Reynolds-Number Flow. Journal of Fluid Mechanics, 1984. 139(Feb): p. 261-290.

29. Tissot, O., et al., Motion of Cells Sedimenting on a Solid-Surface in a Laminar Shear-Flow. Biophysical Journal, 1992. 61(1): p. 204-215.

30. Masliyah, J.H. and S. Bhattacharjee, Electrokinetic and Colloid Transport Phenomena. 2006: Wiley-Interscience.

31. Tha, S.P., J. Shuster, and H.L. Goldsmith, Interaction Forces between Red-Cells Agglutinated by Antibody .2. Measurement of Hydrodynamic Force of Breakup. Biophysical Journal, 1986. 50(6): p. 1117-1126.

32. Frojmovic, M.M. and J.G. Milton, Human platelet size, shape, and related functions in health and disease. Physiological Reviews, 1982. 62(1): p. 185-261.

33. Bostrom, M., D.R.M. Williams, and B.W. Ninham, Specific ion effects: Why DLVO theory fails for biology and colloid systems. Physical Review Letters, 2001. 87(16).

34. Bongrand, P. and G.I. Bell, Cell-cell adhesion: Parameters and possible mechanisms, in Cell Surface Dynamics: Concepts and Models, A. Perelson, C. DeLisi, and F.W. Wiegel, Editors. 1984, Marcel Dekker: New York. p. 459-493.

35. Tandon, P. and S.L. Diamond, Hydrodynamic effects and receptor interactions of platelets and their aggregates in linear shear flow. Biophysical Journal, 1997. 73(5): p. 2819-2835.

36. Van Oss, C.J., Interfacial forces in aqueous media. 2006: CRC.

37. Dukhin, A., et al., Peculiarities of live cells' interaction with micro-and nanoparticles. Advances in Colloid and Interface Science, 2010.

CHAPTER 7

7 AN IN-VITRO VASCULAR MIMETIC MODEL: ENDOTHELIAL DYSFUNCTION STUDY DURING THE PROGRESSION OF ATHEROSCLEROSIS

7.1 Introduction

7.1.1 Atherosclerosis and Endothelial Dysfunction

Atherosclerosis [1, 2], a disease of the arteries, is the most prominent cardiovascular diseases and the primary cause of heart disease and stroke. It is the chief cause of death in most western world and Europe, and also becomes prevalent in developing counties. Research has revealed that atherosclerosis is a multi-factor lesion and a chronic inflammatory disease which could also convert into an acute clinical event by plaque rupture and thrombosis [3]. The underlying pathophysiology of atherosclerosis and its associated risk factors are still unclear.

Endothelial dysfunction has been associated with a number of cardiovascular diseases. It is believed that an early stage of atherosclerosis is endothelial dysfunction [4, 5]. In response to physical and chemical stimuli, endothelial cells (ECs) synthesize and release a number of factors that regulate inflammatory responses, hemostasis and vascular tone. The impairment of physiological situation in different pathologies modifies the amount of secretory substances including vasodilator substance, fundamentally nitric oxide (NO) [5], anticoagulants and

antiplatelets. In addition, the increase of proinflammatory molecules induces procoagulant, vasoconstrictor and proinflamatory conditions [1, 6].

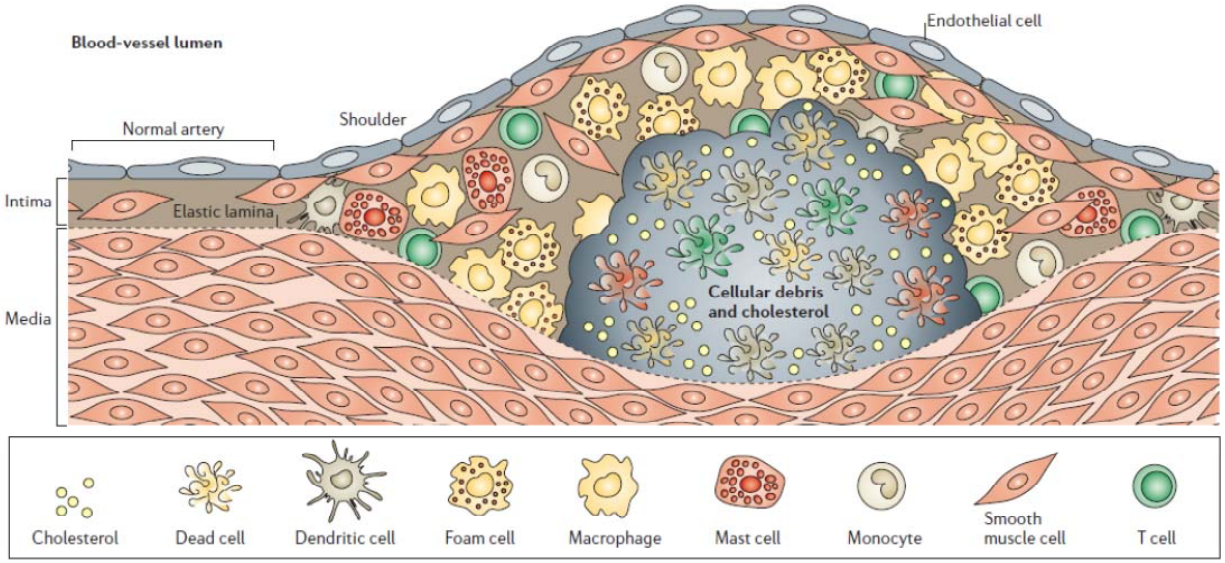

Figure 7-1. Cellular composition of atherosclerotic plaques. Atherosclerotic plaque contains a variety of components including cellular debris, cholesterol and etc. A fibrous cap formed by smooth muscle cells stabilizes the plaque ensures a relatively quiescent status of the plaque. ECs continue serving as sensors to detect physical date from the blood flow, which regulates the vascular tone and determine the fate of the blood vessel. Reproduced from [7].

Atherosclerosis can occur in any artery in the body, especially crucially in the heart. Figure 7-1 illustrates the atherosclerotic plaque which has changed the geometry of the local blood vessel dramatically. The developed atherosclerotic plaque inducing arterial remodelling [8] may cause ECs to be subject to a changed stimuli such as mechanical response due to the new and disturbed blood flow pattern, which will increase the risk of atherosclerotic development. What is more, the response of ECs induced by the redistribution of wall tension at the plaque forming region needs to be investigated. Cell morphology, biomechanical properties and functions are highly sensitive to microenvironment; thus, ECs exhibit characteristics that vary with anatomic location. Different types of shear stress regimens have diverse effects on ECs and may account for

variable responses of ECs to hemodynamics in the circulation [9]. Although atherosclerotic lesion occurs in almost every individual, not each lesion will lead to clinical events while some plaques remain quiescent during the whole life.

Animal models have proved that the branched vascular vessels with disturbed flows are recognized as atheroprone sites. However, it is still incompletely clear that why and how atherosclerosis is further developed and promoted after the formation of subclinical plaques. In literature study, biomechanical factor, such as shear force stress [10, 11], has been reported as one of the most common contributing factors of atherosclerosis. ECs subject to different physical forces will initiate different signalling pathways [12]. The abnormal hemodynamic property locally may become as promoter of atherogenesis [13, 14].

7.1.2 Bio-inspired Vascular Mimetic Model

The use of animal models often comes across feasibility and ethical concerns. The limitations were addressed by developing different in vitro models to replicate the functions in vivo. Microfluidic techniques have been developed and applied in biological assays for about two decades. Various bio-mimic models that reconstitute the critical functions from in vivo tissues or organs were developed by researchers [15, 16]. These models provide repetitive and quantitative investigation for research. With higher level integration, these bio-inspired models can be potentially used for drug discovery and clinical studies in the future. Compared to traditional culturing methods, microfluidic culture allows controlling precisely the microenvironment, and in particular sensing subtle change of experimental parameters controlled. More importantly, microfluidic culture technique is to recapitulate the in vivo microenvironment more

physiologically. To date, the construction of tissue-engineered devices and even the reconstitution of organ level function [16] for biomedical application are now possible.

In this study, an in vitro model to mimic in vivo physiological environment based on microfluidic platforms was developed to simulate the formation of atherosclerotic plaque. The responses of cells to external stimuli in vivo can be contributed by various influences such as cells interactions with other cells and the extracellular matrix. However, these interactions are difficult to be replicated by traditional cell culture systems. ECs, lining the innermost surfaces of blood vessels, perform critical homeostatic functions [3] and act as selective filters between blood and interstitial tissue. In order to mimic blood vessels more precisely, ECs based vascular mimetic microfluidic platform was developed. During the progression of atherosclerosis, the "fatty streak" will continuously change the local microenvironment, which will contribute to potential endothelial dysfunction at the atherogenesis prone site. Meanwhile, the changed local hemodynamic environment may also enhance the recruitment of immune cells into the atheroprone site. Thanks to microfluidic technology, this disease state will be mimicked by the pneumatic valve technique through constructing a multilayer microfluidic system. Combining with computational fluid dynamic (CFD) simulation, the flow profile and shear stress distribution can also be fully illustrated. The bio-inspired vascular mimetic model can be used to study the fundamental mechanisms of atherogenesis especially how atherosclerosis was promoted after the formation of early plaques.

7.1.3 AFM and Cell Biology

Changes of tissue level property are often manifested at the cellular scale. Research has shown that mechanical property of atherosclerotic tissue is distinct at the plaque region [17]. Atomic

force microscope (AFM) has been used to study the biomechanical property of vascular artery tissue with developed atherosclerosis [18]. We proposed to study endothelial dysfunction from an indirect way by investigating the change of biomechanical properties of endothelial cells.

7.1.4 Objectives

In this study, a cell-based in vitro vascular mimetic model was developed from microfluidic cell culture system. With microfluidic technology and pneumatic micro-valve technique, the model is able to simulate the formation of atherosclerotic plaque. The development of atherosclerosis involves with a complex interaction between immune cells, endothelium, vascular smooth muscle cells and cytokines [19]. The recruitment of blood monocytes is a required step at the early atherosclerotic lesion. With this model, the hemodynamic effect on the rolling and adhesion events was investigated. Combined with AFM, this model was used to examine the biomechanical property, including elasticity and viscoelastcity especially the membrane performance, of endothelial cells after the development of atherosclerotic plaque.

Overall, the proposed research involves using an in-vitro vascular mimetic model to investigate endothelial dysfunction during the development of atherosclerosis. The objective is to develop a functional in-vitro artificial vascular system to mimic the development of atherosclerotic plaque. In addition, AFM was used to investigate endothelial dysfunction. The biomechanical property change of ECs is taken as pathogenesis indicator to explore the mechanism of atherogenesis. This bio-inspired in-vitro model could also be employed in various applications such as drug screening and toxicity study.

7.2 Experimental Procedures

7.2.1 Design and Fabrication

In this study, a three-layer PDMS structure was designed to mimic the atherosclerosis model. Poly(dimethylsiloxane) (PDMS) is typically used for microfluidic systems research as the primary substrate material of many prototype devices. Except the prerequisite biocompatibility, PDMS possesses many desirable qualities required in this research, including high flexibility, low chemical reactivity and high formability via softlithography [20]. In addition, the transparency is another important property which assists the following examination by light microscope. PDMS has relatively low elastic modulus [21] which makes it an ideal material for making thin membrane, which can be easily deformed through applying pneumatic pressure. Overall, PDMS is an ideal material to build up the model to mimic blood vessel and simulate the formation of atherosclerotic plaque in vitro.

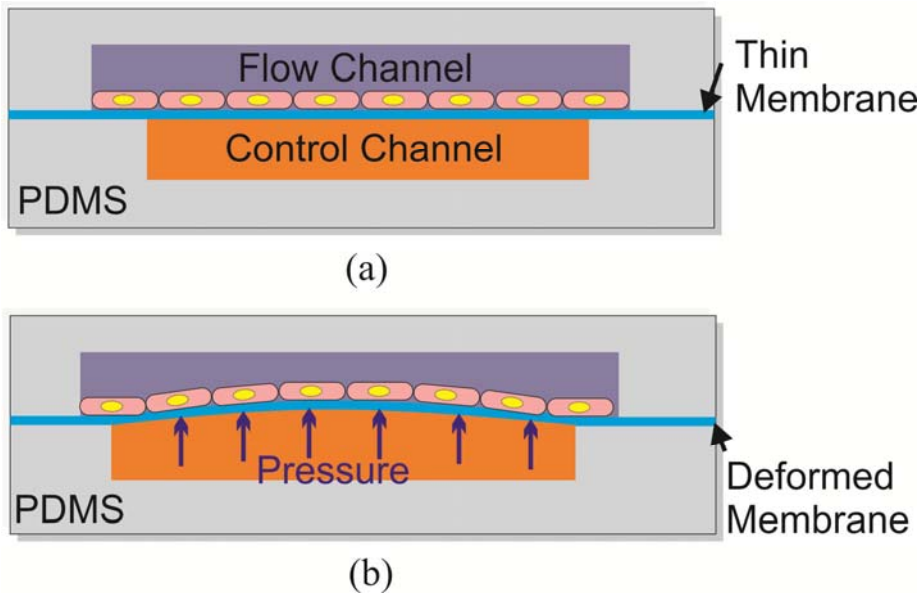

Figure 7-2. The schematic of pneumatically activated microfluidic valve design. (a) Original state of the flow channel and control channel; (b) the deformed shape of flow channel under the pressurization from the control channel.

Figure 7-2a shows the schematic of three-layer PDMS structure. This model was originated from the pneumatically activated microfluidic valve design. The upper layer is covered by a thin PDMS membrane forms the flow channel. The substrate, which has open channels, is bonded with the other side of the thin membrane to form the control channel. Figure 7-2b shows pressure applied in the control channel through connecting the control channel with auxiliary equipment such as gas cylinder. The pressure will deflect the thin PDMS membrane and squeeze the upper channel layer, which is coated with monolayer of endothelial cells.

Mold Fabrication:

The detail of mold fabrication process was described in chapter 5. Depending on the desired size of the channel, either photolithography method or micromachining method can be applied. Two

mold masters were fabricated, one is used for cell culture channel and the other is for control layer.

Thin Membrane Fabrication:

Normally, PDMS solution is poured in a flat bottom container such as petri-dish to create a block of elastomer with desire thickness. However, due to the high viscosity, the thickness of PDMS can't spread uniformly on the substrate. In this study, we used hexane to dilute the PDMS solution to decrease the viscosity and hydrophobicity of the solution. A weight ratio of 1:1 for hexane and PDMS mixture was used. The weight ratio could also vary according to the desired thickness of the PDMS membrane. The diluted solution can easily spread at the bottom of the petri-dish which placing the petri-dish on a horizontal substrate.

Multi-layer PDMS:

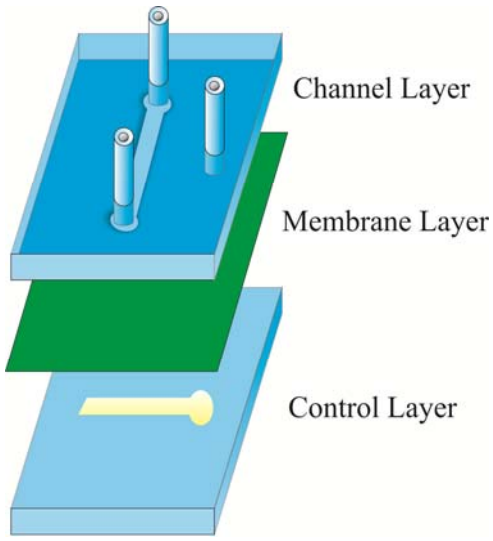

Figure 7-3. Multi-layer PDMS device, the three layers are the channel layer, the membrane layer and the control layer.

PDMS is shipping in two parts: the base and curing agent. The mixing ratio of base and curing agent at 10:1 is used to crosslink the liquid polymer and obtain a solid elastomer. PDMS can be cured at various temperatures by controlling the curing time. It takes 24 hours to cure at room temperature and 2 hours at 80^{o}C. Higher temperature can also be used to further reduce the curing reaction time. The flexible curing time is beneficial for the bonding process which will be detailed described in the following content.

The bonding between each layer of PDMS is critical for successfully fabricating a multi-layer PDMS device. Figure 7-3 describes the schematic of three separate layer used in this study, the channel layer, the membrane layer and the control layer. In the channel layer, there are three tubes inserted in the PDMS block. The detailed procedures of making an integrated microfluidic channel using PDMS and silicone tubes were describe in chapter 5. Here I will not repeat the process. Two of the tubes function as the flow inlet and the flow outlet for the cell culture. In order to make all the connections to peripheral equipments from the top layer, I moved the tube from the bottom layer to the top layer. The third tube which will be connected to the bottom control layer functions as the pressure inlet.

Bonding Process:

One of the key benefits of using PDMS as materials for all the three layers lays the ability of PDMS bonding to itself easily through relative simple methods. In the following I will briefly discuss three methods which were tried and used in this study.

The first method is plasma bonding. To plasma bonding, a clean surface has to be ensured. The bonding sides of PDMS were taped to remove any dust and cloth. Once cleaned, both substrates

were placed in the vacuum chamber of oxygen plasma equipment (STS Plasma Enhanced Chemical Vapour Deposition, Western Nanofabrication facility). After exposed to oxygen plasma for 30s, the methyl groups on the surface were replaced by a large number of hydroxide groups. Within 10 minutes, the two substrates were bonded together and bake at 60^{o}C to 75^{o}C for at least 30 minutes.

As mentioned, the curing process could be controlled by both temperature and time. The second method requires controlling the temperature and curing time. The following protocol was taken to achieve a relatively permanent bonding.

1. Mix the PDMS solution (50 g) with the base and curing agent at ratio 10:1.
2. Take 2 ml of PDMS solution and dilute it with hexane (weight ratio: 1:1), mix the new diluted PDMS solution thoroughly using vortex mixer.
3. Pour 20 ml PDMS solution on the master of top layer which was silicone tubes on it, and pour 15 ml PDMS solution on the master of the bottom layer. Pipette 3 ml diluted PDMS solution and spread on the 100 mm petri-dish, then put the petri-dish on a flat surface.
4. Heat the top layer at 60^{o}C for 1.5 hours and the bottom layer for 1 hour; peel off the top layer and use tweezers to take off the adhesive to open the tubes
5. Heat the membrane at 75^{o}C for 10 minutes and place the top layer on the membrane. Then heat the two layers together for 20 minutes.
6. Peel off the top layer with the membrane and open the pressure inlet with tweezers; then peel off the bottom layer flip the channel side to top and bond to the other size of the membrane. Heat the whole device at 80^{o}C for another hour and press the device slight using a weight.

The difference between the second and third methods is that the ratio of the base to curing agent. In the third method, instead of using 10:1 as ratio for all the three layers, the top and bottom layers use ratio of 30:1 while the membrane uses 3:1. The idea is leaving extra reaction sites for the base and curing agent to continue crosslinking after they are bonding together.

7.2.2 Bio-inspired Model Mimicking Formation of Atherosclerotic Plaques

Cell Culture: Human aortic endothelial cells (HAEC, Lonza) were grown in Endothelial Growth Medium-2 (Lonza, supplemented with EGM2 kit). Cells were incubated in a humidified, 5% CO_2 environment at 37°C. Cells were passaged after they reached 70% confluency using Trypsin-EDTA (0.05% Trypsin; 1 mM EDTA·4Na, Invitrogen). Passages 5-6 were collected in the 1 ml sterile freezing vial (90% Fetal Bovine Serum and 10% Dimethyl sulphoxide) and Passages 7-8 were used for the following experiments.

Jurkat cells were cultured in RPMI 1640 medium (Sigma Aldrich, Canada) supplemented with 1% glutamine, 100 U/ml penicillin, 100 μg/ml streptomycin and 10% fetal bovine serum (FBS).

Device Treatment and Cell Loading: It includes the following main steps, autoclaving the device, coating with extracellular matrix molecules, loading cells and culture cells with perfusion. All the detail procedures were described at the culture processes in chapter 5.

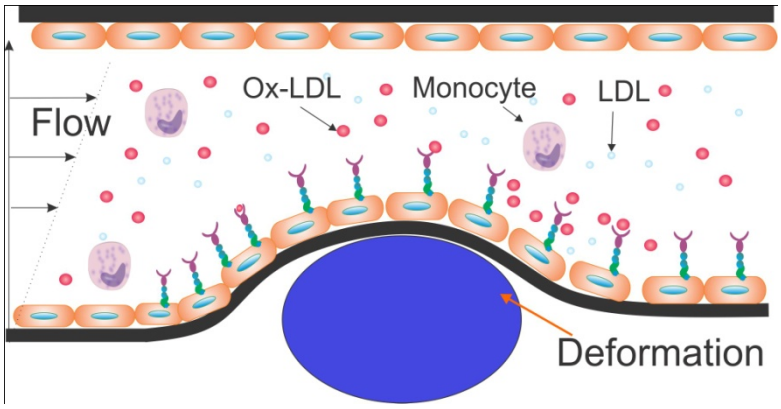

Figure 7-4. The schematic of the changed blood vessel caused by the formation of atherosclerotic plaque. The blue ellipse indicates the formation of plaques.

When human aortic endothelial cells were introduced into the growing channel, they attached to the pre-coated extracellular matrix (ECM) and formed a monolayer after around 24 hours. The time for cells growing into confluent largely depends on the loading density. Cells remained viable as the fresh media equilibrated with CO_2 and O_2 perfuse into the channel for the following days. After the cells grew into confluent, the control channel which had been connected to another syringe pump was activated to deform the membrane. This bump structure was used to simulate the plaque formed during the generation of atherosclerosis, which will narrow the blood vessel as shown in Figure 7-4.

7.2.3 Fluid Dynamics, Cell Rolling and Cell adhesion

Due to the formation of the plaque in the blood vessel, the flow profile became disturbed. In order to examine the flow profile and shear force distribution in the channel, CFD simulation was performed using Ansys Fluent software. In this study, we used CFD simulation to examine the detail profile at the disease site of the blood vessel.

After cells growing at the deformation state of the membrane for another 8-12 hours, endothelial cells were treated with tumour necrosis factor alpha (TNF-α, 200 units/ml) for 60 minutes to activate the adhesion molecules. Then Jurkat cells (5×10^5 cells/ml) were injected into the channel with different flow rate to investigate the rolling flux, rolling speed and cell adhesion event using light microscope. The rolling speed was calculated from the video recorded with CCD camera.

7.2.4 Immunofluorescence

10 mL of prewarmed phosphate-buffered saline (PBS, pH 7.4) was filled into the syringe. The sample was rinsed with around 2 ml of PBS by connecting the syringe to the inlet and fixed by 3.7% formaldehyde solution in PBS for 10 minutes at room temperature, followed by washing cells with another 2 mL PBS. Cells were permeabilized with 0.1 % Triton X-100 in PBS for 3 minutes, washed by PBS and blocked with 1% bovine serum albumin (BSA) for 20 minutes. Then cells were stained with FITC conjugated phallotoxins (Sigma) at a final concentration of 10 μg/mL for 30 minutes. The sample was washed with 10 mL PBS. An optional staining of nuclei was followed. Cells were stained with Hoechst 33342 at a final concentration at 5 μg/mL in PBS for 10 minutes and washed with PBS. Then the sample was filled with fluoroshield and examined by fluorescent microscope (IX81, Olympus).

7.3 Results

7.3.1 Characterization of the Device and Cell Morphology

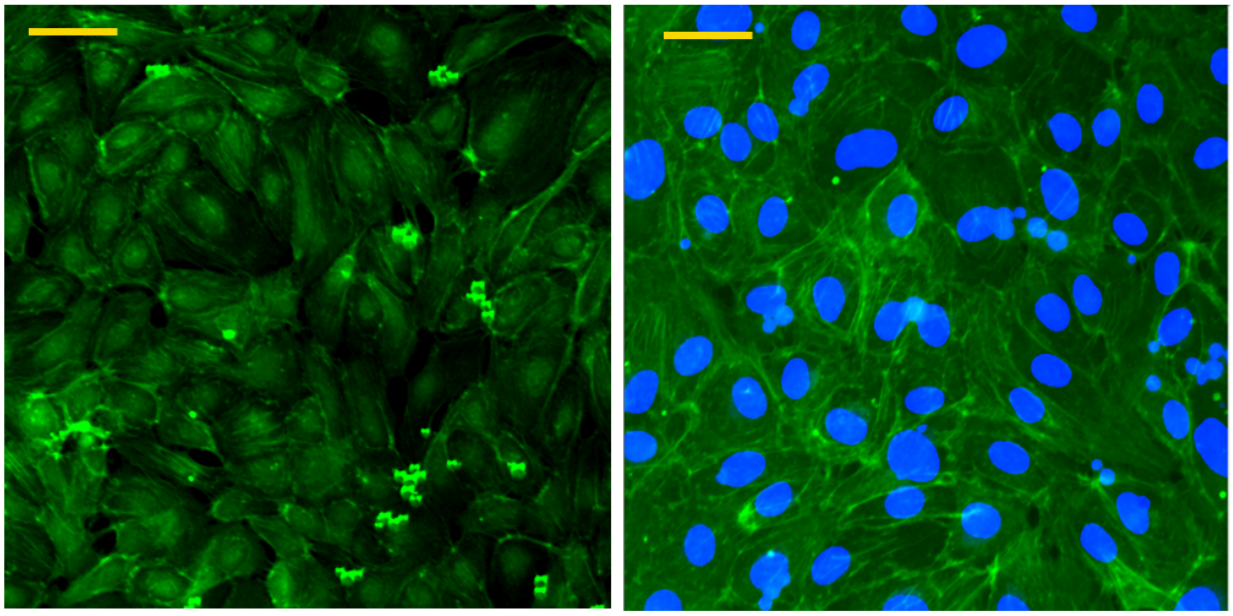

Figure 7-5. Endothelial cell growing in the channel into confluent at low flow rate (0.1 dyne/cm^2). (a) Staining of actin fibres; (b) staining of actin fibres and nuclei. The scale bar is 50 μm.

After loading and attachment, endothelial cells were cultured for around 24 hours under relatively lower shear stress (0.1 dyne/cm^2) before initiating the deformation. The time for cells to become confluent depends on the density of cell loaded and cell number at confluence varies from 1000 cells/mm^2 to 2500 cells/mm^2. The channel has a culture area of 0.12 cm^2 (0.6 mm × 20 mm) and height as 0.4 mm which mainly determines the loading density of cells. With an initial loading density of 1.6 × 10^6 cells/mL for this type of channel, Figure 7-5 shows cells grown for around 20 hours and 24 hours respectively, which shows that cells could grow into

confluent in around 20-24 hours. We found that F-actin didn't show obvious alignment when shear force is low.

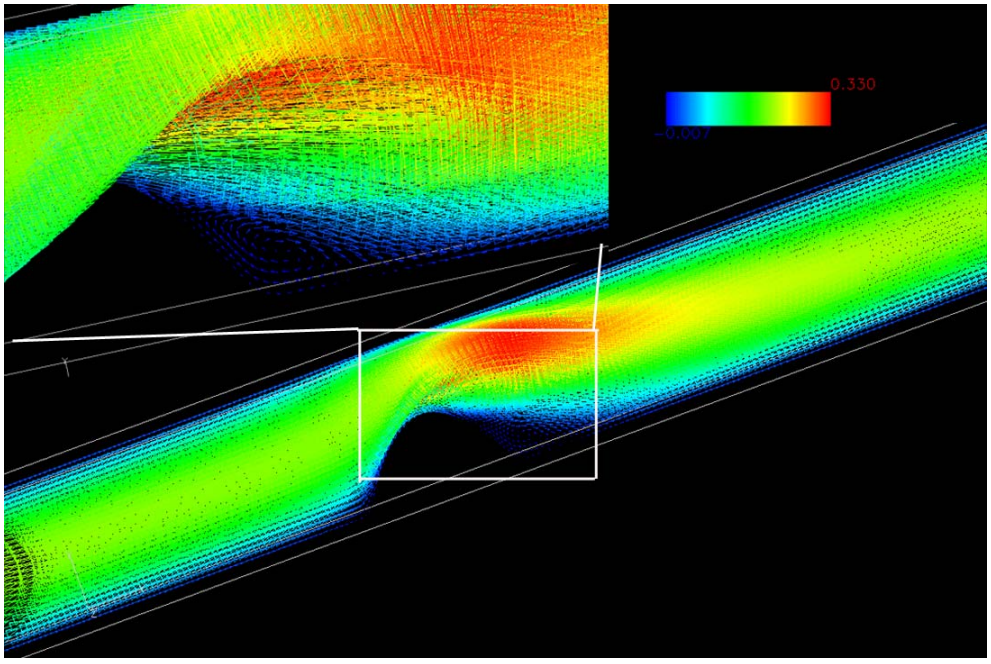

(a)

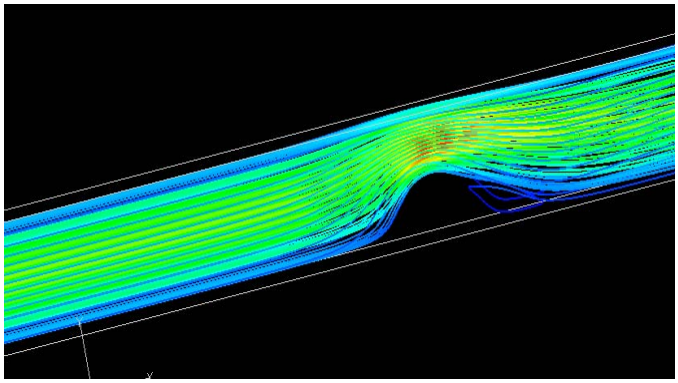

(b)

Figure 7-6. Stream lines of the flow inside the channel with a 50% blockage of the channel. (a) Streamlines of the flow in the channel; (b) particle tracking shows the disturbance of the flow.

The flow profile and shear force distribution were evaluated with computation fluid dynamic simulation by Ansys Fluent. The simulated atherosclerotic plaque models were built in Gambit 2.4.6. Figure 7-6 shows the streamlines of the flow profile at 50% blockage of the blood vessel condition. When the shear stress becomes higher to a threshold, eddies became evident at the downside of the deformation position.

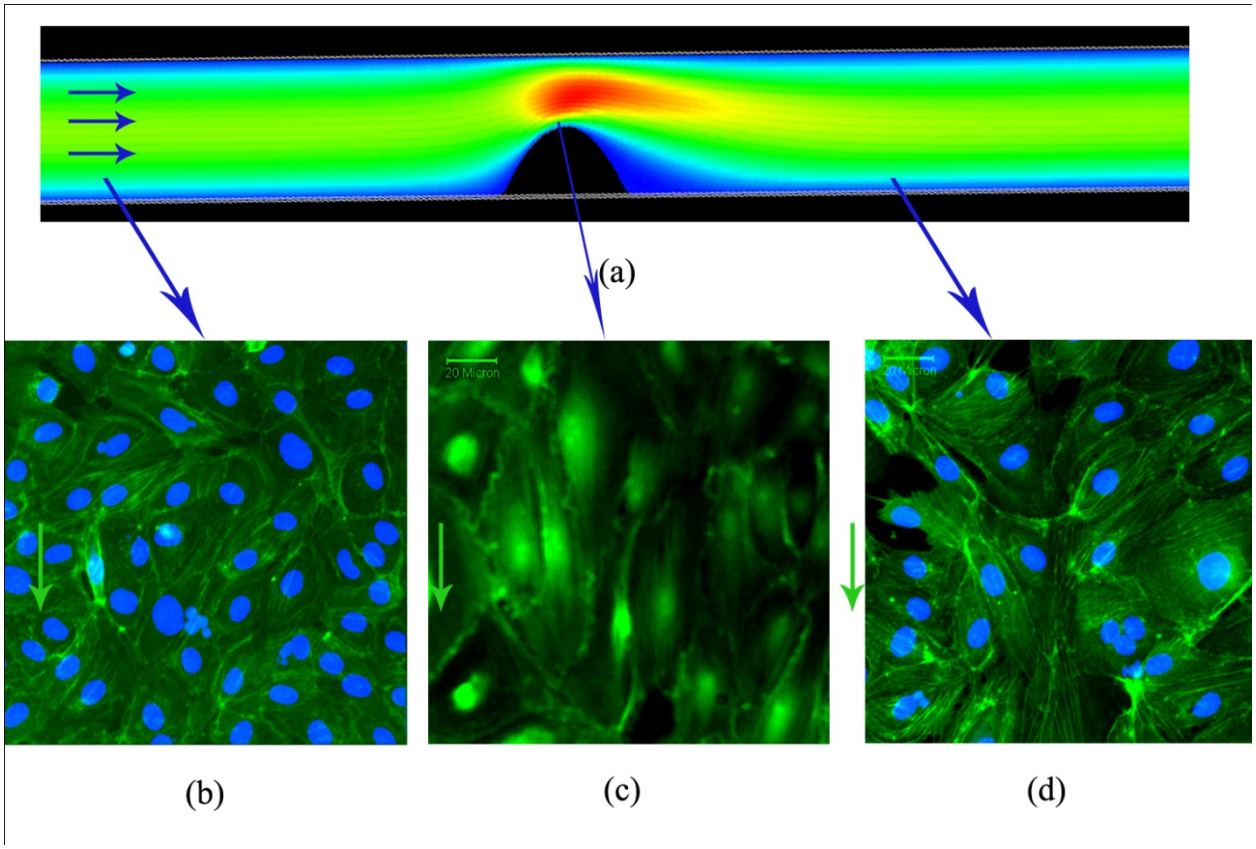

Figure 7-7. The response of ECs after introducing higher shear rate for around 8 hours. (a) The contour of velocity profile; (b), (c) and (d) are cells from different sites indicated by the arrows.

After cells have grown into confluent, the membrane was deformed by the pneumatic pressure. The responses of ECs under different shear force from different location in the channel were examined. Figure 7-7a shows the contour image coloured by velocity magnitude from the simulation results. Figure 7-7b shows cells from a normal site (upstream and away from the deformation site), Figure 7-7c are cells from the higher shear force part (on top of the deformation) and Figure 7-7d shows cells from the site with disturbed flow (downside of the

deformation). Both normal sites and top of the plaque showed alignment of actin fibres while the downside of the plaque didn't show obvious alignment of stress fibres.

7.3.2 Hemodynamic Force and Biomechanical Properties of ECs

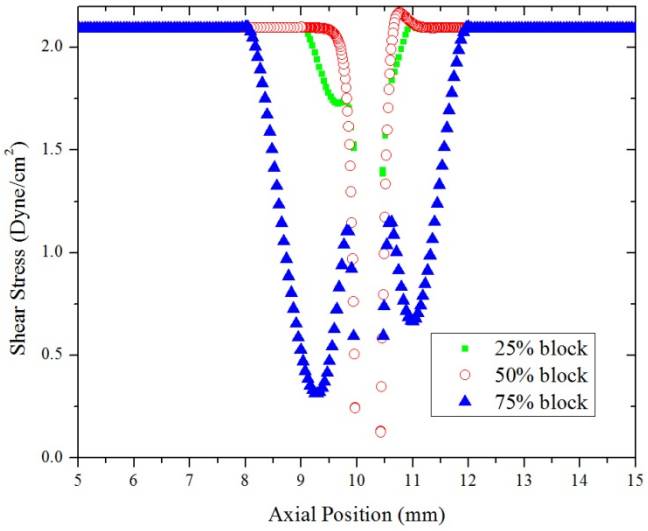

Figure 7-8. The distribution of shear stress on the walls, excluding the deformation part, for different scale of vascular blockage under the same flow at the inlets. Green circle represents 25% blockage; red hollow circle indicates 50% blockage, and blue triangles illustrates 75% blockage of the blood vessels.

Endothelial shear stress plays a critical role in the development of atherosclerosis. Recently, research shows new insight into atherosclerosis that endothelial shear stress acts as promoter rather than initiator during the development of atherosclerotic lesion [22]. Figure 7-8 shows the distribution of endothelial shear stress at the normal sites after the development of atherosclerotic plaque. Shear stress at the wall shows larger scale of disturbance as the magnitude of the blockage increases. A considerable amount of research from in-vivo, ex-vivo and in-vitro has been accumulated to show the responses of ECs under shear stresses. Other than morphology,

shear stress also affects the function, gene expression and more importantly, the biomechanical property of ECs, which will be investigated in the following study.

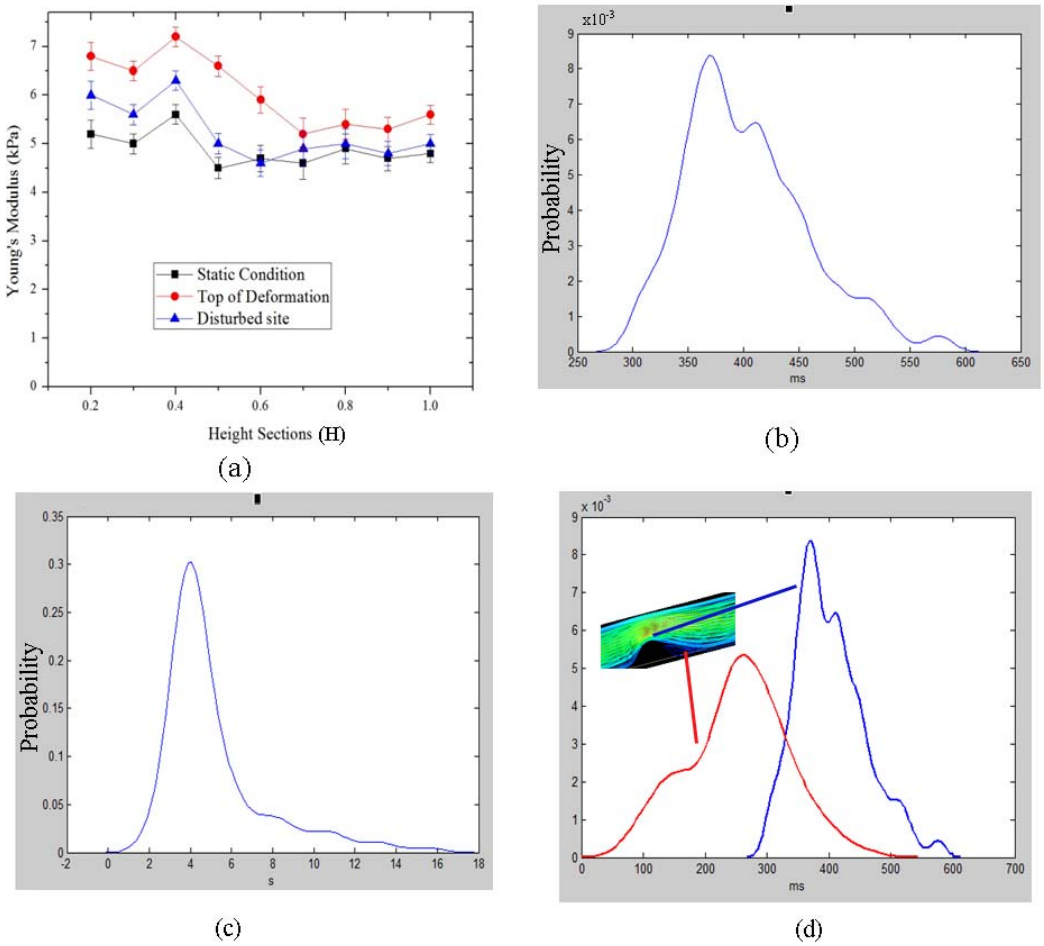

Figure 7-9. The biomechanical properties of ECs at different conditions. (a) The elastic moduli for cells at different conditions. H=1 is the top of the cells. Young's moduli for cells at static condition is 4.9 ± 0.22 kPa; while on top of deformation with higher shear stress is 6.05 ± 0.26 kPa and at disturbed site is 5.24 ± 0.21 kPa; (b) and (c) are the two stress relaxation times for viscoelastic measurement for ECs on top of the deformation; (d) the comparison of shorter relaxation time, corresponding to the membrane property, between ECs on top of the deformation and at the disturbed site.

Figure 7-9 shows the biomechanical properties of ECs from various sites in the channel. Figure 7-9a shows the comparison of Young's moduli for cells at static condition, higher shear force condition (on top of the deformation) and disturbed site (at the downhill site of the deformation) inside the channel. It illustrates that Young's moduli of ECs on top of the deformation site are

highest; cells from the disturbed sites show very similar elasticity with cells at static condition, and a little higher than that of static conditions at lower height sections. This might be caused by the relatively higher density of action stress fibres at the lower height sections at the disturbed sites.

The viscoelastic responses of ECs were also investigated. Figure 7-9b and c shows the stress relaxation times for endothelial cells from the top of the deformation site. As we have discussed in Chapter 3, the membrane property can be identified from the value of shorter stress relaxation time τ_1. Therefore, the shorter stress relaxation time of cells from the top and disturbed area was compared. Figure 7-9d shows that cells from the disturbed area have a smaller τ_1 than that from other locations, which may contribute to form more compliant property of cell membrane at these sites.

7.3.3 Rolling Flux and Rolling Velocity of Immune Cells

In order to predict the relation between adhesion parameters and changed biomechanical environment, rolling flux and rolling velocity of Jurkat cells were measured at different axial positions in the channel. Jurkat cells are T lymphocyte cells, which were transfected to express $\alpha_4\beta_1$ (VLA-4) and $\alpha_5\beta_1$ to specifically interact with vascular adhesion molecule-1 (VCAM-1) and intercellular adhesion molecule-1 (ICAM-1). Alpha(4) integrin has important role in the recruitment of leucocytes [23]. VLA-4 plays a critical role in supporting the tethering and rolling in shear flow [24]. The channel, coated with a monolayer of ECs and deformed under the channel, is closely mimicking the blood vessel with the formation of atherosclerotic plaque. ECs were activated by tumor necrosis factor alpha (TNF-α) to induce adhesion molecules knows as ICAM-1, VCAM-1, and E-selectin [25] to help simulate the inflammatory effect. In order to

characterize the effect of altered hemodynamic force at various locations of the blood vessel after the formation of atherosclerotic plaque, the recruitment density of immune cells were studied.

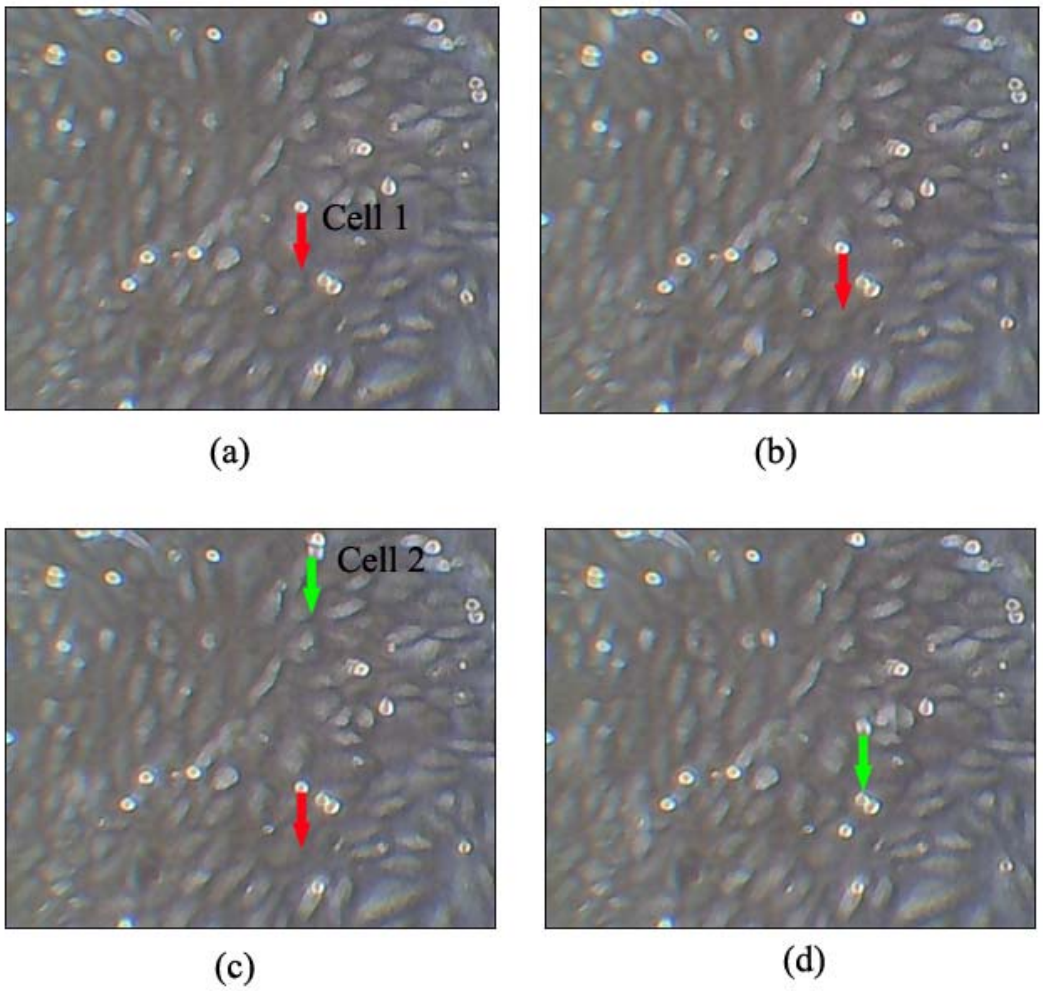

Figure 7-10. Cells rolling on the endothelium. The red arrow indicates the rolling of cell 1 at 5.2 μm/s while the green arrow indicates cell 2 which has a higher rolling speed at 22 μm/s. The time spot of the timeline for them are (a) 5.67 s, (b) 9.97 s, (c) 11.27 s and (d) 14.53 s.

Figure 7-10 shows a typical rolling event for immune cells on top of endothelial cells. Cell 1 has lower rolling speed compared to cell 2. In this specific case, cell 1 finally adhered on the monolayer of endothelial cells while cell 2 escaped.

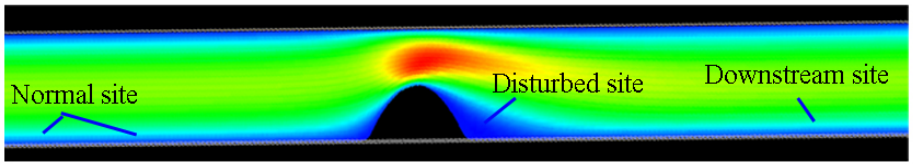

(a)

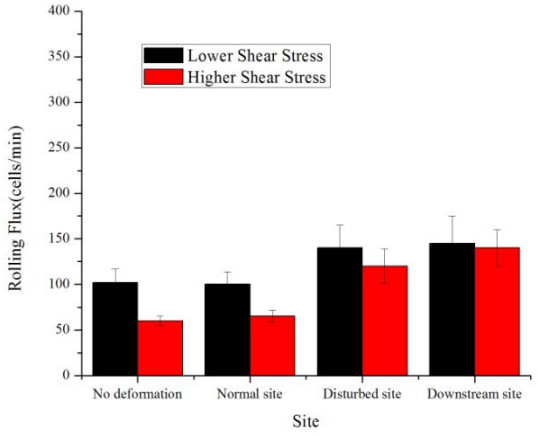

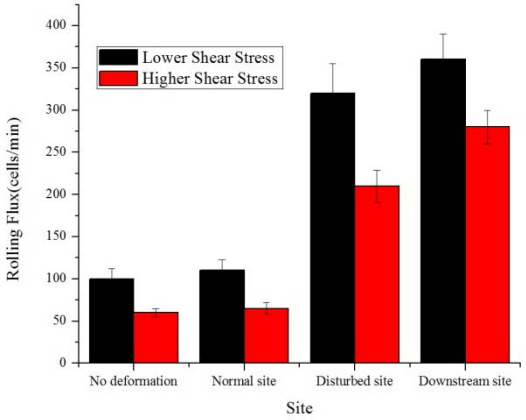

(b) (c)

Figure 7-11. Rolling flux of Jurkat cells at different location in the channel. Error bars are SD from n > 3 experiments. No deformation refers to control experiment without blockage. (b) and (c) are the cases for 25% and 50% blockage of the channel respectively. High and low shear forces are 15 dyne/cm^2 and 1.5 dyne/cm^2, respectively. From ANOVA test, the difference between normal site and disturbed site is not significant for 25% case ($p = 0.068$) and significant for 50% case ($p < 0.05$).

The rolling flux of Jurkat cells at different location in the simulated blood vessel was examined and the results were shown in Figure 7-11. It shows that the rolling flux at the disturbed shear stress site increased around three times as compared to the upstream normal sites for 50% blockage of the channel and the difference was significant (ANOVA test, $p < 0.05$), while 25% blockage indicates less increasement and the difference was not significant (ANOVA test, $p = 0.068$).

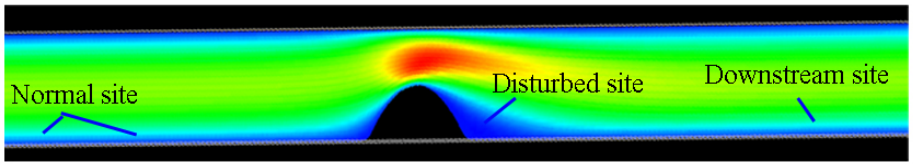

(a)

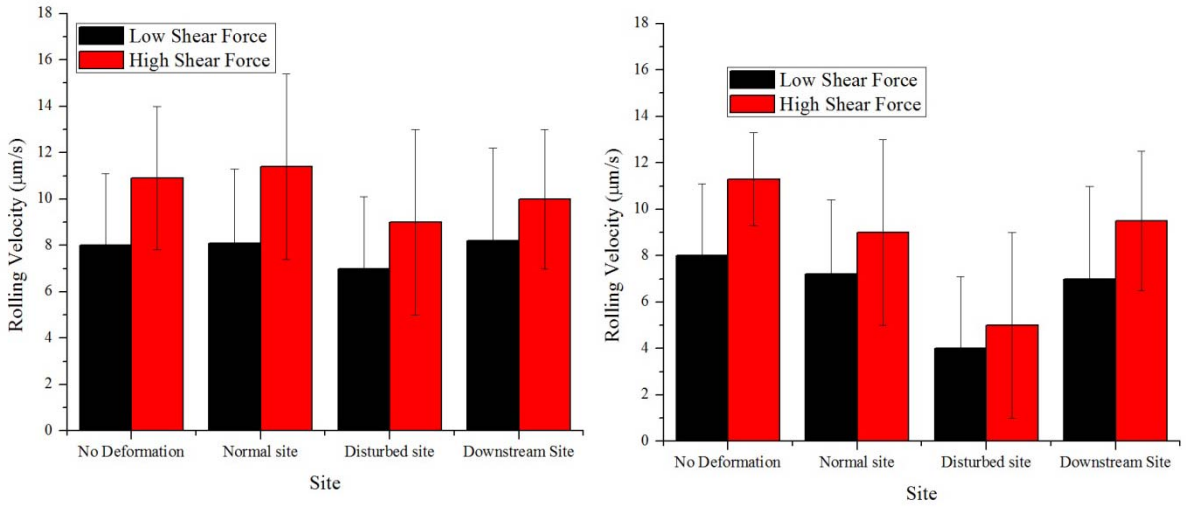

(b) (c)

Figure 7-12. Rolling velocity of Jurkat cells at different location in the channel. Error bars are SD from n > 10 cells. No deformation refers to control experiment without blockage. (b) and (c) are the cases for 25% and 50% blockage of the channel respectively. From ANOVA test, the difference between normal site and disturbed site is not significant for 25% case ($p = 0.23$) and significant for 50% case ($p < 0.05$).

Figure 7-12 illustrates the average rolling speed at different locations. The rolling speed varies from different locations with different shear stress. After the cells passed the plaque to the disturbed sites, the rolling velocity shows a decreasing trend, which indicates the disturbed shear

stress will increase the possible adhesion events. However, the rolling speed doesn't have a linear relationship with the shear stress. For the higher shear force (above 15 dyne/cm^2), the rolling speed doesn't show prominent increase compared to the lower shear force case (1.5 dyne/cm^2). Indeed, some cells even showed lower rolling speed at higher shear force, which may be contributed by multiple bonds or catch bonds.

Overall, the rolling speed has a range from several micrometers to tens of micrometers per second. The disturbed shear force has shown significant effect on both the rolling flux and rolling velocity of Jurkat cells. From shear force distribution at the atheroprone site, we found that there is a gradient shear force distribution at the downstream side of the plaque, which may be the reason that rolling cells tend to decrease the rolling speed when cells flow downward from the plaque, which may contribute to higher adhesion density at the disturbed and downstream sites.

7.3.4 Adhesion of Immune-cells

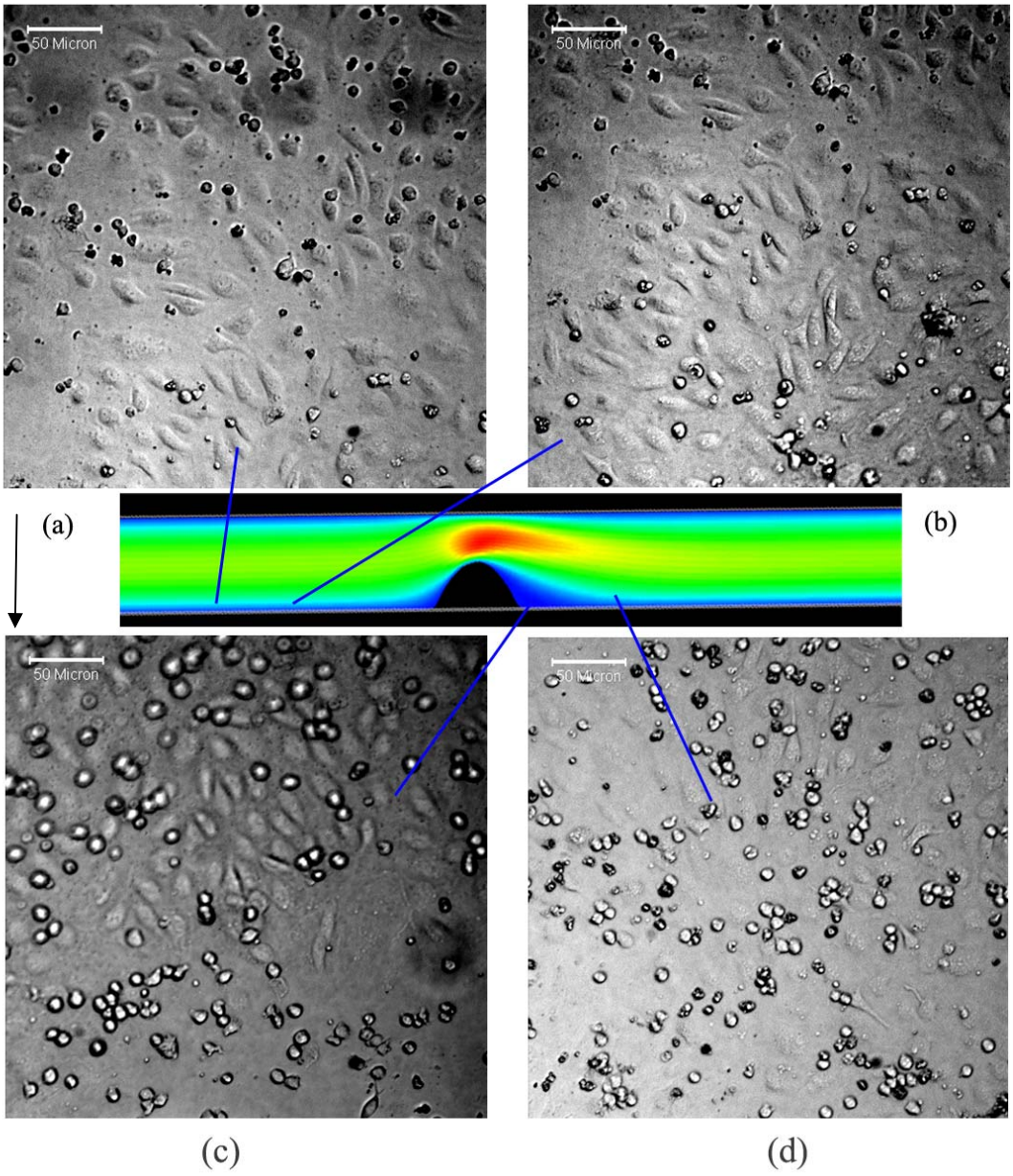

Figure 7-13. Adhesion evens of Jurkat cells at different locations of the blood vessel. Those blue lines indicate the positions where the adhesion events were taken. The arrow indicates the flow direction.

Figure 7-13 shows the adhesion events for Jurkat cells at the different sites of the channel. Figure 7-13a and b were the taken from the upstream of the channel. Figure 7-13c was from the downside of the plaque in the channel. Figure 7-13d is taken from the downstream of the channel.

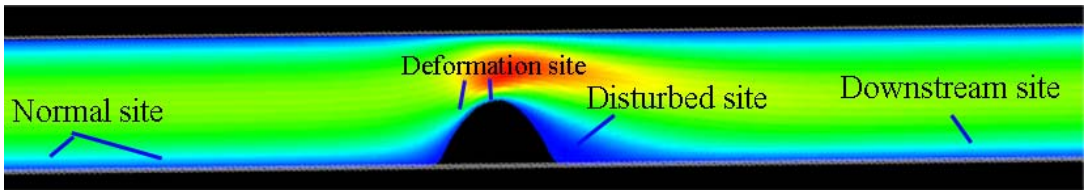

(a)

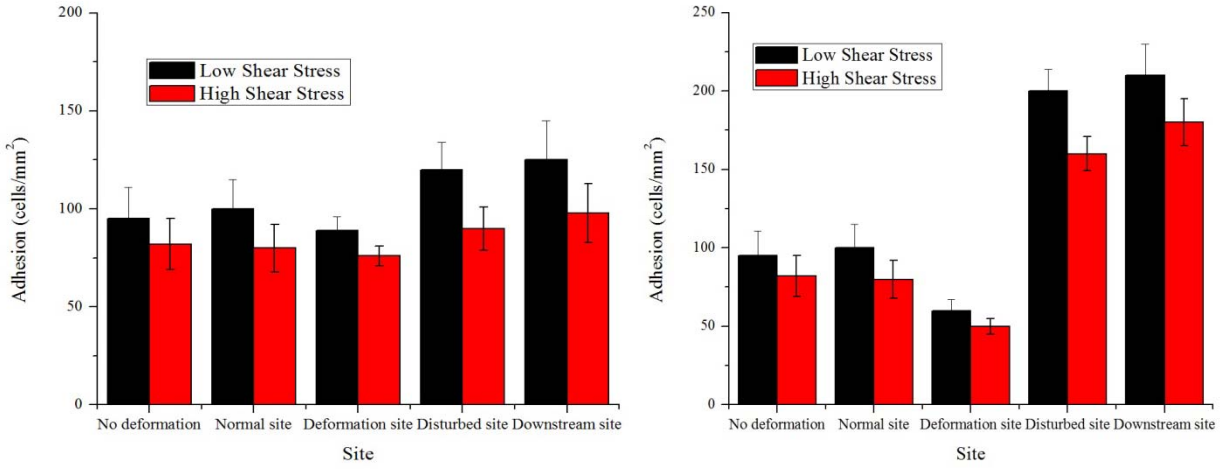

(b) (c)

Figure 7-14. Adhesion statistic from different sites of the blood vessel after fluxing the channel with Jurkat cell solution for around 30 minutes. Error bars are SD from n>3 measurement. (b) and (c) are the cases for 25% and 50% blockage of the channel respectively. No deformation refers to control experiment without blockage. From ANOVA test, the difference between normal site and disturbed site is not significant for 25% case ($p = 0.12$) and significant for 50% case ($p < 0.05$).

Figure 7-14 shows the statistical analysis of adhesion even from different sites of the blood vessel. Under constant shear stress conditions, cells show very low expression of adhesion molecules such as VCAM-1, ICAM-1 and E-/P- selectins and there is slight up-regulation of

VCAM-1, ICAM-1 and E-/P- selectins when cells are exposed to a non-uniform shear stress. Thus, for 25% blockage of the channel, since the shear stress distribution is relatively stable compared to that of 50% blockage, the adhesion doesn't show significant different at different sites. Figure 7-14c shows that when the blockage comes to 50%, which is a relative critical stage for atherosclerosis development, the adhesion at the disturbed site increase critically. It is clear that the impact of the blockage on the performance of blood vessels increases as the blockage scale rises up.

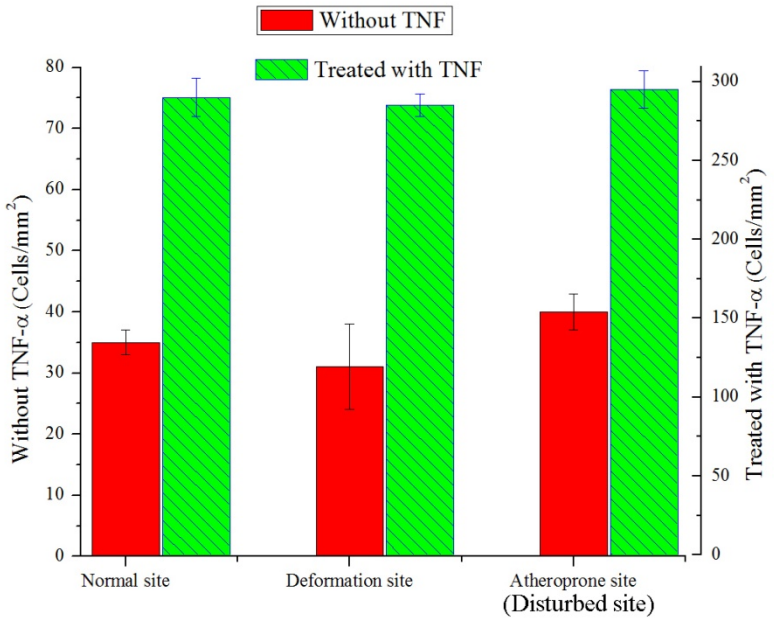

Figure 7-15. Adhesion event for static condition. Instead of fluxing with Jurkat cells, the channel is treated with Jurkat cells at static condition for 1 min. Error bars are SD from n>3 counts.

In order to investigate if the disturbed shear stress has increased the expression of adhesion molecules, including VCAM-1 and ICAM-1, to enhance the adhesion events at the disturbed sites, the adhesion of Jurkat cells was examined under static condition after dissembling the model with 50% of blockage. Jurkat cell solution with a concentration of 10^5 cells/ml was

injected in the channel. After 1 minute, the solution was fluxed with PBS solution to remove all the low adhesion cells and the adhesion event on different site of the channel was shown in Figure 7-15. The green columns, with treating with TNF-α to further activate the adhesion molecules, illustrate the adhesion events at the disturbed site are not significantly different from other sites (ANOVA test, $p = 0.4$), while the red column shows that adhesion events at disturbed site are significant different from normal sites, which indicates that the disturbed shear stress has contributed to the activation of adhesion molecules.

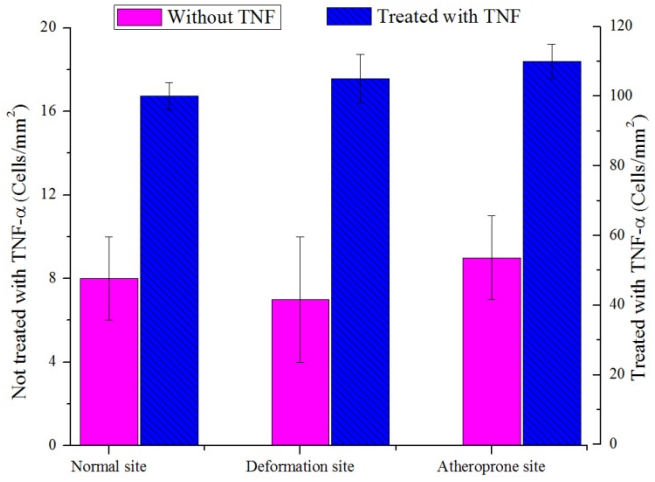

Figure 7-16. Adhesion event after fluxing the channel with Jurkat cell solution for around 20 minutes. Error bars are SD from n>3 counts. For endothelial cells not treated with TNF-α, the adhesion events didn't show significant difference among all sites. For TNF-α treated case, the adhesion events between normal site and atheroprone site are significantly different (ANOVA test, $p < 0.05$).

Since VCAM-1 and ICAM-1 were not massively up-regulated without inflammation, thus, the monolayer of endothelium was activated with TNF-α. As we know, TNF-α will increase more than 10-fold expression of VCAM1 and ICAM1, therefore, the expression of VCAM-1 and ICAM-1 could be seen as relatively uniform inside the whole channel after treating ECs for

sufficient time. After dissembling the deformation of the channel, Jurkat cell solution was injected into the channel, and the adhesion events were examined. The blue column, with ECs treated with TNF-α, in Figure 7-16 shows that adhesion events for ECs from disturbed site are higher than that from other sites, which indicates the mechanical property change of ECs has contributed to the adhesion events as well.

7.4 Discussion

The development of atherosclerosis is believed to be closely related to flow shear stress pattern and it is site-specific manner which mainly affect the branch sites [26, 27]. However, not all the atherosclerotic plaque remain at quiescent state during their whole life, some plaques will keep developing and cause clinical event eventually. In this study, based on microfluidic cell culture model, we simulated the formation of atherosclerotic plaque inside the blood vessel and investigated how the atherogenic factors, such as disturbed shear stress and changed biomechanical property of endothelial cells, promote the development of atherosclerosis.

7.4.1 Hemodynamic Shear Force Effect

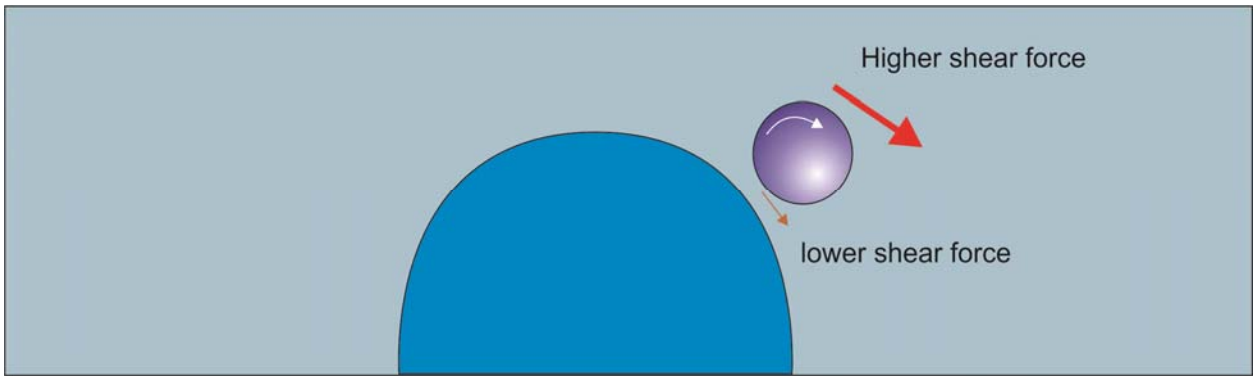

Figure 7-17. The un-symmetric hemodynamic forces cause the self rotating of immune cells. This phenomena will induce cells have higher velocity in the direction to the substrate.

Figure 7-17 shows a cell passing the plaque site was subject to an unbalanced shear force which initiated the rotation of the cell. Therefore, the rolling flux largely increased at the atheroprone site (downside of the plaque). In addition, due to the formation of plaque, shear stress at the downside of the plaque largely decreased which was shown in Figure 7-8. Thus, the rolling velocity at these sites decreased. As we know, cell capture is the first step for cells to initiate the rolling process. After cells were captured, the adhesion of molecules were established, the lower shear stress and the rotation of the cell will contribute to the formation of bonds between adhesion molecules. As the shear stress increased, some bonds become more firmly bonded [28] which contribute to the adhesion of immune cells.

7.4.2 Biomechanical Factors

The perfusion of media was maintained after the formation of plaque. Due to the disturbance of the flow shear stress in the channel, the distribution of mechanical property of cells has changed. The force volume measurement of cells shows that cells at the higher shear stress part have larger elasticity while cells showed lower elasticity at the atheropone site. Cell stiffness is mainly determined by the underline cytoskeleton structure especially the stress fibre underneath. Therefore, the stiffness may have less direct effect on the rolling or adhesion event of immune cells injected.

Viscoelastic property is another important factor since cells are intrinsically viscoelastic materials. However, due to the heterogeneity of cells in the vertical direction, both cell membrane and cytoplasm contribute to the overall property of the cell. From the model we used in Chapter 3, we were able to determine the membrane property for endothelial cells by the bilayer viscoelastic model. Endothelial cells at the atheroprone site shows more compliant

membrane property compared to other sites, which may contribute to the capture event of immune cells. Imagining a ball was hitting on a substrate, the compliant substrate will have more contact area with the ball while the harder surface will have smaller contact area. Thus, the hysteresis effect of the compliant membrane will have increase the bonding number for adhesion molecules. In addition, when the cells are rolling on the compliant surface, the velocity will decrease and further contribute to the formation of adhesion bonds.

7.4.3 Basics for Cell Rolling

As we have mentioned, the results show that capture efficiency and rolling speed doesn't have linear relationship with either shear force or rolling flux. When the shear stress increase to higher, the rolling flux decreased and the adhesion events also decreased, however, the adhesion to rolling flux ratio doesn't decrease but increase slightly. The same phenomena also appeared at the downside of the deformation part. Due to the increased gradient of shear stress, some of the cells show decreased rolling velocity when cell are rolling into the higher shear stress region. These phenomena may be correlated to the bond strength and lifetime adhesion bonds. The initial formation of the adhesion bond is preferred at lower shear stress, but the bond strength shows most efficiency at relatively higher shear stress and the lifetime of the bond also increase at higher shear stress.

7.5 Conclusion

A bio-inspired vascular mimetic microfluidic cell culture model was built to simulate the formation of atherosclerotic plaque. Combined with this model, CFD simulation was used to study the flow profile and shear stress distribution inside the channel and AFM was used to

investigate the biomechanical properties of endothelial cells in the blood vessel. Using this model, the rolling flux, rolling speed and adhesion of immune cells were also investigated. The effect of hemodynamic force and biomechanical property of endothelial cells on the rolling and adhesion events were discussed. The results show that the formation of initial plaque may contribute to the further development of atherosclerotic plaque due to the altered hemodynamic shear stress and local mechanical properties changes of cells.

In literature, most studies focus on the investigation of the initiation of atherosclerotic plaque. In this study, the in-vitro model was built to study the mechanisms of progression of atherosclerotic plaque after the formation of initial atherosclerotic plaque, which induced a series of disturbed states for the blood vessel. However, due to the limitation of in-vitro mimicking ability, the model still needs to be further improved for future study.

7.6 References

1. Ross, R., Atherosclerosis--an inflammatory disease. New England Journal of Medicine, 1999. 340(2): p. 115.

2. Lusis, A.J., Atherosclerosis. Nature, 2000. 407(6801): p. 233-241.

3. Pober, J.S., W. Min, and J.R. Bradley, Mechanisms of Endothelial Dysfunction, Injury, and Death. Annual Review of Pathology-Mechanisms of Disease, 2009. 4: p. 71-95.

4. Davignon, J. and P. Ganz, Role of endothelial dysfunction in atherosclerosis. Circulation, 2004. 109(23): p. 27-32.

5. Suciu, M., The Role of Nitric Oxide (No) and Statins in Endothelial Dysfunction and Atherosclerosis. Farmacia, 2009. 57(2): p. 131-140.

6. Libby, P., et al., Inflammation in Atherosclerosis From Pathophysiology to Practice. Journal of the American College of Cardiology, 2009. 54(23): p. 2129-2138.

7. Hansson, G. and P. Libby, The immune response in atherosclerosis: a double-edged sword. Nature Reviews Immunology, 2006. 6(7): p. 508-519.

8. Gibbons, G. and V. Dzau, The emerging concept of vascular remodeling. New England Journal of Medicine, 1994. 330(20): p. 1431.

9. Kadohama, T., et al., Effects of different types of fluid shear stress on endothelial cell proliferation and survival. Journal of Cellular Physiology, 2007. 212(1): p. 244-251.

10. Malek, A.M., S.L. Alper, and S. Izumo, Hemodynamic shear stress and its role in atherosclerosis. Jama-Journal of the American Medical Association, 1999. 282(21): p. 2035-2042.

11. Cunningham, K. and A. Gotlieb, The role of shear stress in the pathogenesis of atherosclerosis. Laboratory Investigation, 2004. 85(1): p. 9-23.

12. Azuma, N., et al., Endothelial cell response to different mechanical forces. Journal of Vascular Surgery, 2000. 32(4): p. 789-794.

13. Glagov, S., et al., Hemodynamics and Atherosclerosis - Insights and Perspectives Gained from Studies of Human Arteries. Archives of Pathology & Laboratory Medicine, 1988. 112(10): p. 1018-1031.

14. Hastings, N.E., et al., Atherosclerosis-prone hemodynamics differentially regulates endothelial and smooth muscle cell phenotypes and promotes pro-inflammatory priming. American Journal of Physiology-Cell Physiology, 2007. 293(6): p. C1824-C1833.

15. Suuronen, E.J., et al., Building in vitro models of organs. International review of cytology, 2005. 244: p. 137-173.

16. Huh, D., et al., Reconstituting Organ-Level Lung Functions on a Chip. Science, 2010. 328(5986): p. 1662-1668.

17. Holzapfel, G.A., G. Sommer, and P. Regitnig, Anisotropic mechanical properties of tissue components in human atherosclerotic plaques. Journal of Biomechanical Engineering-Transactions of the Asme, 2004. 126(5): p. 657-665.

18. Reichlin, T., et al., Investigating native coronary artery endothelium in situ and in cell culture by scanning force microscopy. Journal of Structural Biology, 2005. 152(1): p. 52-63.

19. Ross, R., Cell biology of atherosclerosis. Annual Review of Physiology, 1995. 57(1): p. 791-804.

20. Quake, S.R. and A. Scherer, From micro-to nanofabrication with soft materials. Science, 2000. 290(5496): p. 1536.

21. Lötters, J., et al., The mechanical properties of the rubber elastic polymer polydimethylsiloxane for sensor applications. Journal of Micromechanics and Microengineering, 1997. 7: p. 145.

22. Mehdizadeh, A. and A. Norouzpour, New insights in atherosclerosis: Endothelial shear stress as promoter rather than initiator. Medical Hypotheses, 2009. 73(6): p. 989-993.

23. James, W.G., D.C. Bullard, and M.J. Hickey, Critical role of the alpha(4) integrin/VCAM-1 pathway in cerebral leukocyte trafficking in lupus-prone MRL/fas(lpr) mice. Journal of Immunology, 2003. 170(1): p. 520-527.

24. Alon, R., et al., The integrin VLA-4 supports tethering and rolling in flow on VCAM-1. The Journal of cell biology, 1995. 128(6): p. 1243.

25. Borish, L.C. and J.W. Steinke, 2. Cytokines and chemokines. J Allergy Clin Immunol, 2003. 111(2 Suppl): p. S460-75.

26. Malek, A.M., S.L. Alper, and S. Izumo, Hemodynamic shear stress and its role in atherosclerosis. JAMA: the journal of the American Medical Association, 1999. 282(21): p. 2035.

27. Nigro, P., J. Abe, and B. Berk, Flow shear stress and atherosclerosis: a matter of site specificity. Antioxidants & Redox Signaling, 2010(ja).

28. Schaff, U.Y., et al., Vascular mimetics based on microfluidics for imaging the leukocyte-endothelial inflammatory response. Lab on a Chip, 2007. 7(4): p. 448-456.

CHAPTER 8

8 CONCLUSIONS

This dissertation presents the results from the majority of my PhD research. Atomic force microscopy is used to study the mechanical properties of endothelial cells and new characterization methods of biomechanical properties of cells were developed from experimental results. The biochemical effect, cholesterol content, on ECs was studied. Then a microfluidic cell culture system was constructed, based on which, a vascular mimetic microfluidic system was developed to simulate the formation of plaque during atherosclerosis process.

8.1 Summary of Findings

Chapter 2 presented a new characterization method to help understand the mechanical property especially elasticity of a single cell by AFM. The new method overcomes the effect of the substrate on the investigation of cell elasticity. By correlating the elasticity with cell morphology, a more detailed description of the elasticity of single cells was given. Chapter 3 described a bilayer viscoelastic model for living cells to investigate the stress relaxation response of endothelial cell, which is to distinguish the contribution of different cell components on responses of cells under mechanical stimuli.

The effect of cholesterol content on ECs was investigated in Chapter 4. From tradition model, the mechanical property of cell membrane is not easily to be distinguished. With bilayer viscoelastic model, the response of plasma membrane was unveiled. It was found that cholesterol would increase the stiffness of plasma membrane, thus brings chaos into cell membrane.

Chapter 5 developed a more practical method for fabricating microfluidic cell culture system. With a mask-free microfabrication technique, a highly integrated, leakage-free, low cost and time effective method was developed to realize the processes in a routine lab. Chapter 6 presented a method to quantitatively determine the intermolecular forces for a cell doublet and cell-substrate interaction model in circulating system. The results indicated that DLVO forces should be integrated with hydrodynamic forces when analysing the intermolecular forces in biological system with high ion concentration.

In Chapter 7, a bio-inspired cell culture system was developed to mimic the development of atherosclerotic plaque. As we know, hemodynamic shear force plays a critical role in the development of atherosclerosis in the branched arteries. After the formation of atherosclerotic plaque, the local hemodynamic shear stress was disturbed which affects the flow profile and the response of endothelial cells. From examining the rolling and adhesion events of immune cells, it is concluded that the deformation site with higher shear stress, the hemodynamic force showed athero-protective effect; while at the downside of the deformation where the disturbed shear force located, hemodynamic force showed atheroprone effect.

8.2 Future Directions

Understanding the systemic pathological factor of atherosclerosis is a complex work. In this dissertation, through in vitro cell culture experiments and vascular mimetic model, biomechanical factors, including mechanical properties of ECS, hemodynamic effect and intercellular forces, related to atherosclerosis were investigated. While the work has shed light on discovering the mechanisms of the progression of atherosclerosis, questions still remain about the coupling of biophysical input and the biochemical output of the system. The biochemical

response represents a very complex direction. In this direction, the distribution of chemotactic factors especially the adhesion molecules could be examined by blocking the effect of certain factors. Another direction is to develop more delicate in vitro model to mimic in vivo environment more physiologically. Through co-culturing smooth muscle cell with endothelial cells, more complex responses during the progression of atherosclerosis could be unveiled.

Curriculum Vitae

Qiuquan Guo Ph.D Candidate

Education and Degrees:

2007-present	Ph.D Candidate in Biomedical Engineering The University of Western Ontario, London, Ontario, Canada
2005-2007	Master of Engineering Science in Physical Electronics Beijing Institute of Technology, Beijing, China
2001-2005	Bachelor in Mechanical Engineering Beijing Institute of Technology, Beijing, China

Honours and Awards:

2007-present	Western Graduate Research Scholarship (WGRS), UWO
2009	Graduate Thesis Research Awards Fund, UWO
2007	Excellent Graduation Thesis Award, Beijing
2006 ~ 2007	Outstanding Graduated Student Award, Beijing
2006	China Aerospace Science Corporation Scholarship, Beijing
2005	First-class of the People's scholarship, Beijing
2005	Excellent Graduated Student Award of Beijing
2004	SONY scholarship, Beijing
2001 ~ 2005	Excellent Student Award of the University, Beijing
2003	Challenge Cup the Structure Design Competition in Beijing

- *The Best Design Award*
- *The Best Structure Analysis Award*
- *Major Award for Structure Loading*

Work Experience:

2007-2011	Research Assistant/Teaching Assistant
	The University of Western Ontario
2005-2007	Research Assistant
	Beijing Institute of Technology

Journal Publications:

1. **Qiuquan Guo,** et al., AFM Reveals Correlation of Morphology and Elasticity of Human Aortic Endothelial Cells, Biomechanics. (submitted)
2. **Qiuquan Guo,** et al., Evaluation of intermolecular forces in a circulating system. Biosystems, 2011. (Accepted)
3. Kar Man Leung, Greg Wanger, **Qiuquan Guo**, et al., Bacterial nanowires: conductive as silicon, soft as polymer. Soft Matter, 2011. 7(14): p. 6617-6621.
4. Mei Liu, Ying Chen, **Qiuquan Guo,** et al., An Economic Method for Large-Scale Patterning and Electric Measurement of Nanowires. Journal of Nanoelectronics and Optoelectronics, 2011. 6(2): p. 144-151.
5. Mei Liu, Ying Chen, **Qiuquan Guo,** et al., Controllable positioning and alignment of silver nanowires by tunable hydrodynamic focusing. Nanotechnology, 2011. 22(12): p. 125302.
6. Binyu Yu, Kar Man Leung, **Qiuquan Guo,** et al., Synthesis of Ag-TiO_2 composite nano thin film for antimicrobial application. Nanotechnology, 2011. 22(11): p. 115603.
7. Yu Liu, **Qiuquan Guo,** et al., Optimization and calibration of atomic force microscopy sensitivity in terms of tip-sample interactions in high-order dynamic atomic force microscopy. Journal of Applied Physics, 2009. 106(12): p. 124507-124507-9.
8. Mei Liu, Yu Liu, **Qiuquan Guo,** et al., Modeling of electroosmotic pumping of nonconducting liquids and biofluids by a two-phase flow method. Journal of Electroanalytical Chemistry, 2009. 636(1-2): p. 86-92.
9. **Qiuquan Guo,** et al., Design of a relaying electroosmosis pump driven by low-voltage DC. Microsystem Technologies, 2009. 15(7): p. 1009-1015.
10. Jinlong Zhang, **Qiuquan Guo,** et al., A lab-on-CD prototype for high-speed blood separation. Journal of Micromechanics and Microengineering, 2008. 18: p. 125025.
11. **Qiuquan Guo,** et al, Micromechanical modeling of local field distribution for a planar composite under plastic deformation. Acta mechanica, 2006. 187(1): p. 139-149.

Conferences:

2010 CMBEC 33, Canada

2010 8th International Conference on Nanochannels, Microchannels, and Minichannels MD and Numerical Simulation of Microscale and Nanoscale Phenomena

2010 CFD Society of Canada 18th Annual Conference, Canada

2009 TEXPO 2009

2009 Biomaterials, Hong Kong, China

2008 The Canadian Society for Mechanical Engineering (CSME), Ottawa

2006 The 3rd mechanics annual conference, Beijing